

Phase I Design Report

Deliverable D4

Composite Bridge Decking

Publication No. FHWA-HIF-13-030
January 2013

HIGHWAYS FOR LIFE

Accelerating Innovation for the American Driving Experience.



U.S. Department of Transportation
Federal Highway Administration

Notice

This document is disseminated under the sponsorship of the U.S. Department of Transportation in the interest of information exchange. The U.S. Government assumes no liability for the use of the information contained in this document.

The U.S. Government does not endorse products or manufacturers. Trademarks or manufacturers' names appear in this report only because they are considered essential to the objective of the document.

Quality Assurance Statement

The Federal Highway Administration (FHWA) provides high-quality information to serve Government, industry, and the public in a manner that promotes public understanding. Standards and policies are used to ensure and maximize the quality, objectivity, utility, and integrity of its information. FHWA periodically reviews quality issues and adjusts its programs and processes to ensure continuous quality improvement.

Technical Report Documentation Page

1. Report No. FHWA-HIF-13-030		2. Government Accession No.		3. Recipient's Catalog No.	
4. Title and Subtitle Composite Bridge Decking: Phase I Design Report				5. Report Date September 2012	
7. Author(s) J. S. O'Connor				6. Performing Organization Code	
9. Performing Organization Name and Address BridgeComposites, LLC 121 Upper Bennett St. Hornell, NY 14843-1451				8. Performing Organization Report No.	
12. Sponsoring Agency Name and Address Federal Highway Administration Highways for LIFE Program – HIHL-1 1200 New Jersey Avenue, SE Washington, D.C. 20590				10. Work Unit No. (TRIS)	
				11. Contract or Grant No. DTFH61-09-RA-00006	
				13. Type of Report and Period Covered	
				14. Sponsoring Agency Code	
15. Supplementary Notes					
16. Abstract <p>This report provides information about the materials, subcomponent shapes, and processes used to fabricate a lightweight decking system. It describes the design criteria and presents the results of physical testing done to validate the finite element analysis. Attention has been given to the structural panels used for decking, as well as to the design details that are critical to the successful deployment of the technology, such as field joint construction, and wearing surface installation.</p> <p>The proposed design is a versatile hollow section that can be deployed in a variety of ways, depending on the design objectives and existing site conditions for a deck replacement project. The composite material provides sufficient strength to carry the factored American Association of State Highway and Transportation Officials (AASHTO) design load and, in cases where the supports are close together, is adequate for deflection control as well. Where steel stringers are spaced more than 3 feet on center, additional material is needed to increase the section's stiffness. Testing has shown that fabrication with epoxy grout in selected cells of the hollow section will increase stiffness by 45 percent, although the grout adds 50 percent or more to the weight of the deck. In cases where it is very important to have a lightweight deck, deflection control can be achieved with additional fiber in the outer wrap. In this instance, the deck weighs approximately 16 psf prior to the application of a 4-psf wearing surface.</p> <p>This report documents Phase I of the project. It is provided as an after-test review to get input from the project's Technical Advisory Panel and other potential stakeholders.</p>					
17. Key Words Composite deck, Fiber-reinforced polymer composite, FRP, bridge decking			18. Distribution Statement No restrictions. This document is available to the public through the National Technical Information Service, Springfield, VA 22161.		
19. Security Classification (of this report) Unclassified		20. Security Classification (of this page) Unclassified		21. No. of Pages 137	22. Price

SI* (MODERN METRIC) CONVERSION FACTORS

APPROXIMATE CONVERSIONS TO SI UNITS

Symbol	When You Know	Multiply By	To Find	Symbol
LENGTH				
in	inches	25.4	millimeters	mm
ft	feet	0.305	meters	m
yd	yards	0.914	meters	m
mi	miles	1.61	kilometers	km
AREA				
in ²	square inches	645.2	square millimeters	mm ²
ft ²	square feet	0.093	square meters	m ²
yd ²	square yard	0.836	square meters	m ²
ac	acres	0.405	hectares	ha
mi ²	square miles	2.59	square kilometers	km ²
VOLUME				
fl oz	fluid ounces	29.57	milliliters	mL
gal	gallons	3.785	liters	L
ft ³	cubic feet	0.028	cubic meters	m ³
yd ³	cubic yards	0.765	cubic meters	m ³
NOTE: volumes greater than 1000 L shall be shown in m ³				
MASS				
oz	ounces	28.35	grams	g
lb	pounds	0.454	kilograms	kg
T	short tons (2000 lb)	0.907	megagrams (or "metric ton")	Mg (or "t")
TEMPERATURE (exact degrees)				
°F	Fahrenheit	5 (F-32)/9 or (F-32)/1.8	Celsius	°C
ILLUMINATION				
fc	foot-candles	10.76	lux	lx
fl	foot-Lamberts	3.426	candela/m ²	cd/m ²
FORCE and PRESSURE or STRESS				
lbf	poundforce	4.45	newtons	N
lbf/in ²	poundforce per square inch	6.89	kilopascals	kPa

APPROXIMATE CONVERSIONS FROM SI UNITS

Symbol	When You Know	Multiply By	To Find	Symbol
LENGTH				
mm	millimeters	0.039	inches	in
m	meters	3.28	feet	ft
m	meters	1.09	yards	yd
km	kilometers	0.621	miles	mi
AREA				
mm ²	square millimeters	0.0016	square inches	in ²
m ²	square meters	10.764	square feet	ft ²
m ²	square meters	1.195	square yards	yd ²
ha	hectares	2.47	acres	ac
km ²	square kilometers	0.386	square miles	mi ²
VOLUME				
mL	milliliters	0.034	fluid ounces	fl oz
L	liters	0.264	gallons	gal
m ³	cubic meters	35.314	cubic feet	ft ³
m ³	cubic meters	1.307	cubic yards	yd ³
MASS				
g	grams	0.035	ounces	oz
kg	kilograms	2.202	pounds	lb
Mg (or "t")	megagrams (or "metric ton")	1.103	short tons (2000 lb)	T
TEMPERATURE (exact degrees)				
°C	Celsius	1.8C+32	Fahrenheit	°F
ILLUMINATION				
lx	lux	0.0929	foot-candles	fc
cd/m ²	candela/m ²	0.2919	foot-Lamberts	fl
FORCE and PRESSURE or STRESS				
N	newtons	0.225	poundforce	lbf
kPa	kilopascals	0.145	poundforce per square inch	lbf/in ²

*SI is the symbol for the International System of Units. Appropriate rounding should be made to comply with Section 4 of ASTM E380.
(Revised March 2003)

TABLE OF CONTENTS

1. INTRODUCTION.....	1
2. TESTING.....	3
Testing Program	3
Materials.....	3
Tube Subcomponents	3
Structural Panels.....	4
Assembly.....	5
Details.....	8
3. AFTER-TEST REVIEW.....	9
4. CONCLUSIONS	11

APPENDIX A: DETERMINATION OF PRELIMINARY DESIGN PROPERTIES

APPENDIX B: DETERMINATION OF LAMINA DESIGN PROPERTIES

APPENDIX C: EVALUATION OF “AS-TESTED” PROPERTIES OF FRP LAMINATES

APPENDIX D: GROUT SELECTION REPORT

APPENDIX E: REPORT ON TUBE TESTING

APPENDIX F: REPORT ON STRUCTURAL PANEL TESTING

APPENDIX G: PANEL SHEAR TEST

APPENDIX H: PANEL FATIGUE TEST

APPENDIX I: PANEL-TO-PANEL FIELD JOINT

APPENDIX J: BRIDGE RAILING POST ANCHORAGE PROOF TEST

APPENDIX K: WEARING SURFACE TEST

APPENDIX L: FIRE TEST REPORT

APPENDIX M: AFTER-TEST REVIEW PRESENTATION

LIST OF FIGURES

Figure 1. Photo. The pultruded tube subcomponent consisting of E-glass and vinyl ester resin. ..	6
Figure 2. Photo. Tube subcomponents are bonded together with adhesive to form a panel.	6
Figure 3. Photo. Panel ends are capped and radii between tubes filled with thixotropic resin.....	6
Figure 4. Photo. The panel is wrapped in glass fiber in preparation for infusion with vinyl ester resin.....	7
Figure 5. Photo. Resin is infused for the outer wrap using a vacuum-assisted resin transfer molding (VARTM) method.	7
Figure 6. Photo. Each infused deck panel is stripped and inspected to ensure that fibers have been thoroughly wet-out with resin.	7
Figure 7. Photo. Adhesive and stone are applied for course 1 of the wearing surface.	8
Figure 8. Diagram. Geometry of ice shield profile with single cavity.	13
Figure 9. Graph. Constituent content of test laminates as a percentage of total laminate thickness.	18
Figure 10. Diagram. Fiber directions for in-plane shear strength testing.	20
Figure 11. Diagram. Structure of double bias laminate.	29
Figure 12. Diagram. Pultruded combination tube.....	32
Figure 13. Diagram. Laminate construction for pultruded combination tube.	33
Figure 14. Diagram. Pultruded FRP combination tube.....	42
Figure 15. Diagram. FRP tube cross section.....	48
Figure 16. Diagram. Grout configurations.....	49
Figure 17. Photo and diagram. Testing setup.	50
Figure 18. Photos. Load cells used for FRP testing.....	50
Figure 19. Diagram. Strain gage locations for the FRP tube specimen #30.....	51
Figure 20. Graphs. Load-deflection elastic response of FRP tubes with no grout (left); Load-deflection response up to failure (tubes #30 and #38) (right).....	52
Figure 21. Graph. Load-strain response of FRP tube #30 (no grout, WSU).	52
Figure 22. Photos. Failure modes of FRP tubes with no grout.	52
Figure 23. Graph. Load-deflection behavior up to failure for grouted FRP tubes.....	55
Figure 24. Graph. Load-deflection curve (up to 2,500 lb) of specimens #56, 57, and #31.....	55
Figure 25. Graphs. Load-strain responses of grouted FRP tubes.	56
Figure 26. Photos. Photographs of failure modes of grouted FRP tubes.....	57
Figure 27. Photos. Cementitious grout slipping at the end of FRP tube #60.....	57

Figure 28. Photos. Cross sections of grouted tubes near midspan, after failure.	58
Figure 29. Specifications with photos. Manufacturing details of panels without grout.	60
Figure 30. Diagram. Grout configurations.....	61
Figure 31. Photos and diagrams. FRP panel test setup.	62
Figure 32. Diagrams. Strain gage location for panel #4.	63
Figure 33. Diagrams. Strain gage location for panel #3 (tested to failure).....	63
Figure 34. Graphs. Load-deflection response of FRP panels with no grout.....	64
Figure 35. Graphs. Load-strain response of FRP panels with no grout.....	64
Figure 36. Photos. Failure sequence of FRP panel #3 (no grout).	65
Figure 37. Photos and diagrams. Details of cut sections from panel #3.....	66
Figure 38. Graphs. Load-deflection response of FRP grouted panels.	68
Figure 39. Diagrams. Strain gage location for panel #7.	69
Figure 40. Diagrams. Strain gage location for panel #10.	69
Figure 41. Graphs. Load-strain response of FRP panel #7-CA.	69
Figure 42. Graph. Load-strain plot of FRP panel #10-EA.....	70
Figure 43. Graph. Load-strain (top & bottom) FRP panels.	70
Figure 44. Diagrams. Tested load footprints.	72
Figure 45. Diagrams. Test setup used to evaluate footprint effect.	73
Figure 46. Photos. Test setup details.	74
Figure 47. Graphs. Load-deflection responses of the two footprint tests.	74
Figure 48. Specifications with photo. Manufacturing details of tested panel.....	76
Figure 49. Photo. FRP panel (WSD).	76
Figure 50. Diagram. Cross section dimensions of the FRP panel tested in fatigue.....	76
Figure 51. Photos and diagram. Fatigue test setup.	77
Figure 52. Graphs. Stiffness ratios as function of the number of fatigue load cycles (left); temporary change in stiffness between 500,000 and 650,000 cycles (right).	78
Figure 53. Diagrams and photo. Location of wearing surfaces: applied to top and bottom of deck panel to assess performance in compression and tension.	79
Figure 54. Graph. Load-deflection behavior at different fatigue cycles.....	80
Figure 55. Graph. Stiffness change during daytime.	80
Figure 56. Photos. Bottom wearing surface before and after 500,000 cycles fatigue load.	81
Figure 57. Photos. Top wearing surface before and after 350,000 cycles fatigue load.....	81
Figure 58. Diagrams. Strain gage position.....	81

Figure 59. Graph. Load-strain behavior (SG1).....	82
Figure 60. Graph. Load-strain behavior (SG4).....	82
Figure 61. Graph. Load-strain behavior (SG3).....	82
Figure 62. Graph. Load-strain behavior (SG5).....	82
Figure 63. Graph. Load-strain behavior (SG2).....	82
Figure 64. Photo. Panel-to-panel field joint.....	84
Figure 65. Diagram. Cross section dimensions.	84
Figure 66. Photos and diagrams. End panel connection test setup.	85
Figure 67. Photo. Crack at load of 7 kips.	86
Figure 68. Photo. Crack at maximum load of 14.7 kips.	86
Figure 69. Photo. Failure of the specimen (11.8 kips).....	87
Figure 70. Graph. Load-deflection behavior.....	87
Figure 71. Graph. Net specimen displacement.	87
Figure 72. Graph. Load-strain behavior of the epoxy key.....	88
Figure 73. Photos. The two failed surfaces.....	88
Figure 74. Diagram. Sketch of the crack line.	88
Figure 75. Photos and sketch. Railing post specimen.....	90
Figure 76. Photo and diagrams. Railing post test setup.....	91
Figure 77. Photo and diagram. Detailing of steel beam-structural frame connection.	92
Figure 78. Photos and diagrams. Location of transducers used during the test.....	93
Figure 79. Graph. Load-displacement behavior of railing post end (string pot 2).	95
Figure 80. Photos. Failure mode of the railing post-FRP deck panel connection.	96
Figure 81. Graph and photo. Vertical displacement of the railing post, Test 1.....	97
Figure 82. Diagram. Railing post connection (deformed shape, not to scale).....	97
Figure 83. Photos. HDPE deformation at different loading levels, Test 2.	99
Figure 84. Graph. Horizontal deflection (x-direction), Test 2.....	100
Figure 85. Graph. Vertical displacement (y-direction), Test 2.	100
Figure 86. Graph. String pot 4 movement, Test 2.	101
Figure 87. Photos and graphs. Movement of three bolts on FRP back panel using digital image correlation, Test 1.	102
Figure 88. Diagram and photos. Expansion bolt connection.	103
Figure 89. Photos. FRP specimen used for pull-off tests.....	106
Figure 90. Photos. Dollies mounted to two test areas.....	107

Figure 91. Photos. Failure surfaces of aggregate to adhesive pull-off tests (dollies 4, 5, and 6).	108
Figure 92. Photos. Failure surfaces of adhesive to FRP pull-off tests (dollies 7, 8, and 9).....	108
Figure 93. Photo. Test panel mounted on top of fire chamber.	110
Figure 94. Photo. Support beams spaced at 2 feet.	110
Figure 95. Photo. 1,600-lb water tank used as concentrated load.....	111
Figure 96. Photos. Placement of thermocouples on the test panel.....	111
Figure 97. Photo. The test panel just after the test stopped. Note that the top surface kept cooler and ended up with little deterioration.	115
Figure 98. Photo. Specimen immediately after the test. Note the extent of damage on the bottom.	115
Figure 99. Photo. Close-up of the open end of the panel after the test.	115
Figure 100. Photo. The glass fiber on the bottom has frayed due to burn-off of the resin matrix.	116

LIST OF TABLES

Table 1. Tube testing.....	4
Table 2. Test methods used in characterization.....	14
Table 3. Comparison of fiber architectures.....	16
Table 4. Comparison of laminate properties.....	17
Table 5. Suggested design values.	23
Table 6. Material properties for the definition of a unidirectional lamina.....	25
Table 7. Test methods used in characterization.....	26
Table 8. Test laminates for characterization of lamina properties.....	27
Table 9. Summary of physical test data for laminate samples.....	27
Table 10. Suggested lamina design values for ply based design and analysis.	30
Table 11. Predicted properties of pultruded tube.....	33
Table 12. Ply details for horizontal walls of pultruded tube.....	34
Table 13. Ply details for vertical walls of pultruded tube.	35
Table 14. Areal reinforcement weights (oz/yd ²) of potential tube laminates.	35
Table 15. Test methods used in characterization.....	37
Table 16. Summary of physical test data for tube laminate samples.....	38
Table 17. Summary of physical test data from outer wrap laminate samples.	39
Table 18. Published grout properties.	44
Table 19. Results of grout testing.	45
Table 20. Relative merits of grouts for the application (i.e., fill material).	46
Table 21. Dimensions and thicknesses of FRP tubes (no grout).	48
Table 22. Details of FRP grouted tubes.....	49
Table 23. Test program—FRP tubes no grout.....	51
Table 24. Test program—grouted FRP tubes.	54
Table 25. Details of panels.....	61
Table 26. Test program—FRP panel without grout.....	63
Table 27. Test program—grouted FRP panels.	67
Table 28. Flexure stiffness as function of increasing number of fatigue cycles.....	78
Table 29. Load-displacement data for string pot 2.	94
Table 30. Test 2 HDPE pad deformation.....	98
Table 31. Pull-off test results.....	107

Table 32. Details of thermocouple placement.	112
Table 33. Deflection measurements.....	113

LIST OF ACRONYMS AND ABBREVIATIONS

AASHTO	American Association of State Highway and Transportation Officials
BIN	Bridge Identification Number
CSM	Chopped Strand Mat
DOT	Department of Transportation
DOTD	Department of Transportation and Development
FHWA	Federal Highway Administration
FRP	Fiber-Reinforced Polymer
HDPE	High-Density Polyethylene
LRFD	Load and Resistance Factor Design
LVDT	Linear Variable Differential Transformer
VARTM	Vacuum-Assisted Resin Transfer Molding
WSD	Wide Side Down
WSU	Wide Side Up

EXECUTIVE SUMMARY

This report summarizes project Phase I, which involved the refinement of design, testing, and fabrication methods used to develop a lightweight, corrosion-resistant bridge deck. The deck can be used on any bridge, but it is particularly beneficial for moveable bridges because of its light weight. Fundamentally, the deck described in this report is the same as the design that was developed and tested between 2003 and 2009 for the New York State Department of Transportation (DOT) at the University at Buffalo, Department of Civil Structural and Environmental Engineering. After a careful assessment of various materials and available methods, refinements have been made to improve performance of the deck, facilitate its fabrication, and reduce its cost. Integral with the design and production improvements are the development of suitable construction details such as connections to the supporting steel, a durable wearing surface, and anchorages for railing posts.

The deck described in this report consists of glass fiber-reinforced polymer composite materials and grout when the stringer spacing necessitates additional stiffness.

After finite element analysis and validation by testing, it was found that the composite section was sufficiently stiff for use on the proof-of-concept bridge in Bolivar, NY, which has steel stringers spaced at 2 feet. The Pleasant Street Bridge over Little Genesee Creek (BIN 2215390) is 40 feet long and had a proposed width of 22 feet. Allegany County personnel started a rehabilitation project in August 2012, replaced the deck, and opened the bridge to traffic in September. The process used is similar to the installations envisioned for moveable bridges, which is the primary target of the Highways for LIFE project. A fixed-span bridge was selected to keep the scope contained enough that it could be done under the present project.

This report has been prepared to document the design and testing for review by the project Technical Advisory Panel, whose names and affiliations are shown below:

- Ray Bottenberg, OR DOT.
- Duane Daniels, Larson Design Group.
- Jeremy Ferris, Allegany County, NY.
- Paul Fossier, LA Department of Transportation and Development (DOTD).
- Paul Liles, GA DOT.
- George Patton, E.C. Driver, Inc.
- William Potter, FL DOT.
- Herbert Protin, HDR.
- Tom Sheehan, NY State Thruway Authority, Canals Division.
- Kevin Thompson, former Caltrans State Bridge Engineer.
- Art Yannotti, former NY State Bridge Engineer.

1. INTRODUCTION

This report summarizes project Phase I (Tasks 2 through 13). The broad objective of Phase I was to identify the most suitable materials, subcomponents, assembly methods, installation details, and wearing surface for the manufacture and deployment of a bridge deck designed to incorporate glass fiber-reinforced polymer (FRP) composite materials. Tasks 2 through 6 involved preliminary design, and Tasks 7 through 13 involved testing. The preliminary design tasks are documented in a previously published report, FHWA-HIF-12-021.

The primary focus of this project has been on moveable bridges for two reasons: the lightweight nature of the deck and the fact that it provides a solid surface that protects the structure. These are especially beneficial for moveable bridges. However, over the course of the project, the Federal Highway Administration (FHWA) modified the title of the project to be simply “Composite Bridge Decking,” since the deck’s advantages are not restricted to use on just one class of bridges. The deck system can be also used on conventional fixed bridges, with similar benefits. Constructability was shown on a 40-foot-long, fixed bridge in Allegany County, NY, as part of a proof-of-concept installation. Deck-work started on August 28, 2012, was completed successfully, and the bridge was opened to traffic on September 27, 2012.

2. TESTING

TESTING PROGRAM

The testing program consisted of an evaluation of the following:

- Materials.
- Tube subcomponents.
- Assemblies.
- Structural panels.
- Details.

Upon conclusion, the researchers provided a summary of the testing program to the project Technical Advisory Panel, and the Panel provided comments. See section 3.

MATERIALS

Publication FHWA-HIF-12-020, Laminate Specification and Characterization, describes the FRP materials considered and tested for this project. Appendices A through C provide addenda to the Laminate Specification and Characterization report. Appendix D summarizes the testing and selection of grout material.

TUBE SUBCOMPONENTS

Table 1 details the testing of the tube specimens, and Appendix E presents findings of these tests.

Table 1. Tube testing.

Test Type	No. of Specimens (10-ft span)	Description	Purpose
1	1	Empty tube with strain gages to obtain load-deflection data.	Calibrate finite element analysis.
2	1	Tube filled (wide cell) with the #1 choice of grout, tested with strain gages to obtain load-deflection data. Tested wide side up.	Calibrate finite element analysis and assess performance of the bond interface. Compare performance of grouts.
3	1	Tube filled (narrow cell) with the #1 choice of grout, tested with strain gages to obtain load-deflection data. Tested wide side down.	Same as above but with narrow cell filled.
4	1	Tube filled (wide cell) with the #2 choice of grout, tested with strain gages to obtain load-deflection data. Tested wide side up.	Calibrate finite element analysis and assess performance of the bond interface. Compare performance of grouts.
5	1	Tube filled (narrow cell) with the #2 choice of grout, tested with strain gages to obtain load-deflection data. Tested wide side down.	Same as above but with narrow cell filled.
6	3	Simple deflection test of a tube filled (wide cell) with the #1 choice of grout, tested wide side up, then wide side down.	Check consistency of interface performance and relative performance of tube up vs. down.
7	3	Simple deflection test of a tube filled (narrow cell) with the #1 choice of grout, tested wide side up, then wide side down.	Check consistency of interface performance and relative performance of tube up vs. down.
8	3	Simple deflection test of a tube filled (wide cell) with the #2 choice of grout, tested wide side up, then wide side down.	Check consistency of interface performance and relative performance of tube up vs. down.
9	3	Simple deflection test of a tube filled (narrow cell) with the #2 choice of grout, tested wide side up, then wide side down.	Check consistency of interface performance and relative performance of tube up vs. down.

STRUCTURAL PANELS

Twelve full-depth panels measuring 3 feet by 11 feet were tested to determine response under flexure, shear, and ultimate failure. The following describes the three panel types that were tested:

- *Baseline:* One panel type was tested without any grout to give a true indication of how much benefit is derived from the grout fill. Additionally, discussions with bridge owners revealed that they do not always need the added grout because they prefer a lighter deck. For instance, if the steel stringer spacing is only 2 feet, an unfilled panel is adequate; tight stringer spacing like this is often the case if the bridge was originally designed for 2-inch-thick timber deck. Also, there may be times when a historic bridge will always be posted for weight restriction because of the condition of the primary members. In this case a deck capable of carrying extremely heavy trucks is unwarranted. Testing determined that, in these situations, a deck can function perfectly without the addition of grout. Four panels of this type were tested in flexure.
- *Top filled:* Panels were tested that had grout in the top of all the tubes, similar to the original prototype. Half of the tubes had the wide cell filled and the others had the narrow cell filled. This was expected to give good plate action to the surface of the deck, helping to distribute the wheel loads. Most decks are designed as simply supported spans between stringers, so putting grout in the top portion of each tube is consistent with this approach. Two panels were made with each grout (epoxy and cementitious), resulting in a total of four panels of this type being tested in flexure.
- *Alternating Grout:* Conversations with the Florida DOT have highlighted the fact that decks on moveable bridges sometimes have compressive stresses in the top surface, and at other times the top surface is in tension. For example, when the span is being lifted, the stresses typically reverse. For these situations, it may be desirable to have grout in both the top and bottom of the panels so that compressive loads can be carried efficiently for either positive or negative bending. Tests were done with grout only in the wide cell, alternating between the top and bottom. Two panels were made with each grout (epoxy and cementitious), resulting in a total of four panels of this type being tested in flexure.

Documentation of the testing is presented in the following appendixes:

- Appendix F summarizes flexure testing of the structural panels as well as ultimate failure.
- Appendix G explains the short panel shear test with a concentrated load.
- Appendix H summarizes a panel fatigue test.

ASSEMBLY

Figures 1 through 7 illustrate the assembly of deck panels from tube subcomponents.

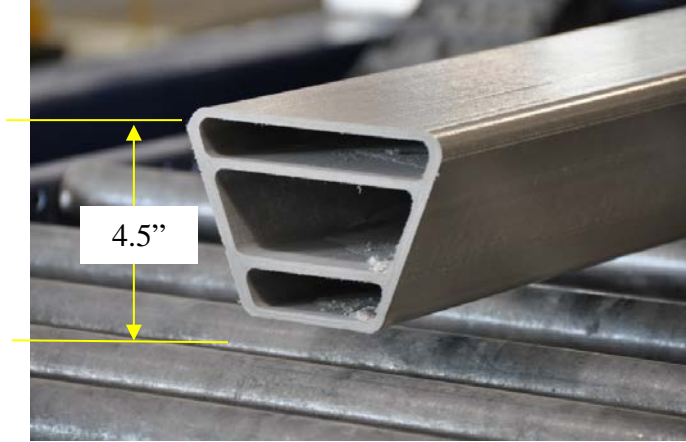


Figure 1. Photo. The pultruded tube subcomponent consisting of E-glass and vinyl ester resin.



Figure 2. Photo. Tube subcomponents are bonded together with adhesive to form a panel.



Figure 3. Photo. Panel ends are capped and radii between tubes filled with thixotropic resin.



Figure 4. Photo. The panel is wrapped in glass fiber in preparation for infusion with vinyl ester resin.



Figure 5. Photo. Resin is infused for the outer wrap using a vacuum-assisted resin transfer molding (VARTM) method.



Figure 6. Photo. Each infused deck panel is stripped and inspected to ensure that fibers have been thoroughly wet-out with resin.



Figure 7. Photo. Adhesive and stone are applied for course 1 of the wearing surface. (The black rectangle is a bearing pad for the bridge railing post.)

DETAILS

Special testing categorized as “details” includes:

- Panel-to-panel field joint.
- Bridge railing anchorage.
- Connection to steel.
- Wearing surface.
- Fire testing.

Documentation of these tests is provided as follows:

- Appendix I describes the results of testing on the grouted panel-to-panel field joint.
- Appendix J describes the results of testing the bridge rail post anchorage and connections to supporting steel.
- Appendix K gives results of wearing surface pull-off tests.
- Appendix L provides the laboratory report for fire testing.

3. AFTER-TEST REVIEW

On August 14, 2012, the research team provided the project Technical Advisory Panel with an update and summary of the testing that had been done. The presentation used for this is included in Appendix M.

The Technical Advisory Panel's comments are listed below, followed by the project team's responses:

- Question: How is the wearing surface repaired/refreshed?
 - Response: Since the second course of the wearing surface is only ¼ inch thick, a new ¼-inch surface can be applied if the additional 3 psf weight is not critical. Otherwise, the polymer concrete wearing surface can be milled off and resurfaced with a fresh course of the same material.

- Question: Will this be available in various panel sections/sizes? Will there be a table for design engineers to use as a design guide?
 - Response: The deck design is valid for a range of spans, and this can be tabulated to give designers the ability to pick the suitable deck type for their stringer spacing. Spans between 2 and 10 feet were tested. Sections were tested with various stiffening materials: empty, epoxy grout in the top only, and epoxy grout alternating between top and bottom.

- Question: What about dynamic loading?
 - Response: An impact factor was applied to the American Association of State Highway and Transportation Officials (AASHTO) design load. The field testing that is planned may provide additional information about the actual dynamic loading induced by truck loads.

- Question: Previous FRP decks have had trouble with the deck-deck joints, deck-steel connections, and the wearing surface. What has been done to prevent those problems?
 - Response: "Details" have been given a lot of attention in the design/analysis, material testing, and proof testing stages of the project. The modeling and subsequent testing assures us that the proposed details will function well in service.

- Comment: In the preliminary design stage, a reviewer's only concern had been about the type of grout used. He was pleased to see that we addressed that issue by selecting a low-modulus grout that will be compatible with the fairly flexible deck panels.

4. CONCLUSIONS

The testing performed in Phase I helped determine the best selection of material, subcomponents, assembly method, and details. Through these tests, cementitious grout was found to be insufficient because of its low bond strength with the pultruded tube. Epoxy grout is preferred. In some applications, the panel will perform adequately without any grout because of its innate robustness and stiffness.

The bridge railing test demonstrated that the anchorage connection meets the Test Level-2 loading requirements found in AASHTO's Load and Resistance Factor Design (LRFD) Bridge Specification. When load on the bridge rail post was increased to failure, it resulted in a type of damage that will be easily repairable using epoxy grout. Further testing may show that higher test levels can be achieved by filling this area of the FRP deck with epoxy grout to resist a punching failure.

The deck panels are suitable for the intended application under standard AASHTO loading.

APPENDIX A: DETERMINATION OF PRELIMINARY DESIGN PROPERTIES

OVERVIEW

The trapezoidal profile used to create the replacement deck slabs in this project was developed from an earlier design developed at the University of Buffalo. In July 2010, XC Associates fabricated a protective ice shield for a bridge in Erie County, NY, using this profile design. The trapezoidal shape was slightly different than that proposed for the current project in that it only used a single grout cavity rather than two (see figure 8). The structure was fabricated from two trapezoids each approximately 0.1 inch thick. The smaller trapezoid was designed to be adhesively bonded inside the larger trapezoid. A series of these tubes were then adhesively bonded together to form a wall unit. To ensure the structural integrity of the wall unit, the assembly was completely wrapped by an outer laminate.

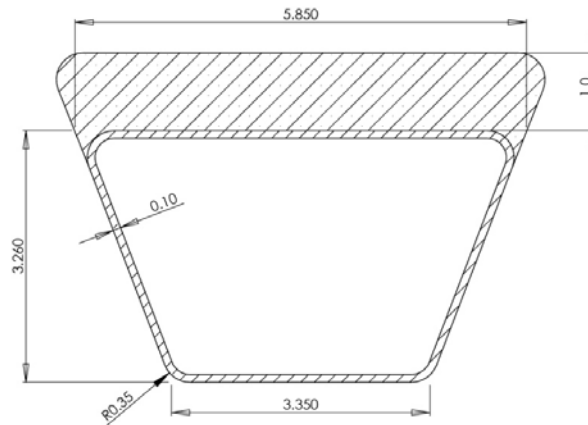


Figure 8. Diagram. Geometry of ice shield profile with single cavity.

The current bridge deck required significantly higher load bearing capacity than the ice wall units. To establish a feasible design, engineers planned to work from earlier finite element analysis models to determine suitable dimensions and FRP laminate configurations for the current deck application. To do this it was necessary to develop preliminary design properties which could be used in the finite element analysis modeling. Once the design had been developed, samples of the final laminates could then be produced and tested to validate predicted behavior.

This appendix outlines work done to develop design properties from the laminate configuration utilized in the earlier ice wall project. It also includes comparative testing performed on two alternative laminates of similar configuration produced by a different manufacturer.

TEST METHODS UTILIZED IN CHARACTERIZATION WORK

The test methods used in this characterization are outlined in table 2. These tests yield strength and modulus values in both primary directions (denoted as 0° for the primary fiber axis and 90° for the direction normal to that axis). Properties are determined in both tension and compression.

In-plane shear strength was also determined. The fiber content of each panel was also determined to allow proper comparison of the resulting properties from each laminate.

Table 2. Test methods used in characterization.

ASTM Test No.	Title	Properties Obtained	Symbol
D3039/3039M-08	Standard Test Method for Tensile Properties of Polymer Matrix Composites	Ultimate tensile strength (0°)	σ_{11T}
		Ultimate tensile strain (0°)	ϵ_{11T}
		Modulus of elasticity (chord) (0°)	E_{11T}
		Ultimate tensile strength (90°)	σ_{22T}
		Ultimate tensile strain (90°)	ϵ_{22T}
		Modulus of elasticity (chord) (90°)	E_{22T}
D6641/D6641M-09	Standard Test Method for Compressive Properties of Polymer Matrix Composite Materials Using a Combined Loading Compression (CLC) Test Fixture	Ultimate compression strength (0°)	σ_{11C}
		Ultimate compression strain (0°)	ϵ_{11C}
		Modulus of elasticity (chord) (0°)	E_{11C}
		Ultimate compression strength (90°)	σ_{22C}
		Ultimate compression strain (90°)	ϵ_{22C}
		Modulus of elasticity (chord) (90°)	E_{22C}
D7264/D7264M-07	Standard Test Method for Flexural Properties of Polymer Matrix Composite Materials	Ultimate flexural strength (0°)	σ_{11F}
		Ultimate flexural strain (0°)	ϵ_{11F}
		Flexure Modulus (chord) (0°)	E_{11F}
		Ultimate flexural strength (90°)	σ_{22F}
		Ultimate flexural strain (90°)	ϵ_{22F}
		Flexure Modulus (chord) (90°)	E_{22F}
D3171-09	Standard Test Method for Constituent Content of Composite Materials Test Method I, Procedure G: Matrix Burnoff in a Muffle Furnace	Fiber fraction - mass	m_f
		Fiber fraction - volume	v_f
D2344/D2344M-00	Standard Test Method for Short-Beam Shear Strength of Polymer Matrix Composite Materials and Their Laminates	Short Beam Shear Strength	

LAMINATES EVALUATED

The laminate produced by XC Associates was produced using Vectorply E-glass fabrics and Derakane 8084 vinyl ester resin. The fabric layup sequence was [E-QX2600 / E-LT5500 / E-

QX2600] with E-QX2600 being a 25.18 oz/yd² Quadraxial E-glass fabric and E-LT5500 being a 54.33 oz/yd² Biaxial E-glass fabric. The resulting ply sequence was:

0°	6.40 oz/yd ²
+45°	6.27 oz/yd ²
90°	6.24 oz/yd ²
-45°	6.27 oz/yd ²
0°	50.97
	oz/yd ²
90°	3.36 oz/yd ²
0°	6.40 oz/yd ²
+45°	6.27 oz/yd ²
90°	6.24 oz/yd ²
-45°	6.27 oz/yd ²

The Compmillenia panels were also produced using Vectorply E-glass fabrics, though different fabrics were selected due to materials held in-stock at Compmillenia. The fabric layup sequence in these panels was [E-LT3200 / E-LM1810 / E-BX2400 / E-LM1810 / E-LT3200], with E-LT3200 being a 31.36 oz/yd² biaxial fabric, E-LM1810 being a 27.06 oz/yd² uniaxial fabric with mat backing and E-BX2400 being a 23.90 oz/yd² double bias fabric with fibers oriented at +45°/-45°. The resulting ply sequence from this configuration was:

90°	13.44
	oz/yd ²
0°	17.92
	oz/yd ²
0°	17.92
	oz/yd ²
CSM	9.00
	oz/yd ²
+45°	11.95
	oz/yd ²
-45°	11.95
	oz/yd ²
0°	17.92
	oz/yd ²
CSM	9.00
	oz/yd ²
0°	17.92
	oz/yd ²
90°	13.44
	oz/yd ²

Compmillenia provided two sample laminates with the alternative layup. One was produced using a standard vinylester (CoRezyn VE8121) and the other with an alternative fire retardant vinylester resin (CoRezyn VE8441). While the ply sequence of these panels are different from

each other, the total weight of directional reinforcement in each panel is relatively close, as shown below in table 3.

Table 3. Comparison of fiber architectures.

Direction	Ice Shield (oz/yd ²)	Compmillenia (oz/yd ²)
0°	63.8	71.7
90°	15.8	26.9
+/- 45°	25.1	23.9
CSM	0	18.0
Theoretical Thickness	0.106 in.	0.15 in.

TEST RESULTS

Table 4 summarizes the results obtained through physical testing.

Table 4. Comparison of laminate properties.

Property	Symbol	XCA Ice Wall		Compmillenia VE-8121		Compmillenia VE-8441		
		Mean	Std. Dev.	Mean	Std. Dev.	Mean	Std. Dev.	
Modulus	Tension	E_{T0}	4.36 MSI	0.15 MSI	2.48 MSI	0.20 MSI	2.56 MSI	0.18 MSI
		E_{T90}	2.02 MSI	0.25 MSI	1.86 MSI	0.26 MSI	1.99 MSI	0.44 MSI
	Compression	E_{C0}	2.89 MSI	0.42 MSI	2.36 MSI	0.35 MSI	2.37 MSI	0.24 MSI
		E_{C90}	2.18 MSI	0.48 MSI	1.84 MSI	0.13 MSI	1.93 MSI	0.13 MSI
	Flexure	E_{F0}	1.83 MSI	0.09 MSI	2.05 MSI	0.08 MSI	1.91 MSI	0.07 MSI
		E_{F90}	1.77 MSI	0.08 MSI	2.38 MSI	0.07 MSI	2.51 MSI	0.07 MSI
Ultimate Strength	Tension	σ_{T0}	84.51 KSI	1.70 KSI	49.80 KSI	2.05 KSI	47.31 KSI	3.42 KSI
		σ_{T90}	28.57 KSI	2.05 KSI	29.75 KSI	1.81 KSI	28.40 KSI	0.44 KSI
	Compression	σ_{C0}	60.08 KSI	3.35 KSI	54.41 KSI	4.03 KSI	45.58 KSI	5.07 KSI
		σ_{C90}	30.09 KSI	1.34 KSI	32.32 KSI	2.07 KSI	27.22 KSI	2.20 KSI
	Flexure	σ_{F0}	37.78 KSI	1.81 KSI	66.08 KSI	4.06 KSI	56.63 KSI	3.60 KSI
		σ_{F90}	47.40 KSI	1.72 KSI	64.56 KSI	4.30 KSI	61.54 KSI	3.40 KSI
Strain at Max. Stress	Tension	ϵ_{T0}	2.30 %	0.13 %	2.44 %	0.14 %	2.37 %	0.20 %
		ϵ_{T90}	2.40 %	0.12 %	2.13 %	0.11 %	2.23 %	0.21 %
	Compression	ϵ_{C0}	2.62 %	0.38 %	2.43 %	0.54 %	2.14 %	0.27 %
		ϵ_{C90}	2.38 %	0.95 %	2.07 %	0.40 %	1.44 %	0.13 %
	Flexure	ϵ_{F0}	3.52 %	0.25 %	4.23 %	0.11 %	3.84 %	0.22 %
		ϵ_{F90}	3.58 %	0.22 %	3.06 %	0.14 %	2.77 %	0.16 %
In Plane Shear Strength	τ_{12}	13.30 KSI	0.41 KSI	14.02 KSI	0.59 KSI	13.98 KSI	0.60 KSI	
	τ_{21}	15.41 KSI	1.51 KSI	13.59 KSI	0.46 KSI	13.69 KSI	0.82 KSI	
Short Beam Strength		5.81 KSI	0.28 KSI	4.98 KSI	0.26 KSI	5.16 KSI	0.26 KSI	
Fiber Content (%)	mass	m_f	70 %		54 %		52 %	
	volume	v_f	48 %		31 %		30 %	
Thickness		t	0.113 in	0.0012 in	0.218 in	0.004 in	0.222 in	0.003 in

OBSERVATIONS ON PHYSICAL TESTING

From the test data it was observed that the two Compmillenia panels were very similar in terms of mechanical properties. There was only a minimal difference in the fiber volume fraction achieved in each panel; thus, the mechanical performance is very similar. The variation in ultimate strength values reflects the slight difference seen in corresponding strain values. The laminates display a highly linear elastic behavior up to failure, and the strength differences simply relate to the different amount of physical elongation seen prior to failure. Given the level of within-sample scatter seen in each sample sets it would seem reasonable to conclude that the different resin used in these panels makes a minimal difference to the mechanical performance.

BEHAVIOR IN THE PRINCIPAL FIBER DIRECTION (0°)

Under tension, the XC Associates panel displays considerably higher properties in the dominant fiber direction (0°). This is indicative of the fact that this panel possesses a significantly higher proportion of its total panel thickness with fibers in that direction. As can be seen from figure 9, in the Compmillenia panel approximately 16 percent of the total thickness of the laminate is occupied by fiber that runs in the 0° direction, compared with 29 percent in the XC Associates ice wall laminate (184 percent difference). It would thus be reasonable to expect that the 0° properties of the XC Associates ice wall panel would be a little under double those of the Compmillenia panels. This is seen in the test data. E_{T0} for the ice wall is 170-175 percent of the Compmillenia panels, and σ_{T0} for the ice wall is 170 percent of the Compmillenia panel. Statistical analysis indicates that data from the two Compmillenia panels are from a common statistical population, which would be expected based on the identical architecture.

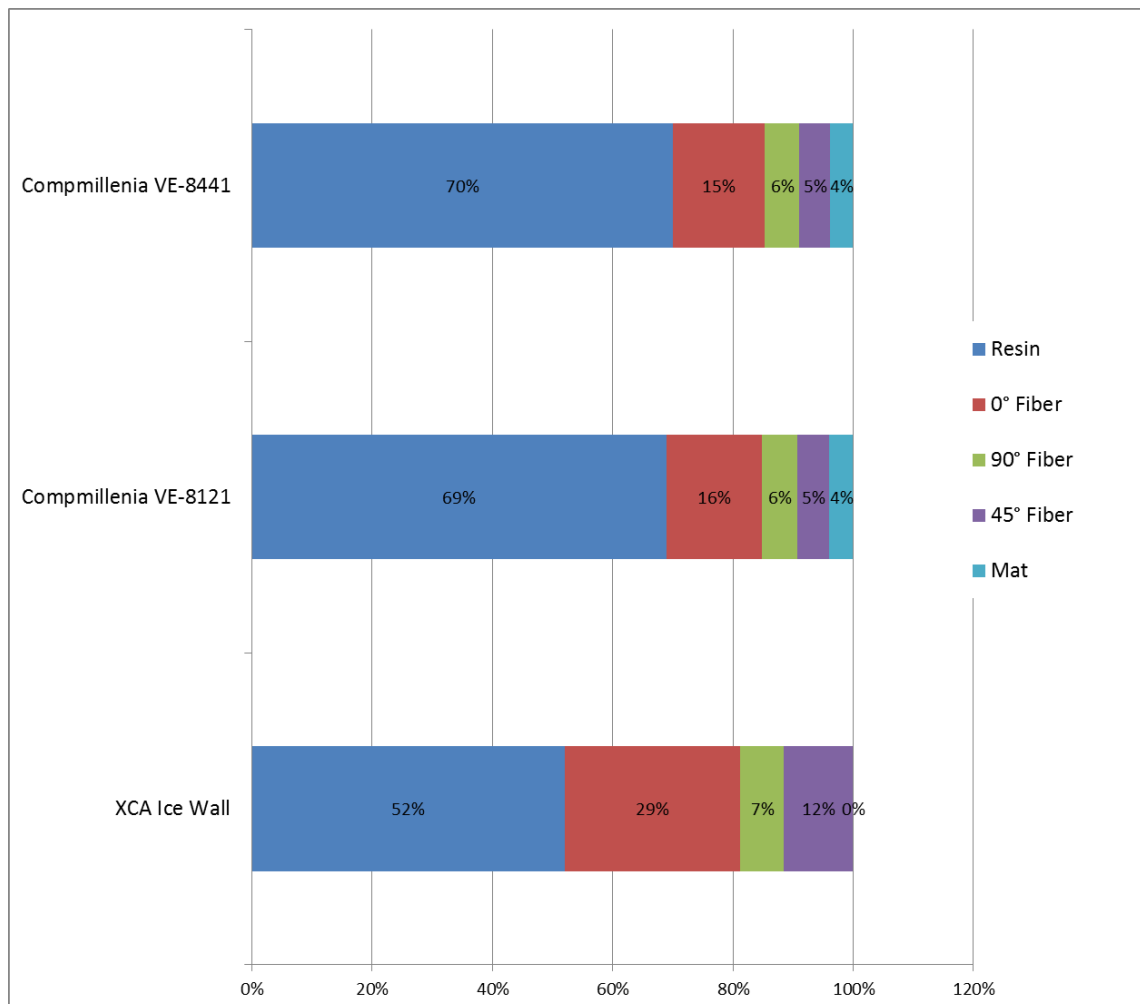


Figure 9. Graph. Constituent content of test laminates as a percentage of total laminate thickness.

From the strain data it can be observed that all of the specimens fail at approximately the same strain. Previous in-house testing has indicated tension capacity in the fiber direction is dominated by the fiber and that the average failure strain of unidirectional glass fiber laminates is around

2.4 percent (standard deviation of 0.56 percent) irrespective of the amount of reinforcement or the resin type. Observation of the average strain limits of the three laminates tested here indicates they all fail close to this level. Statistical analysis of the data indicates that the three strain data sets are part of the same statistical population. It is therefore reasonable to conclude that it is the fiber oriented along the load direction which is controlling the failure of these laminates under tension. When the fibers in the load direction reach their strain limit, rupture occurs and results in catastrophic failure of the laminate.

For compression properties in the principal fiber direction, it can be seen that the resin begins to play a more significant role in the mechanical properties obtained. In terms of ultimate capacity, the strain at break results of the three samples are found to be from the same statistical population, with a population mean of 2.41 percent. This again indicates that the fiber oriented in the load direction is primarily responsible for determining the laminate failure.

However, unlike the behavior under tension, when the laminates are tested in compression parallel to the principal fiber direction, there is not a direct correlation between the fiber content and the resulting modulus (E_{C0}). In this instance, the difference between the ice wall laminate modulus and the modulus for the Compmillenia panels is only around 22 percent, not the expected 70 to 80 percent. This would indicate that the other laminate constituents play a more significant role under compression. Similar results are seen with the strength data (σ_{C0}), where the ice wall panel only displays 10 percent (VE-8121) and 32 percent (VE-8441) strength improvements over the Compmillenia panels.

BEHAVIOR IN THE OFF-AXIS FIBER DIRECTION (90°)

In the 90° direction it can be seen that the proportion of the laminate thickness aligned with the load (90° fibers aligned with 90° axial load) is relatively close for all the panels (7.24 percent vs. 5.94 percent and 5.74 percent). It would therefore be anticipated that for fiber dominated properties the observed values in the 90° direction would be relatively close to each other. This is consistent with the observed data.

When normalized against the amount of fiber in the 90° direction as a proportion of laminate thickness, both the tension and compression modulus (E_{90T} , E_{90C}) are statistically from the same populations, indicating the dominant role of the fiber in the compression response of the laminates.

In terms of strength and strain data on ultimate capacity, the values obtained in testing are relatively close. However, deeper analysis of the data indicates statistically significant variations which cannot be fully explained by the proportion of load bearing fiber. Strain data in tension indicate that the Compmillenia panels are statistically from the same population, but there is significant variation between these values and those of the ice wall panel (average 2.14 percent vs. 2.44 percent). The reason for this variation is unknown and would require further testing to verify. It is thought that some of the variation may be due to the overall architecture of the laminates. With the Compmillenia panels all of the 90° fiber is located on one side of the laminate, while in the ice wall panel the 90° fiber is more evenly distributed throughout the thickness of the panel. It may be that having adjacent plies in other directions helps to preserve

the integrity of the fibers to higher strain levels by better distributing load through the laminate thickness.

Under compression loads the data display significantly greater variation in terms of ultimate capacity. Statistical analysis of the compression strain data indicates statistically significant differences between all three sets of data. The average compression failure strains for the ice wall, VE-8121, and VE-8441 panels are 2.38 percent, 2.07 percent, and 1.44 percent, respectively. Statistically, the ice wall and VE-8121 data are from the same population, but the data for the VE-8441 panel are significantly lower. An examination of the failed specimens does not provide any obvious reason for the discrepancy in failure strains. Failure in inherently compression is more variable than corresponding tensile failure due to the increased number of possible failure mechanisms. Buckling can occur on both a macroscopic specimen level and a microscopic fiber level, with the latter being particularly difficult to identify. Examination of the stress-strain curves for the VE-8441 sample does not indicate any obvious buckling in the specimens. Additionally, all of the failures were properly within the gage length, so there was no obvious premature failure due to the grips. At this point it is possible to identify the difference between the samples, but it is not possible to further explain these variations.

SHEAR BEHAVIOR

In addition to axial tension and compression, shear strength was evaluated both in-plane and through the thickness between the individual laminate plies. In-plane shear testing was conducted using a V-notch shear test. Two different orientations were tested, as shown in figure 10.

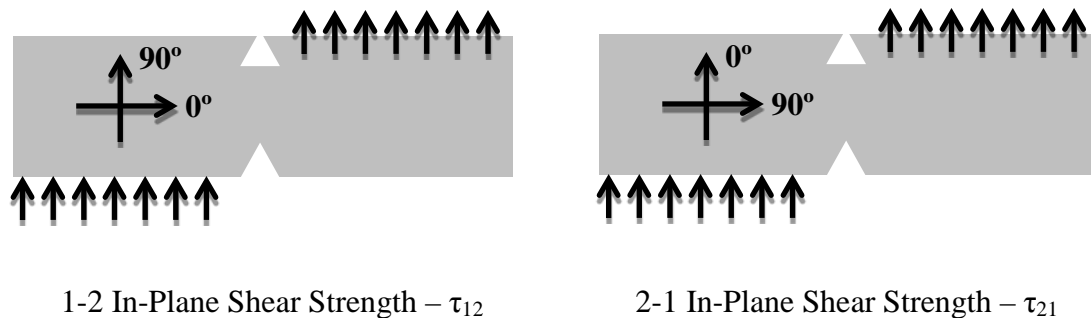


Figure 10. Diagram. Fiber directions for in-plane shear strength testing.

The V-notch shear test induces principal tension and compression stresses at $+45^\circ$ and -45° . On the basis of the previous discussions it would therefore seem reasonable to expect the in-plane strength of the laminates to be significantly influenced by the fiber oriented at $\pm 45^\circ$.

Statistical analysis of the data from the two Compmillenia panels indicate they are from a single population, indicating that the behavior is fiber dominated. There is also no statistically significant difference between the τ_{12} data and the τ_{21} data. If the resin or the fiber oriented off the $\pm 45^\circ$ axis were playing a significant role in determining the in-plane shear strength, it would be expected that statistically significant differences would be evident in the four data sets. The

absence of such differences would indicate that the fiber in the $\pm 45^\circ$ directions does control the shear capacity.

As would be expected from the significant difference between their $\pm 45^\circ$ fiber percentages, there is a statistically significant difference between the shear strengths of the ice wall and Compmillenia panels. However, while the ice wall panel displays an increase in in-plane shear capacity, there is not a direct correlation with the amount of $\pm 45^\circ$ fiber present. The ice wall panel has an average shear strength of 12.4 ksi while the Compmillenia panels have an average of 11.3 ksi. This is a strength increase of only around 10 percent for the ice wall panel despite it having 12 percent of its thickness as $\pm 45^\circ$ versus only 5 percent for the Compmillenia panels. All three panels have a similar load versus deflection behavior trend.

Interlaminar shear capacity was evaluated using a short beam shear test. This test uses a relatively short span under flexural loading to induce shear failure of the specimen between the individual plies, typically at the neutral axis. The interlaminar strength is generally considered to be a resin dominated property; however, the orientation of plies on either side of the failure plane will also play a role in the capacity obtained. The Compmillenia panels display relatively uniform results and were found to be statistically from the same population. Given the identical fiber architecture and similarities in the resin properties, this result would be consistent with expectations. The results for the ice wall panel are higher than the ones for the Compmillenia panels. It is thought that this is attributable to the differences in fiber architecture and resin properties, although no direct correlation can be established at this time.

COMPARISON OF PANEL RESULTS

Some of the discrepancies between the ice wall panel and the two Compmillenia panels are due to the slightly different fiber architecture used by the two manufacturers. In a commercial context where manufacturers were relying on existing reinforcement stocks to produce the panels, the selection of the different reinforcements was entirely reasonable. Most manufacturers seem to work with a selection of preferred reinforcement products and then adapt designs around those products. The challenge for design engineers is how to accommodate those differences and to provide a valid comparison between two different options.

As can be seen from the test data, many of the properties in question tend to be fiber dominated due to the reinforcement architecture selected. Once properties are correlated against the actual amount of reinforcement used, what initially appear to be differences in panel quality can be identified as the simple result of varied reinforcement quantities. This is similar to reinforced concrete. Two finished beams may look similar from the outside and may have both been manufactured to high quality. However, if their internal reinforcement is different, one will provide significantly higher capacity than the other. The result is not the result of a quality flaw but rather stems from what would be an intentional design decision. The same is true for composites.

Beyond fiber architecture, the other principle reason for the difference in panel performance is the resin content of the panels. This is purely the result of manufacturing methodology. The ice wall panel was produced using a VARTM (vacuum infusion) process which infuses the resin into

the fiber under vacuum, while the Compmillenia panels were produced by wet layup followed by a vacuum consolidation. The resin content differences that result from these processes are inherent to the processes themselves.

Both processes place the laminate under a plastic film to create an envelope which is then evacuated to create a pressure differential between the inside of the envelope and ambient atmospheric conditions. This pressure differential is used to consolidate the laminate with the aim of achieving a higher proportion of fiber in the final product. However the mechanism for achieving that consolidation is different with each method. VARTM first consolidates the dry reinforcement and then allows a limited amount of resin into the pre-consolidated fiber. For a vacuum bagged wet layup the reinforcement is initially wet out with resin under ambient conditions. Once the reinforcement and resin have been successfully combined (typically with a resin excess), the wet laminate is placed under the vacuum film and the pressure differential is induced to essentially squeeze out excess resin. While both processes use the same consolidation pressure, the VARTM process typically produces higher fiber percentages. This is because it is far easier to compact the dry fiber layers in VARTM than it is to displace a relatively viscous liquid from within the fibers to compact the wet layup. The result would be that, for a given fiber architecture and resin, a VARTM produced product would be slightly thinner than a vacuum bagged wet layup one. However, it is important to remember that the actual amount of reinforcement would not change—all that would happen is that one panel would possess less resin than the other.

For properties which are fiber dominated, the actual structural capacity of the two laminates would not be changed because the amount of reinforcement would be the same. However, the resulting properties, which are generally characterized in terms of force per unit area, would appear higher for the VARTM laminate due to the reduced thickness. It is essential to remember that thickness is essentially a manufacturing variable, not an inherent characteristic of the material.

Therefore, when comparing the ice wall panel and the two Compmillenia panels, it is necessary to separate manufacturing effects from the potential viability of the laminates. In producing the sample panel, Compmillenia indicated that a VARTM process could be used in the production of bridge components but that their standard production method was vacuum bagged wet layup. From the data obtained it would be reasonable to anticipate that if Compmillenia switched to a VARTM process the resulting laminate properties would be correspondingly higher.

CONCLUSION

From the test results it can be concluded that all three test panels provide mechanical performance consistent with the fiber architecture and the manufacturing method used. Both manufacturers produced panels that exhibited sufficient quality to be utilized in an actual bridge deck fabrication.

Assuming that a laminate specification is developed that reflects the original ice wall laminate construction and that it specifies the use of a VARTM process, the properties in table 5 could be specified for design calculations.

Table 5. Suggested design values.

Property	Symbol	Mean	B-Basis Value
Modulus	Tension	E_{T0}	4366 KSI
		E_{T90}	1988 KSI
	Compression	E_{C0}	2889 KSI
		E_{C90}	2180 KSI
Ultimate Strength	Tension	σ_{T0}	84.56 KSI
		σ_{T90}	29.15 KSI
	Compression	σ_{C0}	60.05 KSI
		σ_{C90}	30.17 KSI
Strain at Max. Stress	Tension	ϵ_{T0}	2.30 %
		ϵ_{T90}	2.44 %
	Compression	ϵ_{C0}	2.62 %
		ϵ_{C90}	2.05 %
In Plane Shear Strength	τ	12.34 KSI	10.15 KSI
Short Beam Strength		5.80 KSI	5.16 KSI
Fiber Content (%)	mass	m_f	70 %
	volume	v_f	48 %
Thickness		t	0.113 in

Given the statistical nature of material failure, it is customary to use statistically based capacity values for engineering design. In this instance, B-basis values are given for the ultimate strength and strain capacity properties. The B-basis value is a 95 percent lower confidence bound on the tenth percentile of a specified population of measurements. Composite Materials Handbook 17 (formerly MIL-HDBK-17) adopts A-basis and B-basis values for characteristic properties of composite materials in engineering design. For the current project, A-basis values (95 percent confidence on the first percentile) are seen as overly conservative, particularly given that validation testing will be conducted at all stages of the design and development process. B-basis values are therefore recommended for capacity characterization.

APPENDIX B: DETERMINATION OF LAMINA DESIGN PROPERTIES

OVERVIEW

The detailed analysis of FRP structures and sub-components is a typically a complex undertaking requiring the use of advance finite element analysis techniques. Due to their inherent brittleness and the directional nature of composite laminates, simplified analysis methods developed for isotropic materials such as steel often do not provide sufficient detail to ensure adequate structural performance with FRP composites. To utilize these methods it is necessary to develop good representative material properties which may be input into finite element models.

Physically, FRP laminates are constructed from a series of ply layers which after curing perform as a single unified layer. In instances where the laminate ply sequence is predetermined, it is possible to construct and test a laminate of the specified construction and to then input those properties into a finite element model. However, in most instances the designer does not know the ply sequence beforehand and will use an iterative process which moves between various ply sequences and structural forms to find an optimal combination of both.

Thankfully, modern finite element analysis packages typically possess laminated plate elements which allow the designer/analyst to specify various reinforcements and orientations. The individual layer properties can be entered and are ultimately combined in the model using classical laminate theory. The basic building block of this approach is the individual unidirectional ply or lamina. Thus, properly defining the properties of a unidirectional lamina is the key to developing viable structural models.

FRP materials are orthotropic in nature, which means the characterization of their mechanical behavior is more complex than for isotropic materials such as steel. The full set of material properties required to define the unidirectional lamina is given in table 6.

For commercial manufacturing purposes it is often convenient to produce a specified ply sequence using a multi-axial fabric. These fabrics combine dry reinforcement for two, three, or four laminae in a single fabric where the separate layers are stitched together with a non-load-bearing thread. Analytically, these fabrics are simply multiple unidirectional lamina placed on top of each other in different orientations, so it is technically not necessary to separately characterize these fabrics if unidirectional lamina properties have already been established. However, some designers prefer to characterize these fabrics in addition to the unidirectional lamina.

In addition to directional layers, it is relatively common for laminates to include layers of randomly oriented short fibers. In dry form these are layers are known as chopped strand mat (CSM) and consist of randomly oriented fibers of approximately 2 inches held together in fabric form by a compatible binder. These layers are essentially isotropic and must be characterized separately from the unidirectional lamina.

This appendix outlines the results of testing undertaken to characterize a unidirectional lamina and a CSM lamina of E-glass and vinyl ester. Additional testing was undertaken on a biaxial lamina (two plies at 0° and 90°) and a double bias lamina (two plies at +45° and -45°).

Table 6. Material properties for the definition of a unidirectional lamina.

Property	Direction	Symbol
Modulus of Elasticity	0	E_1
	90	E_2
In-plane Shear Modulus	0-90	G_{12}
	90-0	G_{21}
Tensile Strength	0	σ_{1T}
	90	σ_{2T}
Compression Strength	0	σ_{1C}
	90	σ_{2C}
Ultimate Tensile Strain	0	ϵ_{1T}
	90	ϵ_{2T}
Ultimate Compression Strain	0	ϵ_{1C}
	90	ϵ_{2C}
In-plane Shear Strength	0-90	τ_{12}
	90-0	τ_{21}
In-plane Poisson Coefficient	0-90	ν_{12}
	90-0	ν_{21}
Lamina Thickness	not applicable	t

TEST METHODS UTILIZED IN CHARACTERIZATION WORK

The test methods used in this characterization are outlined in table 7. These tests yield strength and modulus values in both primary directions (denoted as 0° for the primary fiber axis and 90° for the direction normal to that axis). Properties are determined in both tension and compression. In-plane shear strength was also determined. The fiber content of each panel was also determined to allow proper comparison of the resulting properties from each laminate.

Table 7. Test methods used in characterization.

ASTM Test No.	Title	Properties Obtained	Symbol
D3039/3039M-08	Standard Test Method for Tensile Properties of Polymer Matrix Composites	Ultimate tensile strength (0°)	σ_{1T}
		Ultimate tensile strain (0°)	ϵ_{1T}
		Modulus of elasticity (chord) (0°)	E_{1T}
		Ultimate tensile strength (90°)	σ_{2T}
		Ultimate tensile strain (90°)	ϵ_{2T}
		Modulus of elasticity (chord) (90°)	E_{2T}
D6641/D6641M-09	Standard Test Method for Compressive Properties of Polymer Matrix Composite Materials Using a Combined Loading Compression (CLC) Test Fixture	Ultimate compression strength (0°)	σ_{1C}
		Ultimate compression strain (0°)	ϵ_{1C}
		Modulus of elasticity (chord) (0°)	E_{1C}
		Ultimate compression strength (90°)	σ_{2C}
		Ultimate compression strain (90°)	ϵ_{2C}
		Modulus of elasticity (chord) (90°)	E_{2C}
D5379/D5379M-05	Standard Test Method for Shear Properties of Composite Materials by the V-Notched Beam Method	In-plane shear strength (0-90)	τ_{12}
		In-plane shear strength (90-0)	τ_{21}
D3171-09	Standard Test Method for Constituent Content of Composite Materials Test Method I, Procedure G: Matrix Burnoff in a Muffle Furnace	Fiber fraction - mass	m_f
		Fiber fraction - volume	v_f
D2344/D2344M-00	Standard Test Method for Short-Beam Shear Strength of Polymer Matrix Composite Materials and Their Laminates	Short Beam Shear Strength	

LAMINATES EVALUATED

Four laminates were fabricated for this testing. The test panels are outlined in table 8.

Table 8. Test laminates for characterization of lamina properties.

Panel ID	Reinforcement Fabric	Reinforcement Description	Ply Sequence
LSC-11-LAM-010	E-LA1312	13.42 oz/yd ² stitched unidirectional	[0]4
LSC-11-LAM-011	E-BX1200	12.54 oz/yd ² stitched +45/-45 double bias	[+45/-45]4
LSC-11-LAM-012	E-LT1800	17.92 oz/yd ² stitched 0/90 biaxial	[0/90]3
LSC-11-LAM-013	E-M0010	9.0 oz/yd ² stitched CSM	[CSM]5

TEST RESULTS

Table 9 summarizes the results obtained through physical testing.

Table 9. Summary of physical test data for laminate samples.

Property		Unidirectional Laminate		Double Bias Laminate		Biaxial Laminate		Random Fiber (CSM) Laminate		
		Mean	Std. Dev.	Mean	Std. Dev.	Mean	Std. Dev.			
Modulus	Tension	E_{T0}	2365 KSI	171 KSI	626 KSI	51 KSI	1742 KSI	159 KSI	1094 KSI	99 KSI
		E_{T90}	728 KSI	23 KSI	850 KSI	76 KSI	1957 KSI	195 KSI	974 KSI	122 KSI
	Compression	E_{C0}	2184 KSI	329 KSI	633 KSI	90 KSI	1979 KSI	194 KSI	975 KSI	98 KSI
		E_{C90}	824 KSI	125 KSI	1009 KSI	133 KSI	2019 KSI	233 KSI	1131 KSI	130 KSI
Ultimate Strength	Tension	σ_{T0}	55.85 KSI	3.15 KSI	7.28 KSI	0.27 KSI	32.99 KSI	2.40 KSI	16.60 KSI	1.31 KSI
		σ_{T90}	3.96 KSI	0.27 KSI	15.65 KSI	0.49 KSI	31.82 KSI	4.04 KSI	15.01 KSI	1.48 KSI
	Compression	σ_{C0}	48.32 KSI	1.71 KSI	10.70 KSI	0.66 KSI	39.68 KSI	3.49 KSI	20.51 KSI	0.61 KSI
		σ_{C90}	11.45 KSI	1.40 KSI	12.41 KSI	0.32 KSI	37.22 KSI	1.35 KSI	21.97 KSI	1.46 KSI
Strain at Max. Stress	Tension	ϵ_{T0}	2.46 %	0.14 %	17.73 %	4.97 %	2.13 %	0.16 %	2.01 %	0.28 %
		ϵ_{T90}	0.62 %	0.06 %	10.01 %	1.16 %	2.06 %	0.27 %	1.91 %	0.35 %
	Compression	ϵ_{C0}	3.56 %	1.13 %	3.84 %	0.92 %	2.69 %	0.42 %	3.01 %	0.65 %
		ϵ_{C90}	2.23 %	0.61 %	2.34 %	0.33 %	3.72 %	1.72 %	3.16 %	0.67 %
In Plane Shear Strength	τ_{12}	6.39 KSI	0.25 KSI	10.76 KSI	0.30 KSI	6.08 KSI	0.37 KSI	11.34 KSI	0.00 KSI	
	τ_{21}	4.45 KSI	0.61 KSI	11.21 KSI	0.38 KSI	6.41 KSI	0.26 KSI	- KSI	0.75 KSI	
Short Beam Strength		40.00 KSI	1.83 KSI	17.80 KSI	0.75 KSI	33.00 KSI	2.51 KSI	21.70 KSI	4.74 KSI	
Fiber Content (%)	mass	m_f	40 %		36 %		47 %		35 %	
	volume	v_f	21 %		18 %		26 %		18 %	
Thickness		t	0.126 in		0.148 in		0.116 in		0.135 in	

DISCUSSION OF RESULTS

Unidirectional Lamina Behavior

From the unidirectional lamina results, it can be seen that the properties in the principal fiber direction (0°) are significantly higher than the corresponding properties at 90° to the fiber axis.

As the modulus of elasticity is taken early in the stress/strain response, it would be reasonable to expect the results for tension and compression modulus to be relatively close to each other. This is seen in the test data. Statistical analysis indicates that both the tension and the compression data are from the same statistical population. This is found both parallel and perpendicular to the fibers. This allows for the determination of a single modulus of elasticity for the material under both tension and compression loading. Using the pooled data, the mean modulus of elasticity for the laminate parallel to the fibers (E_1) is 2.34 MSI (standard deviation 0.329 MSI). The pooled modulus of elasticity perpendicular to the fibers (E_2) was found to be 0.77 MSI (standard deviation 0.097 MSI). It is worth noting that while a single statistical value can be established in each direction, there is significantly higher scatter seen in the compression data compared with the tension data.

Failure data for tension and compression do not display the same sort of commonality. This is to be expected due to the different failure mechanisms which drive behavior under tension and compression loading. The data obtained in this testing is seen to be consistent with testing of unidirectional laminae previously undertaken by the author.

Random Fiber Lamina Behavior

As mentioned earlier, the random fiber lamina is expected to be essentially isotropic, and there should be no statistically significant difference in the data obtained at 0° and 90° . Analysis of the modulus of elasticity results indicates that all four data sets (tension and compression at 0° and 90°) are statistically from the same population. This yields a mean modulus of elasticity for the lamina of 1.07 MSI (standard deviation 0.118 MSI).

In relation to capacity, 0° and 90° tensile strengths are found to be from the same population with a mean strength of 15.9 KSI (standard deviation 1.55 KSI). Tensile strain limits are also of the same population, giving an overall mean of 1.96 percent (standard deviation 0.303 percent). Compression strength and strain are similarly seen to be of the same statistical populations, with mean values of 21.18 KSI (std. dev. 1.31 KSI) and 3.08 percent (standard deviation 0.63 percent), respectively.

Based on these findings, shear response was only evaluated in the 0° direction. The mean shear strength was found to be 11.34 KSI with a standard deviation of 0.75 KSI.

Biaxial Lamina Behavior

As mentioned previously, a biaxial fabric is really just two unidirectional layers stitched together at 90° to each other. According to manufacturer data from Vectorply, each layer has an equal amount of unidirectional reinforcement: 8.96 oz/yd². It would therefore be expected that the lamina properties would be equal at both 0 and 90° .

Analysis of the modulus of elasticity values obtained at both 0° and 90° under tension and compression indicated that all the values obtained belong to a common statistical population. It was found that the combined data set had a mean modulus of 1.94 MSI (std. dev. 0.219 MSI).

Analysis of the strength data indicates that statistically significant differences exist between the tension and compression behavior, but within each load type the results at 0° and 90° are of the same population. The mean tension strength (σ_T) was found to be 32.3 KSI (standard deviation 3.25 KSI), and the compression strength (σ_C) was found to be 38.0 KSI (standard deviation 3.02 KSI). Similar results were found in strain capacity, with the mean tensile found to be 2.09 percent (standard deviation 0.219 percent) and the mean compression strain found to be 2.61 percent (standard deviation 0.467 percent).

Double Bias Lamina Behavior

The double bias fabric used in this test series consisted of two unidirectional layers of 6.27 oz/yd² each stitched together at +45° and -45° relative to the principle axis (0°), which is defined as the direction off the fabric roll. The layers are stitched together with a cotton thread running in the 0° direction (see figure 11). As there is an equal amount of reinforcement at each bias angle, it would be expected that properties at 0° and 90° would show to be from a common statistical population. This thought is supported by manufacturer data, which shows equal values for modulus of elasticity and strength in both directions. However, this type of behavior is not supported by the test data. Examination of the modulus and strength data shows significant difference at both 0° and 90° for tension and compression loadings.

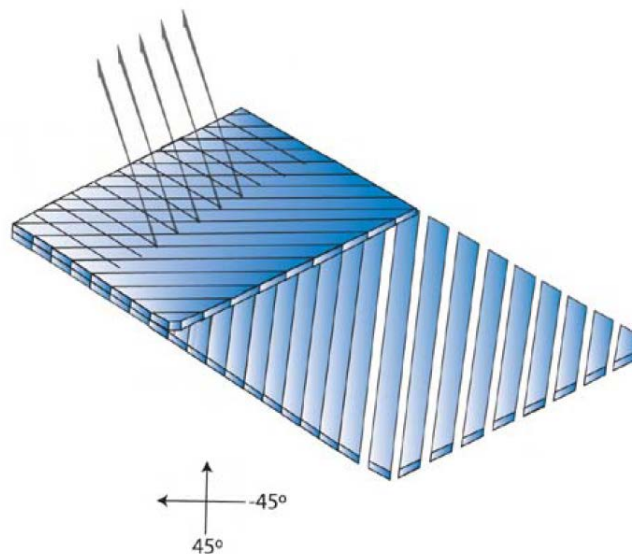


Figure 11. Diagram. Structure of double bias laminate.

It is believed that the reason for the differences observed in the test data stems from the cotton thread used to hold the glass reinforcement fibers in position. Upon further examination it was found that significantly higher stiffness and strength were exhibited when the test direction was parallel to the direction of cotton stitching. Visual examination of the dry reinforcement supported this conclusion, with the fabric demonstrating far more distortion under loading perpendicular to the cotton than with loading parallel to the cotton threads.

The question in characterizing this lamina thus becomes which set of properties should be used when designing with double bias fabrics. It is worth noting that these fabrics are generally used to assist in carrying shear loadings in structures which reduce to principal tensile and compressive stresses parallel to the bias fiber direction. It is also worth noting that the fabrics are often laid down during fabrication without consideration of the cotton stitching. It is therefore thought that the best approach would be to neglect the effect of the cotton and use a conservative approach which characterizes the material based on the properties normal to the cotton direction. In this instance, this translates to the 90° direction.

Analysis of the tension and compression modulus of elasticity data at 90° indicates that the data are from a common statistical population. This translates to a combined modulus of elasticity of 0.935 MSI (standard deviation 0.134 MSI) for the material.

In-plane shear behavior was found to not be affected by the cotton stitching, and statistical analysis of the data in the 1-2 and 2-1 directions showed both sets of results to be from the same statistical population. The in-plane shear strength for the double bias lamina was found to be 10.96 KSI (standard deviation 0.397 KSI).

CONCLUSION

Based on the outcomes of this testing, the values given in table 10 are suggested as design properties for the various lamina forms. The values were obtained using hand lamination and are not normalized for fiber content. This should be accounted for in design calculations and analysis.

Additional care should be taken with using the capacity values. The values given are mean values, and appropriate statistical adjustment should be made using the associated standard deviations to ensure a sufficient margin of safety is created in design work.

Table 10. Suggested lamina design values for ply based design and analysis.

Property		Unidirectional Lamina		Double Bias Lamina		Biaxial Lamina		Random Fiber (CSM) Lamina		
		Mean	Std. Dev.	Mean	Std. Dev.	Mean	Std. Dev.	Mean	Std. Dev.	
Modulus	E0	2340 KSI	329 KSI	935 KSI	134 KSI	1940 KSI	219 KSI	1070 KSI	118 KSI	
	E90	770 KSI	97 KSI							
Ultimate Strength	Tension	σ_{T0}	55.85 KSI	3.15 KSI	15.65 KSI	0.49 KSI	32.30 KSI	3.25 KSI	15.90 KSI	1.55 KSI
		σ_{T90}	3.96 KSI	0.27 KSI						
	Compression	σ_{C0}	48.32 KSI	1.71 KSI	12.41 KSI	0.32 KSI	38.00 KSI	3.02 KSI	21.18 KSI	1.31 KSI
		σ_{C90}	11.45 KSI	1.40 KSI						
Strain at Max. Stress	Tension	ϵ_{T0}	2.46 %	0.14 %	10.01 %	1.16 %	2.09 %	0.219 %	1.96 %	0.303 %
		ϵ_{T90}	0.62 %	0.06 %						
	Compression	ϵ_{C0}	3.56 %	1.13 %	2.34 %	0.33 %	2.61 %	0.467 %	3.08 %	0.63 %
		ϵ_{C90}	2.23 %	0.61 %						
In Plane Shear Strength	τ_{12}	6.39 KSI	0.25 KSI	10.96 KSI	0.40 KSI	6.25 KSI	0.35 KSI	11.34 KSI	0.75 KSI	
	τ_{21}	4.45 KSI	0.61 KSI							
Short Beam Strength		40.00 KSI	1.83 KSI	33.00 KSI	2.51 KSI	33.00 KSI	2.51 KSI	21.70 KSI	4.74 KSI	
Fiber Content (%)	mass	mf	40 %		36 %		47 %		35 %	
	volume	vf	21 %		18 %		26 %		18 %	
Thickness	t	0.126 in		0.148 in		0.116 in		0.135 in		

APPENDIX C: EVALUATION OF “AS-TESTED” PROPERTIES OF FRP LAMINATES

OVERVIEW

Based on earlier testing work, the researchers designed a trapezoidal profile for use in the bridge deck for this project. This profile would be produced using the pultrusion process.

The pultruded combination (combi) tube was a three-cavity trapezoid, as shown in figure 12. The part uses a fire-resistant vinyl ester resin. The reinforcement is E-glass rovings, woven mat, and CSM.

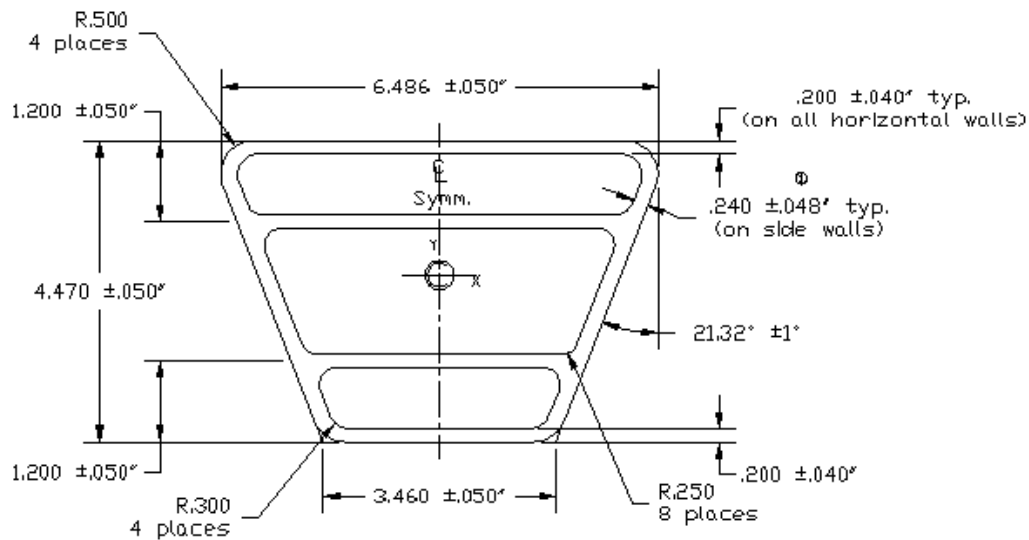


Figure 12. Diagram. Pultruded combination tube.

Figure 13 shows the laminate construction specified for the profile. The original trapezoid concept involved a constant 0.2-inch wall in all areas; however, it did not appear that adequate properties could be obtained with this concept. The final concept used a laminate of 0.2-inch horizontal walls and 0.24-inch walls for the inclined sides.

TRAPEZOIDAL BRIDGE DECK CONSTRUCTION
DIE #6444-1G, PART # CP235
DATE REVISED: 8-3-11 TEW

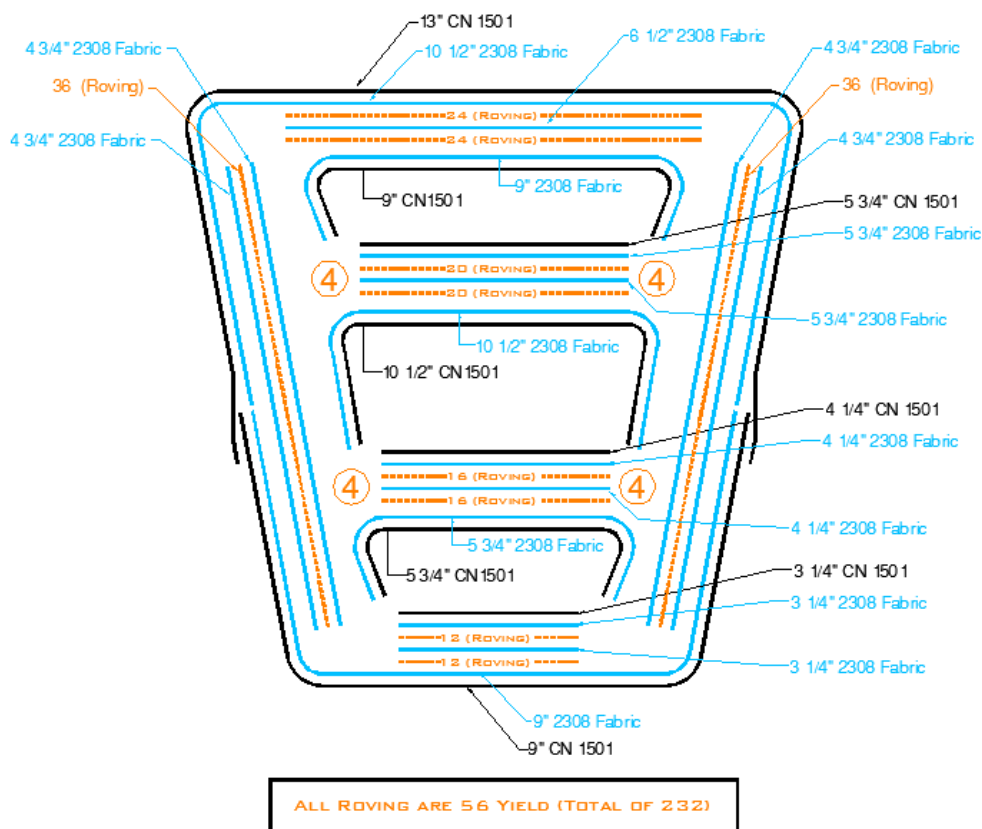


Figure 13. Diagram. Laminate construction for pultruded combination tube.

Predicted properties for this profile construction are given in table 11.

Table 11. Predicted properties of pultruded tube.

Property	Unit	Horizontal Walls	Vertical Walls
Thickness	in	0.2	0.24
Fiber Volume Fraction	%	n/a	n/a
Elastic Modulus – 0° (tension)	MSI	3.39	3.18
Elastic Modulus – 90° (tension)	MSI	2.33	2.39
In-Plane Shear Modulus	MSI	0.74	0.75
Ultimate Tensile Strength – 0°	KSI	63.6	55.6
Ultimate Tensile Strength – 90°	KSI	20.6	22.3
Ultimate Compression Strength – 0°	KSI	54.8	52.6
Ultimate Compression Strength – 90°	KSI	22.3	23.6
Ultimate Shear Strength – In Plane	KSI	8	8.6

The individual ply details of the laminate constructions for the horizontal and vertical walls are given in tables 12 and 13.

Table 12. Ply details for horizontal walls of pultruded tube.

Material	Angle	Areal Weight oz / yd ²	Thickness in.
1 ½ oz CSM	n/a	1.5	0.016
E-TTXM 2308	45	6.27	0.032
	90	11.52	
	-45	6.27	
	CSM	8.10	
Roving - 3.7 ends/in	0	38.3	0.038
E-TTXM 2308	45	6.27	0.032
	90	11.52	
	-45	6.27	
	CSM	8.10	
Roving - 3.7 ends/in	0	38.3	0.038
E-TTXM 2308	45	6.27	0.032
	90	11.52	
	-45	6.27	
	CSM	8.10	
1 ½ oz CSM	n/a	1.5	0.016
TOTALS	0	76.6	0.204
	90	34.6	
	+45/-45	37.6	
	CSM	27.3	

Table 13. Ply details for vertical walls of pultruded tube.

Material	Angle	Areal Weight, oz/yd ²	Thickness, in.
1 ½ oz CSM	n/a	1.5	0.017
E-TTXM 2308	45	6.27	0.032
	90	11.52	
	-45	6.27	
	CSM	8.10	
E-TTXM 2308	45	6.27	0.032
	90	11.52	
	-45	6.27	
	CSM	8.10	
Roving – 7.6 ends/in	0	78.6	0.078
E-TTXM 2308	45	6.27	0.032
	90	11.52	
	-45	6.27	
	CSM	8.10	
E-TTXM 2308	45	6.27	0.032
	90	11.52	
	-45	6.27	
	CSM	8.10	
1 ½ oz CSM	n/a	1.5	0.017
TOTALS	0	78.6	0.240
	90	46.1	
	+45/-45	50.2	
	CSM	27.3	

Table 14 shows a comparison of the total weights of reinforcement used in each portion of the tube profile.

Table 14. Areal reinforcement weights (oz/yd²) of potential tube laminates.

Fiber Direction	Creative Pultrusions Horizontal Wall	Creative Pultrusions Vertical Wall
0	76.6	78.6
90	34.6	46.1
+45/-45	37.6	50.2
CSM	27.3	27.3
Thickness	0.204 in.	0.240 in.

The bridge deck design called for a series of these trapezoidal profiles to be adhesively bonded together into a single panel unit which would form the deck. To ensure that individual units would not separate during service the bonded panel units were wrapped in an additional laminate. This outer laminate wrap also provided additional strength and stiffness to the panel. The specified configuration of this outer wrap was two layers of Knitmat S36007G fabric with a layer of Infusamat S1815CFM fabric in between the two layers. Knitmat S36007G is a stitch-bonded biaxial fabric with 17.92 oz/yd² of unidirectional reinforcement oriented at both 0° and 90° for a total fabric weight of 35.84 oz/yd². Infusamat S1815CFM is a biaxial fabric with 8.96 oz/yd² of unidirectional reinforcement oriented at both 0° and 90°. The biaxial layers are stitched to a 13.5 oz/yd² layer of continuous filament mat (randomly oriented fiber). The fabric is designed specifically for resin infusion processes, with the continuous filament mat providing a medium to improve resin flow into reinforcement fiber during fabrication.

This appendix outlines testing conducted on these various laminates using test samples from the actual production environment. Samples of the trapezoidal tube were taken from the actual production run. The outer wrap laminates were prepared by XC Associates in their facility using production run materials and fabrication methods.

TEST METHODS UTILIZED IN CHARACTERIZATION WORK

The test methods used in this characterization are outlined in table 15. These tests yield strength and modulus values in both primary directions (denoted as 0° for the primary fiber axis and 90° for the direction normal to that axis). Properties are determined in both tension and compression. In-plane shear strength was also determined. The fiber content of each panel was also determined to allow proper comparison of the resulting properties from each laminate.

Table 15. Test methods used in characterization.

ASTM Test No.	Title	Properties Obtained	Symbol
D3039/3039M-08	Standard Test Method for Tensile Properties of Polymer Matrix Composites	Ultimate tensile strength (0°)	σ_{1T}
		Ultimate tensile strain (0°)	ϵ_{1T}
		Modulus of elasticity (chord) (0°)	E_{1T}
		Ultimate tensile strength (90°)	σ_{2T}
		Ultimate tensile strain (90°)	ϵ_{2T}
		Modulus of elasticity (chord) (90°)	E_{2T}
D6641/D6641M-09	Standard Test Method for Compressive Properties of Polymer Matrix Composite Materials Using a Combined Loading Compression (CLC) Test Fixture	Ultimate compression strength (0°)	σ_{1C}
		Ultimate compression strain (0°)	ϵ_{1C}
		Modulus of elasticity (chord) (0°)	E_{1C}
		Ultimate compression strength (90°)	σ_{2C}
		Ultimate compression strain (90°)	ϵ_{2C}
		Modulus of elasticity (chord) (90°)	E_{2C}
D5379/D5379M-05	Standard Test Method for Shear Properties of Composite Materials by the V-Notched Beam Method	In-plane shear strength (0-90)	τ_{12}
		In-plane shear strength (90-0)	τ_{21}
D3171-09	Standard Test Method for Constituent Content of Composite Materials Test Method I, Procedure G: Matrix Burnoff in a Muffle Furnace	Fiber fraction - mass	m_f
		Fiber fraction - volume	v_f
D2344/D2344M-00	Standard Test Method for Short-Beam Shear Strength of Polymer Matrix Composite Materials and Their Laminates	Short Beam Shear Strength	

TEST RESULTS

Table 16 summarizes the results obtained from the trapezoidal tube through physical testing. Predicted values from the manufacturer are provided for comparative purposes.

Table 16. Summary of physical test data for tube laminate samples.

Property		Combi-Tube Side Walls			Combi-Tube Horizontal Walls			
		Tested Values		Predicted Values	Tested Values		Predicted Values	
		Mean	Std. Dev.	Mean	Mean	Std. Dev.	Mean	
Modulus	Tension	E_{T0}	3434 KSI	224 KSI	3180 KSI	4092 KSI	526 KSI	3390 KSI
		E_{T90}	2709 KSI	416 KSI	2390 KSI	1767 KSI	60 KSI	2330 KSI
	Compression	E_{C0}	4178 KSI	515 KSI	- KSI	3999 KSI	382 KSI	KSI
		E_{C90}	3377 KSI	281 KSI	- KSI	4157 KSI	465 KSI	KSI
Ultimate Strength	Tension	σ_{T0}	33.00 KSI	2.77 KSI	55.60 KSI	39.96 KSI	2.11 KSI	63.60 KSI
		σ_{T90}	10.28 KSI	3.10 KSI	22.30 KSI	19.88 KSI	0.96 KSI	20.60 KSI
	Compression	σ_{C0}	54.12 KSI	7.35 KSI	52.60 KSI	70.00 KSI	8.08 KSI	54.80 KSI
		σ_{C90}	37.50 KSI	1.48 KSI	23.60 KSI	54.73 KSI	7.49 KSI	22.30 KSI
Strain at Max. Stress	Tension	ϵ_{T0}	1.01 %	0.13 %	- %	1.07 %	0.09 %	%
		ϵ_{T90}	0.47 %	0.15 %	- %	1.38 %	0.09 %	%
	Compression	ϵ_{C0}	1.49 %	0.21 %	- %	2.06 %	0.36 %	%
		ϵ_{C90}	1.32 %	0.26 %	- %	1.43 %	0.28 %	%
In Plane Shear Strength	τ_{12}	13.79 KSI	1.07 KSI	8.60 KSI	13.29 KSI	1.01 KSI	8.00 KSI	
	τ_{21}	13.45 KSI	0.64 KSI	KSI	15.55 KSI	1.11 KSI	KSI	
Fiber Content (%)	mass	m_f	74 %		- %	72 %		%
	volume	v_f	53 %		- %	51 %		%
Thickness		t	0.24 in		0.24 in	0.19 in		0.20 in

Table 17 summarizes the results obtained for the outer laminate wrap used to tie the individual tubes together into a single cohesive structural unit. Three different laminates were tested for this assessment. The first is a “witness panel” of the specified laminate prepared by XC Associates in their facility. The second is a sample of actual production laminate removed from a tested sample of bridge deck. The first two panels only possess glass fiber reinforcement. The third panel includes the layer of carbon which was added into the final construction to improve the overall stiffness of an unfilled panel.

Table 17. Summary of physical test data from outer wrap laminate samples.

Property		Outer Wrap - Witness Panel		Outer Wrap - From Deck Panel		Final Outer Wrap with Carbon		
		Mean	Std. Dev.	Mean	Std. Dev.	Mean	Std. Dev.	
Modulus	Tension	E_{T0}	2339 KSI	92 KSI	2337 KSI	463 KSI	3280 KSI	164 KSI
		E_{T90}	2410 KSI	205 KSI	1588 KSI	68 KSI		
	Compression	E_{C0}	2915 KSI	346 KSI	2308 KSI	439 KSI	3222 KSI	325 KSI
		E_{C90}	2379 KSI	337 KSI	2420 KSI	201 KSI		
Ultimate Strength	Tension	σ_{T0}	36.71 KSI	1.70 KSI	24.61 KSI	4.69 KSI	50.30 KSI	2.58 KSI
		σ_{T90}	39.14 KSI	4.31 KSI	21.54 KSI	1.63 KSI		
	Compression	σ_{C0}	39.05 KSI	4.23 KSI	36.39 KSI	4.62 KSI	35.71 KSI	4.18 KSI
		σ_{C90}	35.46 KSI	2.68 KSI	36.43 KSI	4.56 KSI		
Strain at Max. Stress	Tension	ϵ_{T0}	1.70 %	0.12 %	1.26 %	0.21 %	2.06 %	0.11 %
		ϵ_{T90}	1.78 %	0.13 %	1.89 %	0.13 %		
	Compression	ϵ_{C0}	1.61 %	0.27 %	1.87 %	0.43 %	1.91 %	0.39 %
		ϵ_{C90}	2.01 %	0.52 %	1.95 %	0.35 %		
In Plane Shear Strength				9.51 KSI	1.12 KSI	9.08 KSI	0.41 KSI	
Fiber Content (%)	mass	m_f	63 %		55 %			
	volume	v_f	41 %		33 %			
Thickness		t	0.13 in		0.15 in		0.17 in	

DISCUSSION OF RESULTS

Tube Performance

As can be observed from table 16, there were some significant discrepancies between the experimental obtained values for the tube walls and the predicted properties. The modulus values obtained are generally higher than the predicted values, and it is not expected that the extra stiffness will cause significant problems in the final structure. The biggest concern was in regard to the strength values, where a number of the test values are only about half of the predicted capacity. It is thought that this may be due to lower overall strain capacity for the tube compared with the type of strain limits normally expected for a unidirectional test laminate. Assuming a relatively linear stress-strain relationship for the material, the predicted values indicate an assumed failure strain in the order of 2 percent. From earlier testing in this project, the failure strains for lamina test panels were in generally excess of 2 percent, so this would seem to be a reasonable assumption. However, when the tube walls were tested, the maximum strain generated was only in the 1 to 1.5 percent range. Given that the behavior of these materials was highly linear up to failure, the lower strain limits translate to a lower strength capacity. The reason for the reduced strains in the fabricated tubes is unknown, and further testing would need to be undertaken to fully understand this behavior. As such testing is beyond the scope of work for this project, it is recommended that analysis of the deck behavior be done using the actual test data.

Outer Wrap Performance

When comparing the “witness panel” for the outer wrap and the laminate sample removed from the actual deck panel, one would expect to see very similar test results. Observation of the data in table 17 shows that the data from the witness panel are consistently higher than the data for the

other panel. Part of the reason for these differences is the difference in fiber volume fraction. The witness panel was prepared under idealized conditions as a small panel on a flat board. This enables the production of a better quality laminate with lower resin content. Working with the larger deck unit, where the laminate must be wrapped around the deck unit, it is harder to achieve the consolidation levels seen in the small panel. It is thought that the sample from the actual deck unit is more representative of the values which will be seen in the final deck.

CONCLUSION

The performance of the “as-tested” composite laminates differed from initial predictions. While preliminary design was performed using the predicted values, these actual test values were provided for final analysis computations and were shown to still provide sufficient performance. Ultimate validation of this performance was demonstrated in the testing of full-scale components.

APPENDIX D: GROUT SELECTION REPORT

OVERVIEW

The design solution selected for the replacement deck in this project utilizes an FRP profile with three cavities (see figure 14). These profiles will be bonded together to form a large deck unit. To improve the stiffness of the deck panel and to increase resistance to localized loading, the upper and lower cavities may be filled with an appropriate grout material. This grout may be used in either the upper or lower cavity or both. Development testing on the original design concept showed a significant increase in deck performance could be gained through use of the grout.

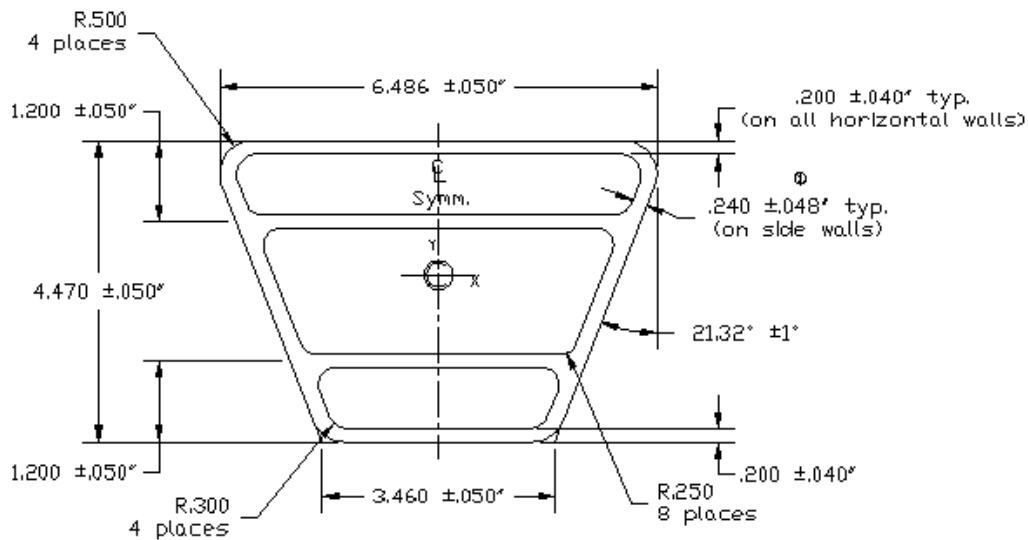


Figure 14. Diagram. Pultruded FRP combination tube

This appendix outlines work done to identify and select several grout products which may be suitable for use in the current design. Testing is performed to validate key selection parameters and a final recommendation is made for the current project.

KEY ISSUES FOR THE GROUT

In assessing potential grout products for the application, the following issues were identified as important evaluation criteria:

- Compression strength.
- Workability.
- Cure shrinkage.
- Cure time.
- Adhesion to FRP substrate.

- Density.
- Cost.
- Industry acceptance.

SELECTION OF TEST MATERIALS

The strategy adopted for selecting an appropriate grout for this structure was to identify several potential grout options based on published data and technical documentation.

There are two basic classes of grout which may be used for this design:

1. Cementitious grout
2. Polymer grout

Both classes were considered in this investigation.

The initial approach in identifying potential materials was to examine the approved material lists of several state DOTs for possible materials. Product manufacturers were then contacted to discuss the suitability of their product. Additional product recommendations from the project team and associated contacts were also considered. From these investigations the following products were identified as being potentially suitable for the current design:

- Target 1121 Cable Duct Grout, Non-shrink cement, Target Products Ltd.
- Target 1118 Unsanded Silica Fume Grout, Non-shrink cement, Target Products Ltd.
- Sikagrout 300 PT, Non-shrink cement, Sika Corporation
- Pro-Poxy 2000, Epoxy, DSC Unitex
- Pro-Poxy 2500, Epoxy, DSC Unitex
- Ipanol E-Grout, Epoxy, IPA Systems, Inc.
- Ipanol E-Flex RM, Epoxy, IPA Systems, Inc.

SUMMARY OF PUBLISHED PERFORMANCE DATA

Table 18 provides performance information on the selected products, obtained from manufacturer data sheets.

Table 18. Published grout properties.

Product	Type	Set Time, hrs	Shrinkage (28 days), %	Compression Strength (ksi)			
				1 day	3 day	7 day	28 day
Target 1121	Cement	3 to 12	<0.2	2.56	4.43	8.10	12.20
Target 1118	Cement	8	exp: 1.5-2.5	2.90	5.08	7.25	8.70
SikagROUT 300PT	Cement	3 to 12	<0.2 exp: <2.0	3.00	5.00	7.00	8.00
Pro-Poxy 2000	Epoxy	0.3 to 4	0.005	-	-	-	14.50
Pro-Poxy 2500	Epoxy	0.5	-	-	-	-	
E-Grout	Epoxy	1.5	0.005	11.00	15.00	15.00	15.00
E-Flex RM	Epoxy	4			6.80		

One of the difficulties in comparing manufacturer data for the cement grouts versus the epoxy grouts is that manufacturer testing is generally different for the two different types of material. Thus, the published data do not provide a straight comparison.

TESTING PROGRAM

In addition to examination of the manufacturer data, physical testing was conducted to obtain additional performance data required for finite element analysis modeling and to confirm published figures. The following tests were conducted:

- ASTM C109 / C109M - 11b Standard Test Method for Compressive Strength of Hydraulic Cement Mortars (Using 2-in. or [50-mm] Cube Specimens).
- ASTM C78 / C78M - 10 Standard Test Method for Flexural Strength of Concrete (Using Simple Beam with Third-Point Loading).
- ASTM C39 / C39M - 12 Standard Test Method for Compressive Strength of Cylindrical Concrete Specimens.

Compression modulus values were obtained using C39 with 3-inch by 6-inch cylinders.

Testing was conducted at 1, 3, 7, and 14 days for compression strength. Compression modulus and modulus of rupture (flexure) were determined at 14 days. Fourteen-day testing was used instead of the standard 28 days because this particular application requires materials with rapid strength development. Full strength development within 7 days is seen as preferable for this application.

TEST RESULTS

Table 19 summarizes the results obtained through physical testing.

Table 19. Results of grout testing.

Product	Compression Strength (psi)				Modulus of Rupture (psi)	Compression Modulus (ksi)
	1 day	3 day	7 day	14 day	14 day	14 day
Target 1121	818	3154	6440	7448	834	952
Target 1118	-	6551	8221	8328	1218	983
Sikagrout 300PT	2275	6904	7644	8581	-	-
Pro-Poxy 2000	9500	8092	-	11475	2099	-
Pro-Poxy 2500	-	-	-	-	2040	743
Ipanol E-Grout	9293	14994	15206	15577	1900	-
Ipanol E-Flex RM	5979	7596	7751	6849	3773	-

OBSERVATIONS ON PHYSICAL TESTING

One of the key challenges of this particular application scenario is the need to flow the grout through a narrow (~1 inch) cavity over a distance of up to 24 feet. This requires a material with good flow characteristics. All of the cement grouts demonstrate highly fluid behavior once properly mixed. While they are initially paste-like, there is a point in the mixing process when the material changes to a highly fluid behavior. It is anticipated that in this state the cement grouts could be pumped or flowed into the cavity.

The Pro-Poxy 2000 and Ipanol E-Grout are more viscous than the cement grouts but still exhibit enough flow where it is thought they could be successfully used in this application. It may be necessary to decrease the aggregate content of the E-Grout below the standard mix level to retain sufficient flow.

The Pro-Poxy 2500 is a mortar material rather than a grout and does not exhibit the flow characteristics required for this application. Therefore, it would not be suitable.

The resin component of the Ipanol E-Flex RM is considerably more viscous than the Ipanol E-Grout resin. This results in a mix with reduced flow characteristics. While not as paste-like as the Pro-Poxy 2500, the E-Flex RM may present challenges in filling the pultrusion cavity. Further testing would need to be conducted on a full-length tube specimen to properly assess the suitability of this material.

Working time is a significant issue in grout selection, as sufficient time must be available to mix and place the material before cure occurs. This is not typically a problem with the cement grouts due to their much longer cure times. For the epoxy grouts, this is more problematic. Once the resin has gelled, further working of the material is not possible. The Pro-Poxy 2000 and Ipanol E-Grout both display longer working times compared with the Pro-Poxy 2500 and Ipanol E-Flex systems. For all systems it will be necessary to carefully stage the mixing of the grout, and

multiple batches will be required to ensure the material going into a particular tube is as fresh as possible. It is thought that the working time of the Pro-Poxy 2000 and Ipanol E-Grout should be sufficient for the application at hand. The E-Flex system appears to be a much faster gelling product and the short gel time available with typical batch sizes may cause problems with filling the tube.

As can be seen from the test data, the epoxy products have a significant performance advantage over the cement products both in terms of final strength and rapid development of that strength. It can be seen that the epoxy products develop around 80 percent of their ultimate strength within 24 hours. This is a significant advantage in achieving the rapid production times envisaged for the bridge deck.

In terms of ultimate compression strength, the Pro-Poxy 2000 and Ipanol E-Grout display significantly higher strength than the cement grout options, with the Ipanol E-Grout exceeding 15 ksi. As expected, the modulus of rupture for the epoxy options is approximately twice that of the cement grouts.

While deflection under load was not measured, it was observed from the tests that the epoxy products deform significantly more than the cement grouts under failure load. The failure of the epoxy is also more progressive, rather than a sudden fracture. It is thought that this may make the epoxy products less susceptible to cracking in service, thereby preserving the integrity of the grouting in the tubes.

CONCLUSION

Table 20 shows an indication of the relative merits of the grouts, using a letter grade.

Table 20. Relative merits of grouts for the application (i.e., fill material).

Grout	Adhesion	Density	Cost	Industry Acceptance
ProPoxy 2000	A	A	C	B
Ipanol E-Grout	A	A	C	B
Ipanol E-Flex	A	A	C	B
Target 1121	C	B	B	A
Target 1118	C	B	B	A
Sika 300PT	C	B	B	A

Based on the investigations undertaken and the testing performed, the project team elected to use Ipanol E-Grout for grouting the FRP tubes in the deck. The E-Grout provided high strength performance at a reasonable cost. It appears to offer the required handling characteristics and working time for filling the tubes. It develops strength rapidly allowing the manufacture of the deck to proceed after only 1 day of grout curing. Further testing of performance in full-size grouted tubes confirmed the suitability of this selection. This brand epoxy grout was chosen over others primarily because of availability.

APPENDIX E: TUBE TESTING REPORT

DESCRIPTION OF TESTED SPECIMENS

For this study, 10 empty (i.e., no grout) and 16 grouted FRP pultruded tubes were evaluate. The shape of the cross section is shown in figure 15. Overall dimensions and thicknesses were measured in nine specimens; see table 21. It appears that variability of the dimensions is in the order of 0.01 to 0.06 inches.

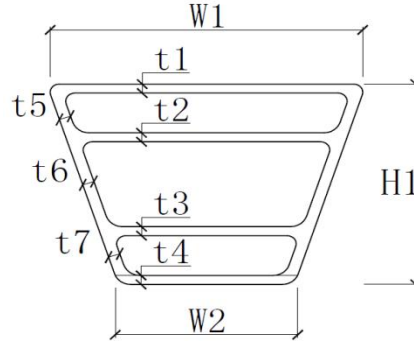


Figure 15. Diagram. FRP tube cross section.

Table 21. Dimensions and thicknesses of FRP tubes (no grout).

Tube ID No.	Weight (lb)	Length (inches)	t ₁ (inch)	t ₂ (inch)	t ₃ (inch)	t ₄ (inch)	t ₅ (inch)	t ₆ (inch)	t ₇ (inch)	W ₁ (inch)	W ₂ (inch)	H ₁ (inch)
#30	57.86	131.94	0.200	0.190	0.222	0.206	0.253	0.260	0.241	6.516	3.608	4.477
#31	57.86	131.91	0.200	0.195	0.230	0.208	0.251	0.252	0.248	6.519	3.620	4.478
#32	57.86	131.88	0.201	0.196	0.223	0.210	0.246	0.254	0.248	6.518	3.607	4.478
#33	58.08	132.09	0.201	0.201	0.224	0.207	0.252	0.253	0.241	6.521	3.594	4.482
#34	58.08	132.06	0.200	0.196	0.227	0.208	0.252	0.256	0.244	6.521	3.597	4.483
#35	57.75	131.84	0.200	0.196	0.231	0.210	0.245	0.256	0.245	6.515	3.599	4.477
#36	57.75	131.91	0.204	0.198	0.226	0.208	0.248	0.255	0.248	6.516	3.600	4.480
#37	57.86	131.91	0.203	0.195	0.223	0.207	0.248	0.254	0.250	6.518	3.604	4.482
#38	57.75	131.88	0.200	0.193	0.224	0.211	0.245	0.256	0.247	6.518	3.612	4.479
#00 (unlabeled)	56.87	131.41	0.203	0.197	0.230	0.196	0.242	0.255	0.239	6.519	3.566	4.474
Average	57.77	131.88	0.201	0.196	0.226	0.207	0.248	0.255	0.245	6.518	3.601	4.479
Max	58.08	132.09	0.204	0.201	0.231	0.211	0.253	0.260	0.250	6.521	3.620	4.483
Min	56.87	131.41	0.200	0.190	0.222	0.196	0.242	0.252	0.239	6.515	3.566	4.474
Range	1.210	0.68	0.004	0.012	0.009	0.016	0.012	0.008	0.012	0.006	0.054	0.008

Of the 16 grouted tubes, half were filled with a cementitious grout and the other half filled with an epoxy grout. Two different grouting configurations were explored: “wide” or “narrow” cells filled. Two different cross section positions were also evaluated: wide side up and wide side down. Figure 16 shows all four possible combinations. The specimens were also checked for dimensional stability, weight, and any visible defects. One specimen, #69, had a lower weight than similar specimens; the manufacturer indicated that it was partially filled with epoxy grout. Specimens were received on February 2, 2012.

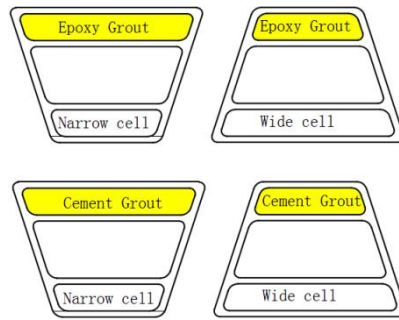


Figure 16. Diagram. Grout configurations.

Table 22. Details of FRP grouted tubes.

Tube ID No.	Grout type	Cell filled	Weight(lbs)	Length(in)	Date filled	cross-section check	
						Height H_1	Width W_1
#68-EW	Epoxy 2.5	Wide	109.6	132.06	1/31/2012		
#69-EW	Epoxy 2.5	Wide	*91.6	132.00	Partially filled	4.462	6.523
#50-EW	Epoxy 2.5	Wide	111.4	132.25	1/31/2012	4.470	6.522
#51-EW	Epoxy 2.5	Wide	111.0	132.13	1/31/2012		
#52-EN	Epoxy 2.5	Narrow	88.4	132.25	1/31/2012		
#53-EN	Epoxy 2.5	Narrow	88.0	132.13	1/31/2012		
#54-EN	Epoxy 2.5	Narrow	88.6	132.28	1/31/2012	4.478	6.513
#55-EN	Epoxy 2.5	Narrow	89.2	132.13	1/31/2012	4.474	6.514
#56-CW	cementitious	Wide	104.2	132.19	1/20/2012		
#57-CW	cementitious	Wide	104.0	132.00	1/21/2012		
#58-CW	cementitious	Wide	103.8	132.00	1/22/2012	4.476	6.520
#59-CW	cementitious	Wide	104.2	132.06	1/23/2012	4.473	6.511
#60-CN	cementitious	Narrow	84.8	132.00	1/24/2012		
#61-CN	cementitious	Narrow	84.8	132.25	1/25/2012		
#62-CN	cementitious	Narrow	85.0	132.13	1/26/2012	4.476	6.522
#63-CN	cementitious	Narrow	85.0	132.19	1/27/2012	4.471	6.516

DESCRIPTION OF TEST SETUP

The FRP tubes were tested under three-point loading (hydraulic actuator at midspan). Steel rollers were used for support between a 10-foot span length. Vertical deformation was measured using one linear variable differential transformer (LVDT) and/or string pot. In some specimens, strain measurements were obtained from uniaxial and rosette strain gage configurations. Two load cells were used to collect load data (22-kip or 110-kip capacity). The 22-kip load cell was used in nondestructive tests to better monitor the low-range of load, whereas the 110-kip load cell was used when the tubes were tested up to failure. A steel plate (12 inches by 4 inches by 0.5 inches) was used under the hydraulic actuator to create a 4-inch-wide distributed load over the FRP specimen.

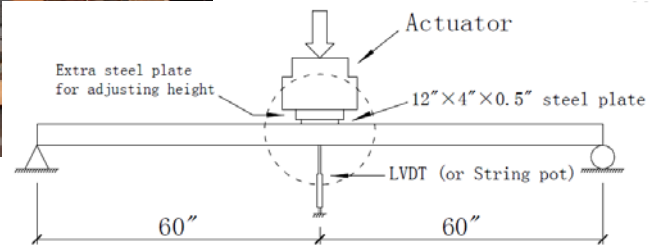
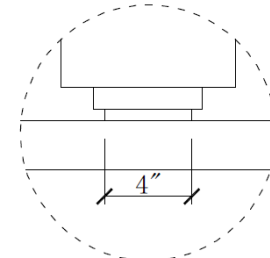


Figure 17. Photo and diagram. Testing setup.



22-kip load cell



110-kip load cell

Figure 18. Photos. Load cells used for FRP testing.

TEST PROGRAM

FRP Tubes with No Grout

All 10 FRP tubes with no grout were tested using the test setup described above. Two of them were tested up to failure, and the remaining eight were loaded and unloaded in the elastic range with two different cross section positions (wide side up, WSU, and wide side down, WSD), to check for any changes in their elastic stiffness response. The FRP tube #38 was initially loaded elastically up to 2.5 kips, and then was loaded up to failure (WSU). Specimen #30 was instrumented with strain gages in three locations: top (SG1) and bottom (SG2) “flange” under point load, and shear span (SG 3-5) at 25.4 inches from point load. This specimen was tested to

failure (WSU). Figure 19 shows the strain gages locations. Table 23 provides additional details on this test program.

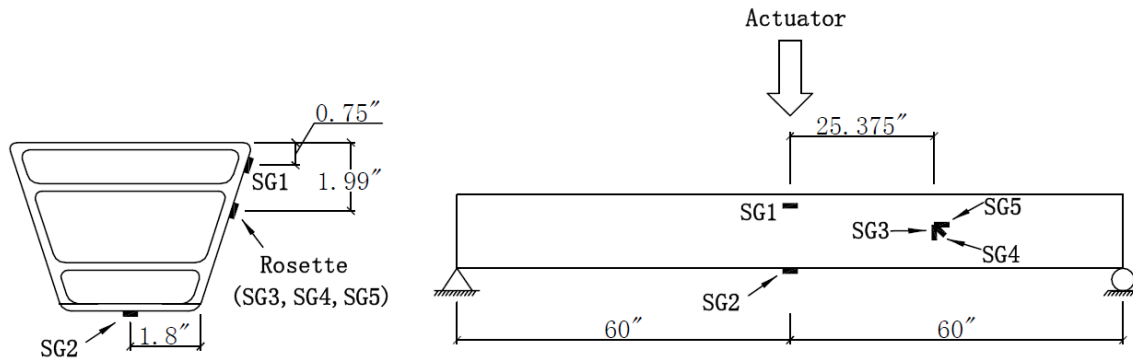


Figure 19. Diagram. Strain gage locations for the FRP tube specimen #30.

Table 23. Test program—FRP tubes no grout.

Tube ID No.	Instrumentation used in test	Cross-section position	Max or Failure Load (kips)	Displacement at max or failure load (inch)	Flexural stiffness k (lbs/inch)	Tested date
#00 (unlabeled)	LVDT & 22 kips load cell	WSU	2	1.36	1419	11/22/2011
		WSD		1.38	1418	11/22/2011
#30	LVDT & 22 kips load cell & strain_pot & 2 strain gages & 1 strain rosette	WSU	5(fail) crushing at top	3.72	1520	12/19/2011
#31	LVDT & 22 kips load cell	WSU	2.5	1.64	1527	01/04/2012
		WSD		1.65	1546	02/02/2012
#32	LVDT & 22 kips load cell	WSU	2.5	1.67	1525	01/04/2012
		WSD		1.67	1542	02/03/2012
#33	LVDT & 22 kips load cell	WSU	2.5	1.65	1541	01/05/2012
		WSD		1.66	1547	02/03/2012
#34	LVDT & 22 kips load cell	WSU	2.5	1.67	1528	02/03/2012
		WSD		1.64	1551	01/05/2012
#35	LVDT & 22 kips load cell	WSU	2.5	1.68	1518	02/03/2012
		WSD		1.65	1534	01/05/2012
#36	LVDT & 22 kips load cell	WSU	2.5	1.68	1522	02/03/2012
		WSD		1.64	1543	01/05/2012
#37	LVDT & 22 kips load cell	WSU	2.5	1.67	1519	01/06/2012
		WSD		1.65	1539	01/06/2012
#38	LVDT & 22 kips load cell	WSU	2.5	1.66	1529	02/03/2012
		WSD		1.66	1533	02/03/2012
	LVDT & 110 kips load cell	WSU	4.5(fail) crushing at top	3.49	1468	02/14/2012

The load-deflection behavior of FRP empty tubes is shown in figure 20. Results indicate that the flexural stiffness (k; calculated as the slope between 300 and 2,000 lb) of the FRP tubes #31-#38 is very similar: $k = 1533$ lb/inch (on average) with a 1.2 percent variation. The flexural stiffness of the FRP tube #00 empty tube is 7 percent smaller: $k = 1419$ lb/inch, possibly related to the smaller tube thickness (table 21 shows that the thickness of the walls, e.g. t_4 , t_5 , t_7 , of this tube is smaller than the other specimens). Flexural thickness values are tabulated in table 23.

Strain data from the test to failure of FRP tube #30 shows that the strain gage on the bottom “flange” (SG2) has a quite linear response up to failure load. By contrast SG1, near the top flange exhibited a nonlinear response beyond 4,000 lb of applied load. The strain gage rosette (SG3-5) displayed a very small magnitude of strain values, as expected.

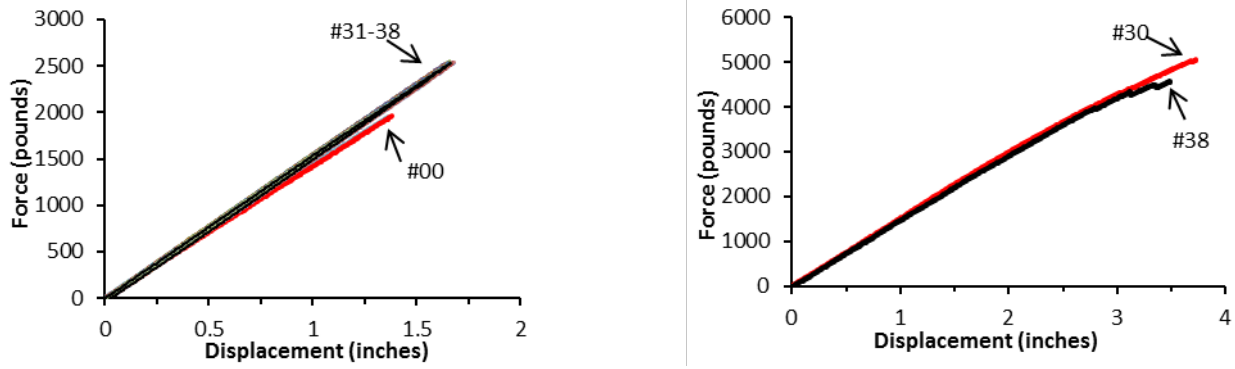


Figure 20. Graphs. Load-deflection elastic response of FRP tubes with no grout (left); Load-deflection response up to failure (tubes #30 and #38) (right).

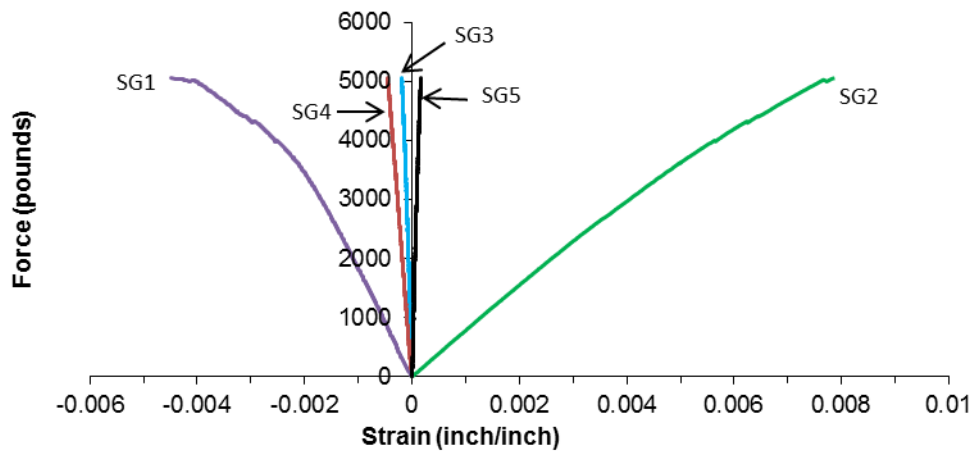
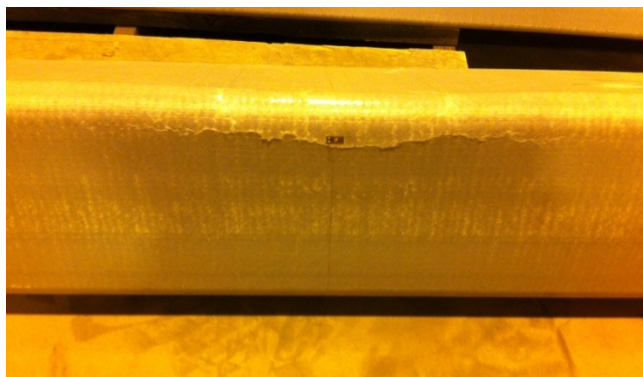


Figure 21. Graph. Load-strain response of FRP tube #30 (no grout, WSU).

The FRP tubes with no grout (#30 and #38, both WSU) failed by crushing of the top flange under the point load. Figure 22 shows photographs of these specimens after failure.



Specimen #30



Specimen #38

Figure 22. Photos. Failure modes of FRP tubes with no grout.

Grouted Tubes

Fifteen grouted tubes were tested using the same test setup described above; the FRP tube partially filled with grout (#69) was not tested. The tested specimens had two different grouts and two different grouting configurations. Table 24 shows the details of this test program, including position of the cross section, instrumentation used, failure loads, displacements and modes. Flexural stiffness was calculated between two load levels in the elastic range (prior to first crack). Because each specimen's load range is different, this information has been included in table 24.

Only four specimens were tested to failure (FRP tubes #50, 52, 57, and 60). The remaining specimens were loaded and unloaded in the elastic range. Figure 23 shows the load-deflection curves of all FRP tubes (with and without grout) tested to failure. It should be noted that the grouted tubes had a higher flexural stiffness than the empty tubes. Epoxy grouted specimens had a higher flexural stiffness than cementitious grouted specimens.

Table 24 shows that the elastic flexural stiffness of epoxy grouted tubes is 34 percent larger, on average, than that of the non-grouted tubes, while the flexural stiffness of cement-based grouted tubes is only 18 percent larger than that of the non-grouted tubes. When the cementitious grout is in compression, the flexural stiffness of the grouted tube is 17 percent larger than that of the grouted tube where the cementitious-based grout is in tension, which in turn has a very small increment of stiffness over the empty tube condition. However, for epoxy grouted tubes, the elastic flexural stiffness has little variation (only 4 percent) whether the grout is subjected to compression or tension. Comparing the effect of grouting either the wide or narrow cell, the epoxy grouted tubes have a 9 percent larger elastic flexural stiffness when the narrow cell is filled (as opposed to the wide cell); the cement-based grouted tubes show little difference.

Specimen #56 had the lowest flexural stiffness (1,600 lb/in.). Analysis of the load-deflection curve indicates that the composite action in this tube vanishes at a very small load, and the specimen behaves as an empty tube. Figure 24 shows a comparison of the load-deflection behavior (in the elastic range) for specimen #56, #57 (similar configuration), and #31 (empty tube).

Table 24. Test program—grouted FRP tubes.

Tube ID No.	Instrumentation used	Cross-section position	Max or failure Load(kips)	Deflection at max or failure load (inches)	Elastic stiffness (lbs/inch) [load range, lbs]	Load and deflection at first crack (kips/inches)	Tested date
#68-EW	String pot & 22 kips load cell	WSD	3.5	2.05	1926 [300-2550]	2.55/1.319	03/02/2012
#50-EW	String pot & 110 kips load cell	WSU	9(fail) Failure at bottom	4.92	1920 [300-4500]	No crack sound heard	02/24/2012
#51-EW	LVDT & 22 kips load cell & 2 strain gages & 1 strain rosette	WSU	7.3	3.89	1993 [300-3500]	No crack sound heard	03/03/2012
#52-EN	String pot & 110 kips load cell	WSD	9.6(fail) Failure at bottom	4.77	2234 [300-4800]	No crack sound heard	02/24/2012
#53-EN	LVDT & 22 kips load cell & 2 strain gages	WSD	7.8	3.84	2182 [300-3900]	No crack sound heard	03/03/2012
#54-EN	String pot & 22 kips load cell	WSU	3.8	2.41	2048 [300-1590]	1.59/0.756	03/02/2012
#55-EN	String pot & 22 kips load cell	WSU	1.8	0.92	2045 [300-1750]	1.75/0.838	03/02/2012
#56-CW	LVDT & 22 kips load cell & 2 strain gages & 1 strain rosette	WSU	5.9	3.89	1600 [300-3000]	No crack sound heard	03/03/2012
#57-CW	LVDT & 22 kips load cell	WSU	2.5	1.42	1970 [300-2000]	2/1.015	02/03/2012
		WSD		1.68		0.4/0.242	
	LVDT & 110 kips load cell	WSU	6.44(fail) Failure at bottom	4.39			02/14/2012
#58-CW	String pot & 22 kips load cell	WSD	3.8	2.58	1728 [30-400]	0.4/0.221	03/02/2012
#59-CW	LVDT & 22 kips load cell	WSD	1.0	0.68	1687 [30-420]	0.42/0.244	03/02/2012
#60-CN	String pot & 110 kips load cell	WSD	7.5(fail) Failure at bottom	4.60	2103 [300-3000]	3/1.431	02/24/2012
#61-CN	LVDT & 22 kips load cell & 2 strain gages	WSD	8.0	5.39	1850 [300-3000]	5.98/3.654	03/03/2012
#62-CN	String pot & 22 kips load cell	WSU	3.8	2.63	1646 [30-300]	0.3/0.174	03/02/2012
#63-CN	LVDT & 22 kips load cell	WSU	1.0	0.66	1714 [30-360]	0.36/0.205	03/02/2012

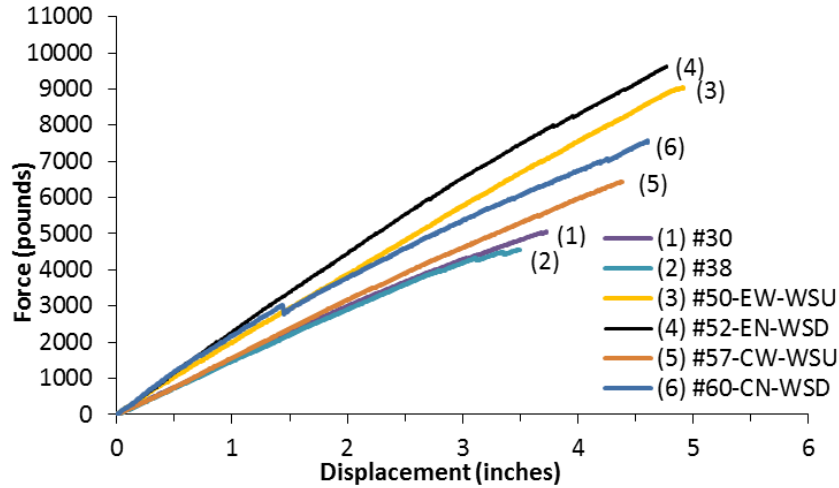


Figure 23. Graph. Load-deflection behavior up to failure for grouted FRP tubes.

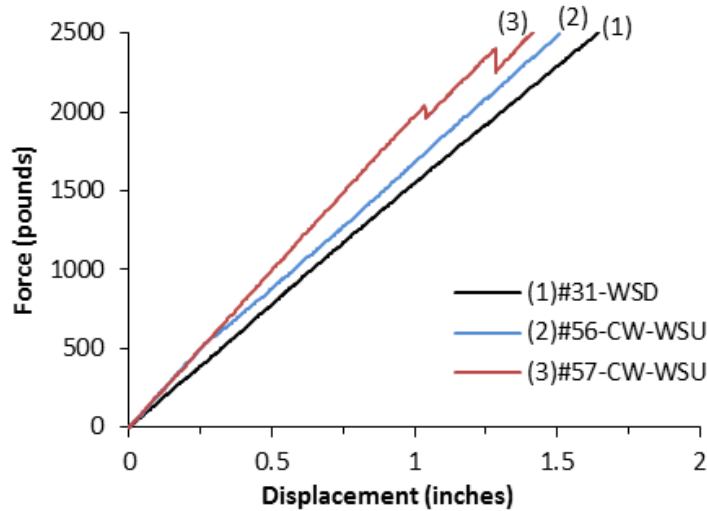


Figure 24. Graph. Load-deflection curve (up to 2,500 lb) of specimens #56, 57, and #31.

Four specimens were instrumented with strain gages. FRP tubes #53 and #61 had one strain gage at the top (SG1) and one at the bottom (SG2). FRP tubes #51 and #56 had, in addition to SG1 and SG2, a strain gage rosette (SG3-5) at 25.4 inches from the point load. Figure 19 shows locations of all the strain gages. Load-strain plots are shown in figure 25. The two strain gage rosettes (FRP tubes #51 and #56) failed during testing, perhaps due to insufficient curing time of the adhesive used prior to test. Strain responses of these specimens confirm the load-deflection behavior, analyzed previously, showing that grouted tubes have a larger section modulus when the narrow cell is filled and subjected to compression. Epoxy grouted tubes have a larger section modulus than cement-based grouted tubes.

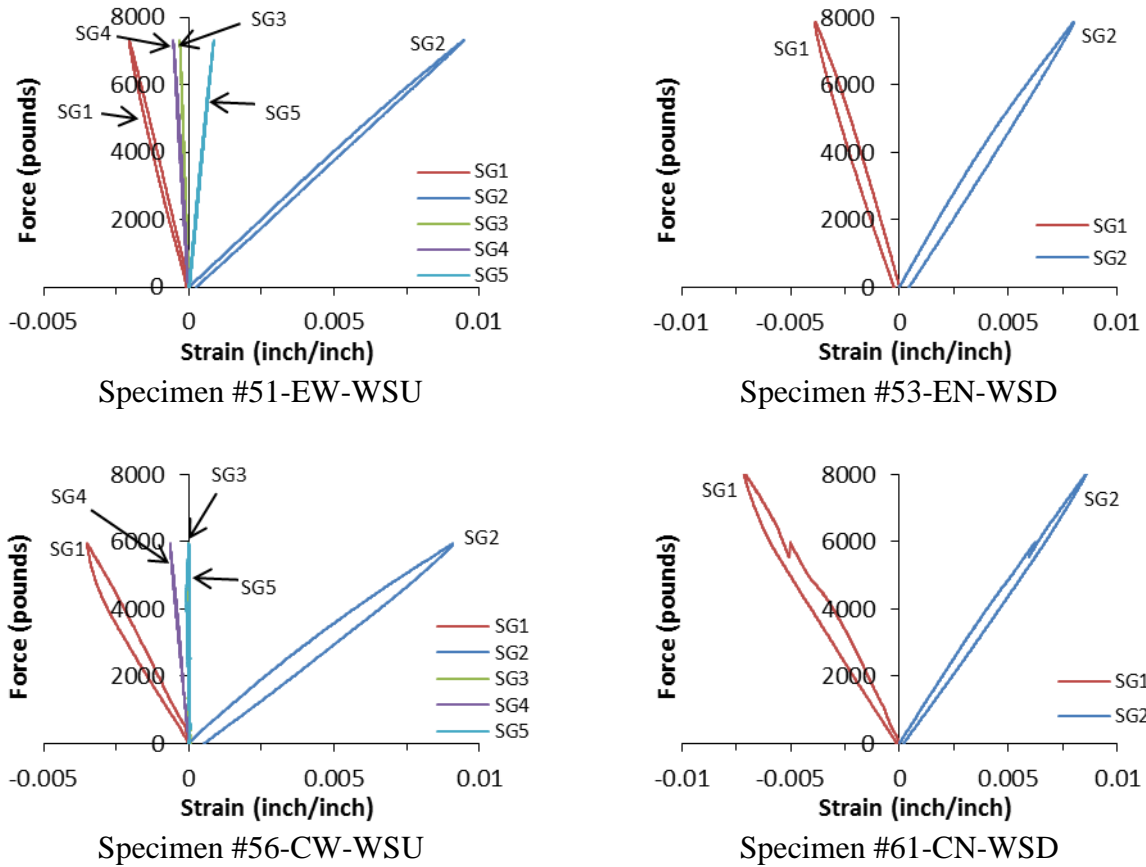
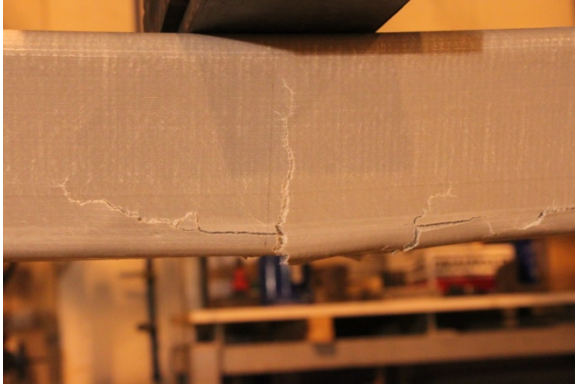


Figure 25. Graphs. Load-strain responses of grouted FRP tubes.

Failure mode for the grouted tubes originated with a tensile rupture of the bottom flange, regardless of the location of the grout (wide or narrow cell in compression). Cracks propagated vertically for all specimens, and also horizontally in specimen #50 (the location of this horizontal crack is 0.5 inches from the bottom, apparently at the splice between wall tube and the bottom horizontal section of the FRP tube). Figure 26 shows photographs of the damage regions for all four tested specimens.



Specimen #50- EW-WSU



Specimen #52-EN-WSD



Specimen #57-CW-WSU



Specimen #60-CN-WSD

Figure 26. Photos. Photographs of failure modes of grouted FRP tubes.

Specimen #60 also showed slip of the cementitious grout (top) during testing at one of the ends of the specimen (the other side was covered by the manufacturer with tape), indicating that the bond between the grout and the FRP tube had failed. The load-deflection curve has a significant load drop around 3,000 lb, probably related to the debonding initiation. Load-strain curves for a cementitious-grouted specimen also registered a significant load drop, in this case around 6,000 lb.

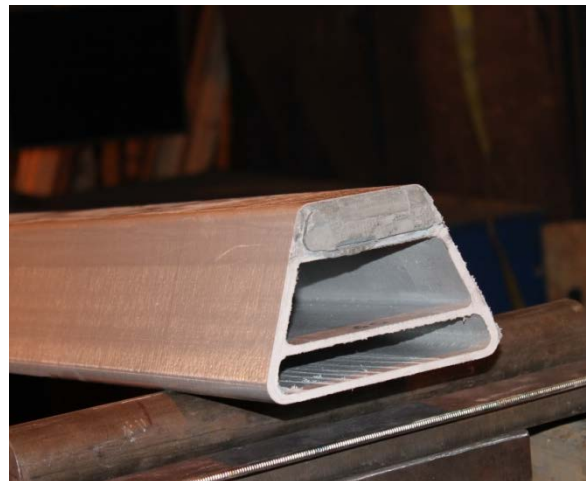
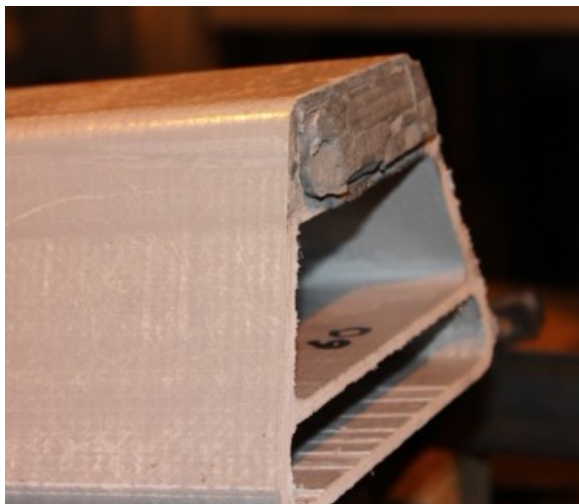


Figure 27. Photos. Cementitious grout slipping at the end of FRP tube #60.

After testing to failure, specimens #50 and #57 were cut using a wet cutting block saw near the damaged region (around the center span) to look in detail at the debonded region. Inspection of the cut surfaces shows that debonding between the epoxy grout and the FRP tube (specimen #50) occurred along the lower interface, whereas cracks between the cementitious grout and the FRP tube (specimen #57) were present along the top interface, as shown in figure 28. Specimen #37 also had a vertical crack inside the cementitious grout, a possible indication of additional damage on this grouted region.



Specimen #50- EW-WSU



Specimen #57-CW-WSU

Figure 28. Photos. Cross sections of grouted tubes near midspan, after failure.

CONCLUSIONS

Based on the experimental program developed, the following conclusions can be drawn:

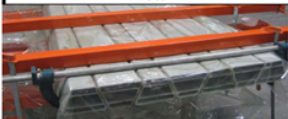
- Simple load-deflection tests of nine empty tubes show that the empty tubes have similar flexural stiffness ($k=1533$ lb/inch) with a 1.2 percent variation. Only one tube had a smaller stiffness, probably due to smaller FRP tube thicknesses.
- Test results show that grouted tubes have a larger elastic flexural stiffness than empty tubes. Epoxy grouted tubes have 34 percent greater stiffness, while cement-based grouted tubes have only 18 greater stiffness than empty tubes.
- For cement-based grouted tubes, the increase in the elastic flexural stiffness is only significant when the grout is in compression, whereas for the epoxy grouted tubes, the increase on flexural stiffness is present regardless of the grout being in compression or tension.
- Failure mode of the empty tubes is by FRP crushing at the top flange, while the grouted tubes (grout in compression) fail by tensile rupture of the bottom flange.
- Inspection of the damaged regions of the grouted specimens tested to failure shows that debonding occurred at the interface between the FRP and the grout. This occurred at load levels that ranged from 40 to 80 percent of the maximum load.
- The cementitious grout appears to have a lower tensile and bond strength, which could be easily cracked during field installation.

APPENDIX F: STRUCTURAL PANEL TEST REPORT

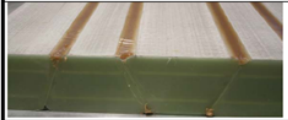
DESCRIPTION OF TESTED SPECIMENS

Twelve panels, each composed of seven FRP tubes, were evaluated for this project. Eleven panels were delivered on May 16, 2012, and one additional panel was delivered 2 weeks later.

Panels #1 to #4 were empty (i.e., no grout); manufacturing details are listed in figure 29.

Test Panel	1						
		Date:					
Panel Size	3'-2" Wide x 11'-0" Long x 4 1/2" High						
Tube #'s	2, 9, 10, 13, 17, 18, 28						
Bond	One layer chop mat and resin						
Weight							
Panel Costs							
Labor Costs				Material Costs			
				(Infill mat, resin, thixo, sanding disk costs)			
Photo				Notes			
				Single Layer Chop mat does not provide appropriate adhesion to both surfaces. Cleaning / Tooling costs excessive			

Test Panel	2						
		Date:					
Panel Size	3'-2" Wide x 11'-0" Long x 4 1/2" High (7 Tubes)						
Tube #'s	3, 4, 12, 14, 19, 23, 26						
Bond	Two layers chop mat and resin						
Weight							
Panel Costs							
Labor Costs				Material Costs			
(2hr assem, 1.5 thix, 6 hr. sand)???				(Infill mat, resin, thixo, sanding disk costs)			
Photo				Notes			
							

Test Panel	3						
		Date:					
Panel Size	3'-2" Wide x 11'-0" Long x 4 1/2" High						
Tube #'s	6, 7, 11, 15, 21, 27, 29 (7 Tubes)						
Bond	Plexus - Top and Bottom Bead with Truss pattern infill						
Weight							
Panel Costs							
Labor Costs				Material Costs			
				(Infill Plexus and Thixotropic Resin Cost)			
Photo				Notes			
				Quick and fast assembly, adhesive costs can be expensive if not controlled. Much cleaner finish than chop mat.			

Test Panel	4						
		Date:					
Panel Size	3'-2" Wide x 11'-0" Long x 4 1/2" High (7 Tubes)						
Tube #'s	5, 8, 16, 20, 22, 24, 25						
Bond	Plexus - Top and Bottom Bead intermediate verticals						
Weight							
Panel Costs							
Labor Costs				Material Costs			
(1.25 hr for assembly, 1 hr. thixo, 1 hr. sanding)???				(Infill Plexus and Thixotropic Resin Cost)			
Photo				Notes			
				Quick and fast assembly, adhesive costs can be expensive if not controlled. Much cleaner finish than chop mat.			

Figure 29. Specifications with photos. Manufacturing details of panels without grout.

Panels #5, #6, #9, and #10 were filled with epoxy grout; panels #7, #8, #11, and #12 were filled with cementitious grout. Two different grouting configurations were provided: “alternate” or “narrow side” cells filled. Two different cross section positions were tested: WSU and WSD. Figure 30 shows all four possible combinations. Specimen details are listed in table 25.

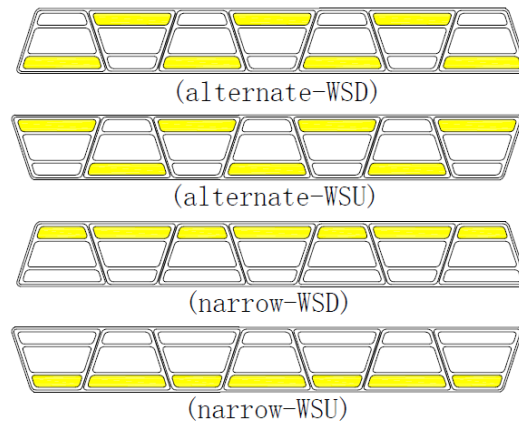


Figure 30. Diagram. Grout configurations.

Table 25. Details of panels.

Panel ID No.	Grout type	Cell filled	Length(in)	Width		Height(in.)	Date received
				Wide side(in.)	Narrow side(in.)		
#1	No	none	132.50	38.50	35.50	4.81	05/16/2012
#2	No	none	132.88	38.50	35.38	4.88	05/16/2012
#3	No	none	132.13	38.31	35.25	4.75	05/16/2012
#4	No	none	132.81	38.25	35.19	4.81	05/16/2012
#5-EN	Epoxy	Narrow side	132.81	38.00	35.13	4.88	05/24/2012
#6-EA	Epoxy	Alternate	132.50	38.25	35.13	4.94	05/16/2012
#7-CA	Cementitious	Alternate	132.75	38.19	35.13	4.81	05/16/2012
#8-CN	Cementitious	Narrow side	132.19	38.19	35.25	4.88	05/16/2012
#9-EN	Epoxy	Narrow side	132.69	38.13	35.19	5.00	05/16/2012
#10-EA	Epoxy	Alternate	132.56	38.13	35.13	4.81	05/16/2012
#11-CA	Cementitious	Alternate	132.81	38.13	35.13	4.88	05/16/2012
#12-CN	Cementitious	Narrow side	132.63	38.00	35.13	4.75	05/16/2012

DESCRIPTION OF TEST SETUP

The FRP panels were tested under three-point loading (hydraulic actuator at midspan). Steel rollers were used for support between a 10-foot span length. A 110-kip load cell was used to collect load data. The test setup is shown in figure 31.

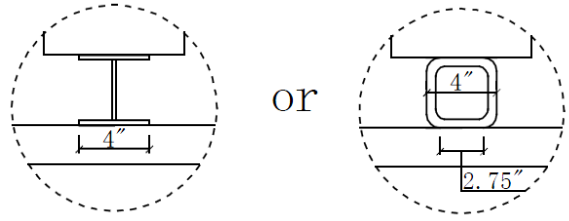
For the empty panels, the vertical deformation was measured using one LVDT and one string pot at the midpoint of the bottom plane. An I-shape steel beam (4-inch by 35-inch contact area) was used under the hydraulic actuator to create a 4-inch-wide distributed load over the FRP specimen.

For the grouted panels, the vertical deformation was measured using one string pot at the midpoint of the bottom plane and two LVDTs placed 15 inches from the string pot, as shown in figure 32. A steel tube measuring 4 inches by 4 inches by 0.375 inches was used under the point load. The contact area of this steel tube is 2.75 inches multiplied by the width of the top plane (35 inches for WSD and 38 inches for WSU).

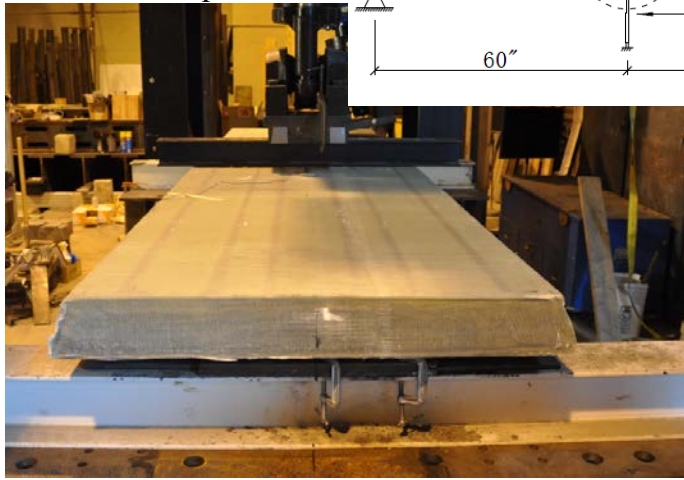
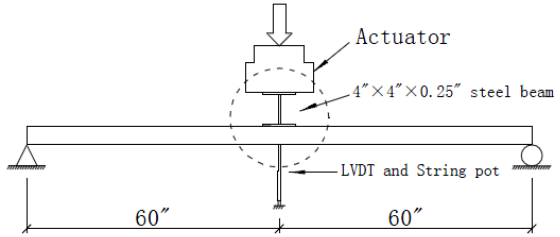
In some specimens, strain measurements were obtained from uniaxial and rosette strain gage configurations.



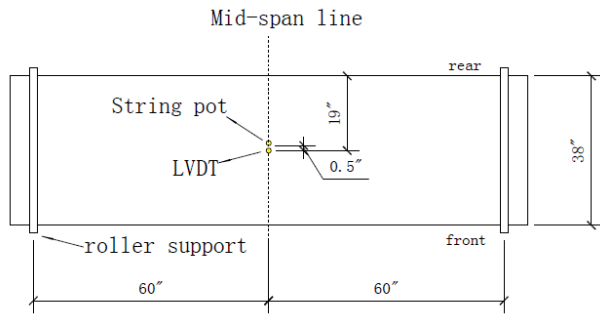
Front view of test setup



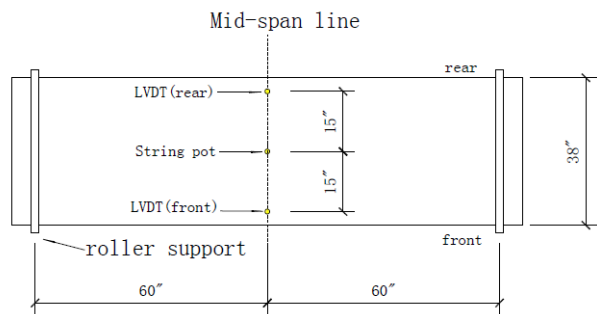
OR



Side view of test setup



Bottom view of test setup (panels #1-#4)



Bottom view of test setup (panels #5-
#12)

Figure 31. Photos and diagrams. FRP panel test setup.

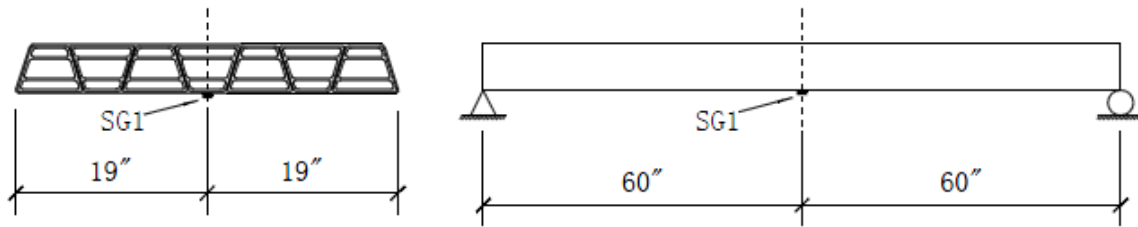


Figure 32. Diagrams. Strain gage location for panel #4.

TEST PROGRAM

FRP Panels with No Grout

The panels with no grout were tested using the test setup described above. They were all loaded and unloaded in an elastic range (up to 20 kips). Panel #1 was tested both WSU and WSD. Panel #2 was tested WSD. Panel #3 was loaded and unloaded (up to 20 kips), then tested to failure. It was instrumented with two strain gages installed at the centerline of the panel width. SG1 was placed at midspan on the bottom surface; SG2 was attached 2.125 inches away from midspan on the top surface; see figure 33. Panel #4 was instrumented with one strain gage at midspan and centerline of the panel width on the bottom surface. Table 26 provides additional details on this test program.

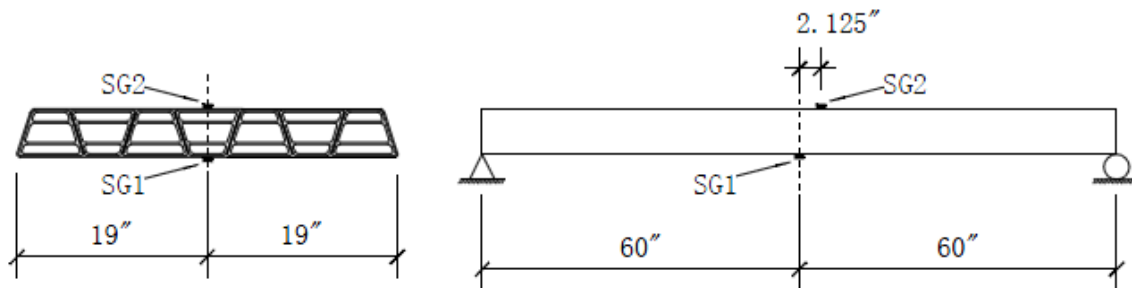


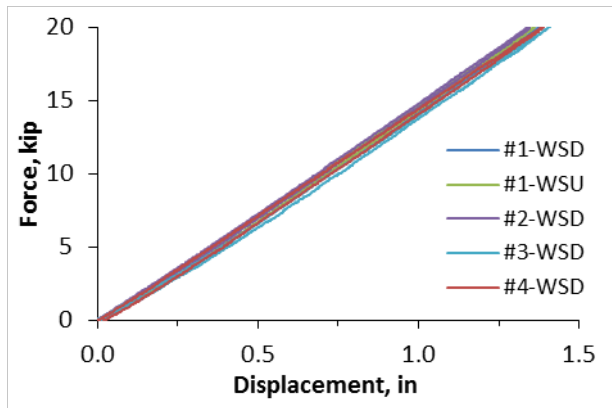
Figure 33. Diagrams. Strain gage location for panel #3 (tested to failure).

Table 26. Test program—FRP panel without grout.

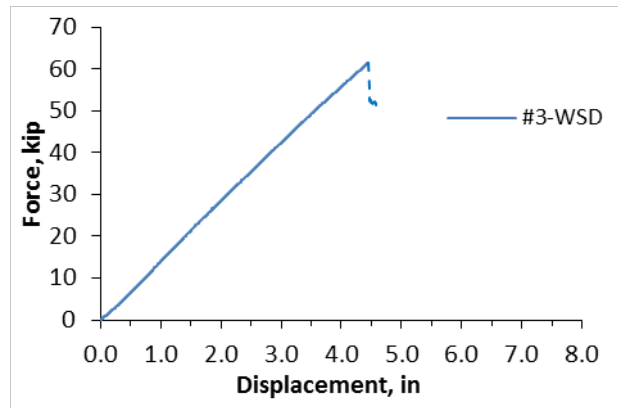
Panel ID No.	Instrument used	Cross-section position	Max or Failure Load(kips)	Displacement at max or failure load (in.)	Flexural stiffness k (kip/in.)	Tested date
#1	String pot & LVDT & 110 kips load cell	WSU	20	1.38	14.49	05/23/2012
		WSD		1.39	14.4	05/23/2012
#2	String pot & LVDT & 110 kips load cell	WSD	20	1.37	14.72	05/22/2012
#3	String pot & LVDT & 110 kips load cell	WSD	20	1.44	14.32	05/22/2012
	String pot & 110 kips load cell & 2 strain gages		61(fail) crush at top	4.45	13.91	05/24/2012
#4	String pot & LVDT & 110 kips load cell & 1 strain gage	WSD	20	1.4	14.05	05/22/2012

The load-deflection behavior of all FRP empty panels in the elastic range (up to 20 kips) is shown in figure 34 (left). Flexural stiffness, k , was calculated as the slope between 1 and 10 kips (except for panel #3). Results indicate that panels #1 through #4 have a very similar stiffness: average $k = 14.32$ kip/inch, with a 2.9 percent variation. Panel #3 exhibited a change in stiffness around 3 kips of load. This is a very small change, possibly due to very localized damage on the panel, though this was not observed visually. Flexural stiffness was calculated between 5 and 15 kips ($k = 14.32$ kip/inch, as shown in table 26).

Strain data from the test of panel #4 has a linear response up to 20 kips of load; see figure 35 (left). Strain data from panel #3 are illustrated in the graph on the right in figure 35. This shows that the strain gage on the top (SG2) behaves quite linearly, whereas SG1, located at the centerline and mid-width of the panel (bottom), exhibited a nonlinear response beyond 40 kips of applied load. Strain behavior during unloading of the specimen after failure is shown with dotted lines.

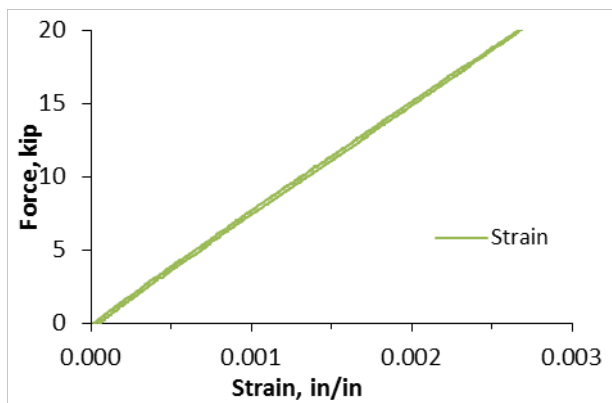


a) elastic response of all FRP panel-no grout

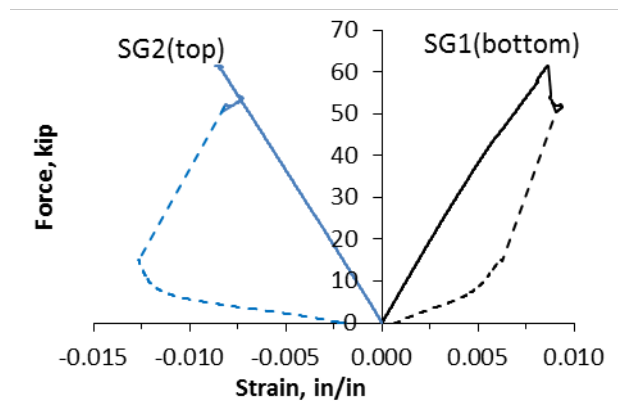


b) response to failure of panel #3

Figure 34. Graphs. Load-deflection response of FRP panels with no grout.



a) Load-strain response of panel #4



b) Load-strain response of panel #3

Figure 35. Graphs. Load-strain response of FRP panels with no grout.

Panel #3 was loaded manually under displacement control. The first crack was heard around 32 kips. Additional cracking noises were heard with incremental loading, and they seemed to come from localized damage regions. At around 62 kips and 4.5 inches of deflection, a significant cracking noise was heard. It appears that one or more of the FRP tubes failed (compression at the top layer), and additional sounds were heard (the load dropped to around 52 kips). At this point, it was observed that the top of the outer wrap buckled in the vicinity of the steel tube. The test continued under increasing displacement, and after just few more major cracking sounds, the load dropped to around 15 kips (perhaps all the FRP tubes had failed at this point). The outer wrap showed a region of damage near the point load. The specimen was unloaded at this point. It was observed that very small permanent deformation (0.5 inches) remained after the specimen was fully unloaded. Residual strain values were also determined: SG1 (bottom) registered 0.07 percent, and SG2 (top) registered 0.18 percent of permanent deformation. Figure 36 shows the sequence of events.



Failure at midspan: buckling of outer wrap



Top surface of the damaged outer wrap

Figure 36. Photos. Failure sequence of FRP panel #3 (no grout).

Figure 37 shows photographs of the cross section of panel #3 after failure. The failed panel was cut into two pieces along the width using a masonry blade, close to the damaged region. It appears that where the outer wrap buckled, the bond between the FRP tubes and the outer wrap was not strong. This may indicate that the tube surfaces may need better surface preparation, such as sanding. By contrast, visual inspection could not detect cracks between the individual FRP tubes. In the future, nondestructive evaluation methods, such as acoustical emission, could be used to investigate the possibility of damage. The top surface of the FRP plates was then exposed, and the compression cracks along the top section of the FRP tubes were photographed.

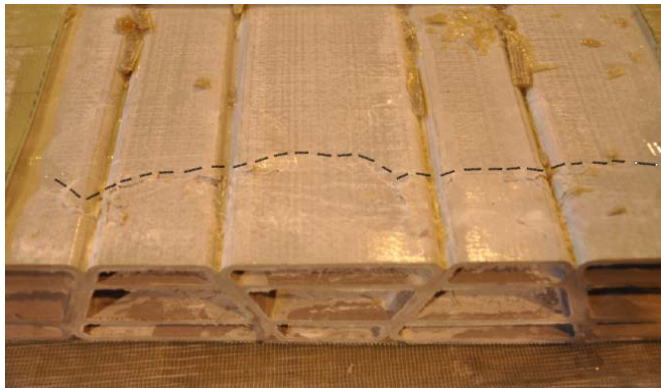
Four pieces of the outer wrap were obtained by additional cuts along the top surface of the FRP panel and were sent to a laboratory to determine “as-built” properties of the laminate. The laminate was tested in tension, compression, and shear to compare with previous test results. Fiber fraction was also determined.



Cutting of the FRP panel #3



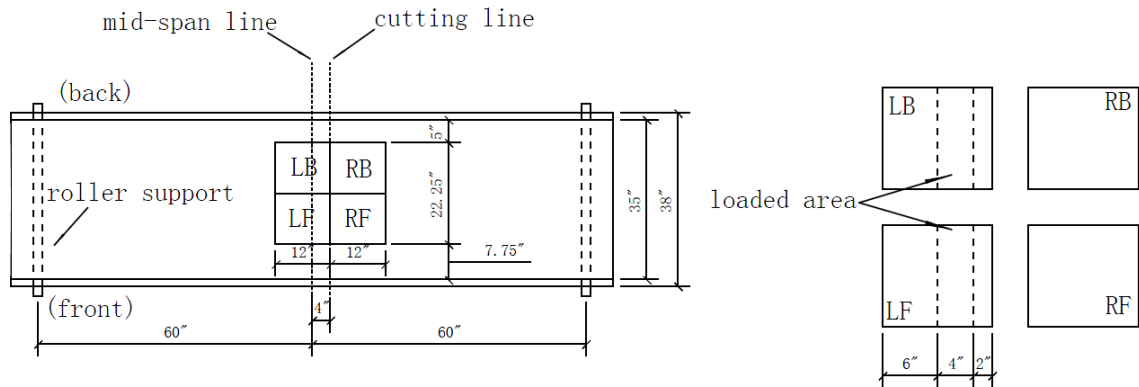
Cross section of panel #3 near damage region



Compression cracks on top of FRP tubes



Cracking detail-top surface FRP tubes



FRP panel #3- cut lines

Figure 37. Photos and diagrams. Details of cut sections from panel #3.

Grouted Panels

Eight FRP grouted panels were tested using the same test setup as used for the non-grouted panels. The tested specimens had two different grouts and two different grouting configurations. Table 27 shows the details of this test program, including the position of the cross section, instrumentation used, and maximum loads and displacements. Flexural stiffness was calculated between two load levels in the elastic range (prior to first crack). Because each specimen's elastic range is different, this information has been included in table 27. Panels #5, #8, #9, and

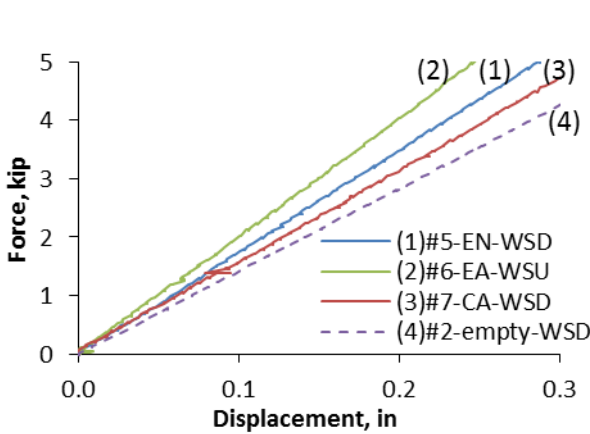
#12 were loaded and unloaded to 20 or 22 kips and then to 38 kips; panels #6, #7, #10, and #11 were loaded and unloaded to 24 kips and then to 40 kips. Deformation of the FRP panel was recorded using two LVDTs and one string pot. No significant difference (in the order of 3.2 percent) was found between the deflections at the centerline vs. the edge.

Table 27 shows that the elastic flexural stiffness of the cementitious grouted panels is very similar— $k= 15.24$ kip/inch, on average—regardless of the location of the filled cells and tested position. This k value is only 6.4 percent higher than for the panels without grout. The flexural stiffness of the epoxy grouted panels (filled in alternate cells) is 45 percent larger, on average, than that of the non-grouted panels; the flexural stiffness of the epoxy grouted panels (narrow side cells filled) is 26 percent larger than that of the non-grouted panels. Thus, the epoxy grouted panels with alternate cell filled are the most efficient panels with respect to flexural stiffness in the elastic range. Figure 38 shows the different load-deflection response of the grouted panels in the elastic range and overall response between epoxy grouted panels (filled with alternate cells and narrow side cells) and a cementitious grouted panel. Non-grouted (empty) panel response is also included for completeness.

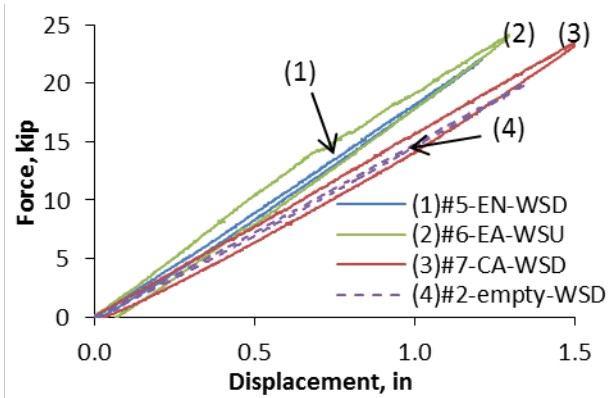
The residual deformation data (after the last unloading cycle) is shown in table 27. The average residual deformation of the cementitious grouted panels was found to be 0.06 inches, while the average residual deformation of the epoxy grouted panels is 0.125 inches. It was noted that for panel #5 (epoxy grouted-EN), no cracking was heard during the loading portion of the test; this panel exhibited the smallest permanent deformation of all epoxy grouted panels.

Table 27. Test program—grouted FRP panels.

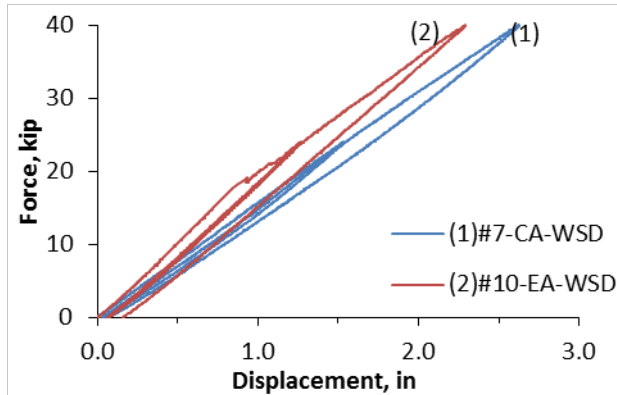
Panel ID No.	Instrument used	Cross-section position	Max Load(kips)	Displacement at max loads (inch)	Flexural stiffness (kip/in.) [load range, kip]	Load and deflection at first crack (kips/in.)	Average residual deformation (inch)	Date tested
#5-EN	String pot & 2 LVDT & 110 kips load cell	WSD	20&38	1.21&2.09	17.94 [1-10]	No crack sound heard	0.05	05/31/2012
#6-EA	String pot & 2 LVDT & 110 kips load cell	WSU	24&40	1.29&2.28	20.91 [1-10]	10.8/0.529	0.129	06/05/2012
#7-CA	String pot & 2 LVDT & 110 kips load cell & 2 strain gage & 2 strain rosette	WSD	24&40	1.53&2.63	15.58 [1-6.5]	6.7/0.429	0.061	06/04/2012
#8-CN	String pot & 2 LVDT & 110 kips load cell	WSU	20&38	1.42&2.73	15.07 [0.5-3]	3.2/0.219	0.074	05/30/2012
#9-EN	String pot & 2 LVDT & 110 kips load cell	WSU	22&38	1.34&2.60	18.09 [1-10]	13.9/0.786	0.171	05/31/2012
#10-EA	String pot & LVDT & 110 kips load cell & 2 strain gages & 2 strain rosette	WSD	24&40	1.27&2.29	20.72 [1-10]	19/0.931	0.151	06/04/2012
#11-CA	String pot & 2 LVDT & 110 kips load cell	WSU	24&40	1.50&2.57	15.02 [1-5]	5.3/0.337	0.056	06/04/2012
#12-CN	String pot & LVDT & 110 kips load cell	WSD	22&38	1.36&2.36	15.29 [1-4]	4.2/0.274	0.047	05/30/2012



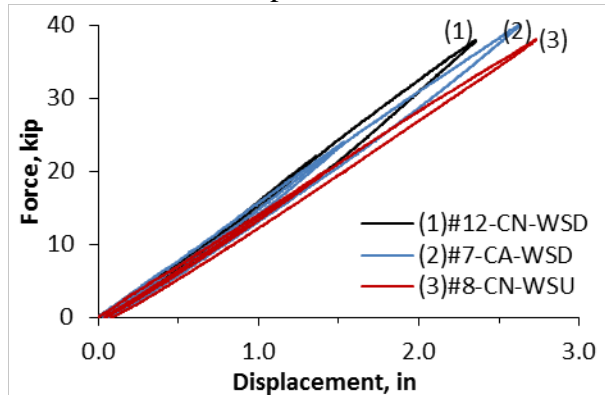
a) Elastic response of FRP panels



b) Overall response up to 20 kips of FRP panels



c) Grout effect on alternate filled cell configuration



d) cementitious grout effect on FRP panels

Figure 38. Graphs. Load-deflection response of FRP grouted panels.

The elastic flexural stiffness of the epoxy grouted panel is 36 percent larger than that of the cementitious grouted panel. However, cracking of the epoxy grout beyond 20 kips of applied load significantly affect the stiffness of the panel, as shown in the graph at the bottom left in figure 38. With increasing loading, the flexural stiffness drops to 16 kip/inch at the load range of 25 to 35 kips, which is only 7 percent larger than the cementitious grouted panel ($k=14.9$ kip/inch) measured at the same load range. The graph at the bottom right of figure 38 shows that even though the position of the cementitious grout does not affect the flexural stiffness of the FRP panels on the elastic range (before first cracking), it does affect the load-deformation behavior in the cracked region.

Two grouted panels (#7 and #10) were instrumented with strain gages (uniaxial and rosette configuration). Panel #7 has one strain gage at the top (SG1), one strain gage at the bottom (SG2), and two strain gage rosettes on each side (SG3-5, SG6-8). Panel #10 has one strain gage at the top (SG1), one strain gage at the bottom (SG2), and one strain rosette on the front side (SG3-5). Strain gage positions are shown in figures 39 and 40.

Figures 41 through 43 show load-strain plots. Figure 43 shows a comparison of the strain behavior at the top and bottom of the FRP panels #7-CA and #10-EA. Up to a load of 20 kips, the strain-load curves for SG1 (top) and SG2 (bottom) look quite symmetrical for both panels. Beyond 20 kips, the epoxy grouted panel (#10-EA) cracks in tension (SG2); in contrast, SG1 doesn't show any disturbance. SG2 in panel #10 has a similar response as SG2 for panel #7 (cementitious grout-CA).

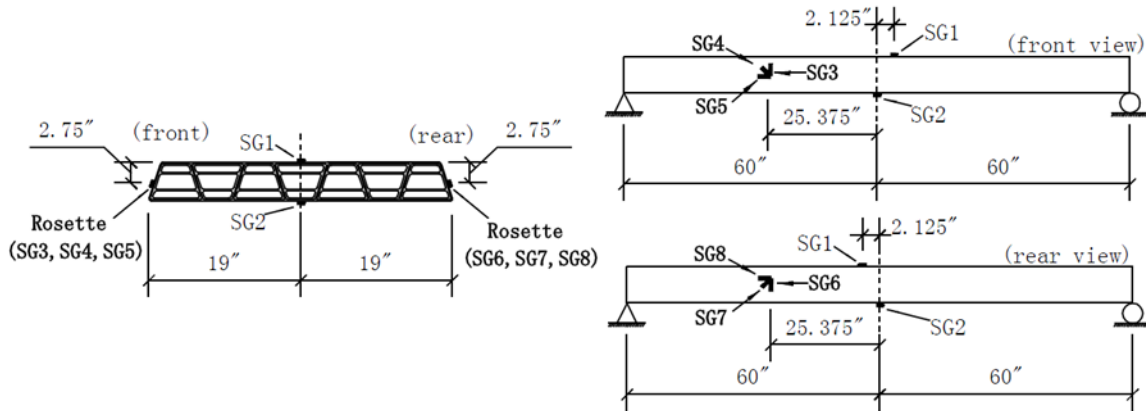


Figure 39. Diagrams. Strain gage location for panel #7.

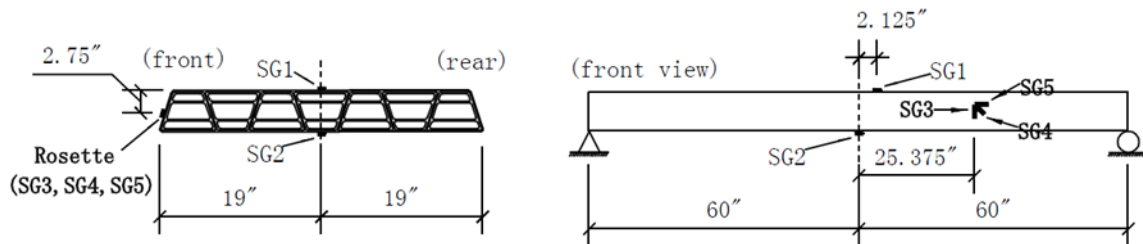


Figure 40. Diagrams. Strain gage location for panel #10.

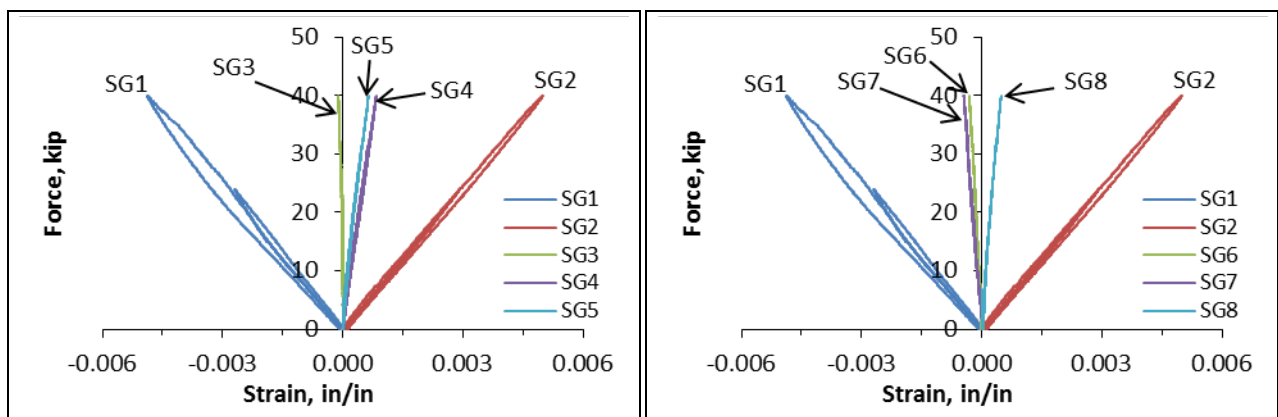


Figure 41. Graphs. Load-strain response of FRP panel #7-CA.

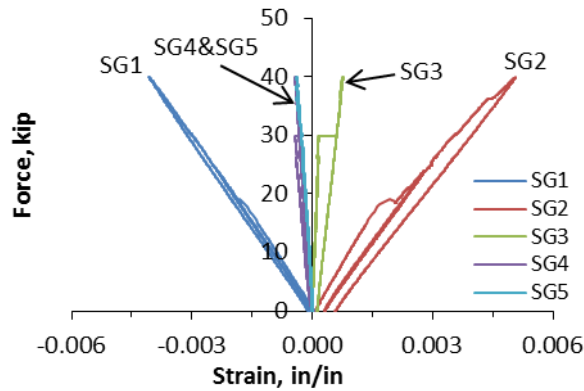


Figure 42. Graph. Load-strain plot of FRP panel #10-EA.

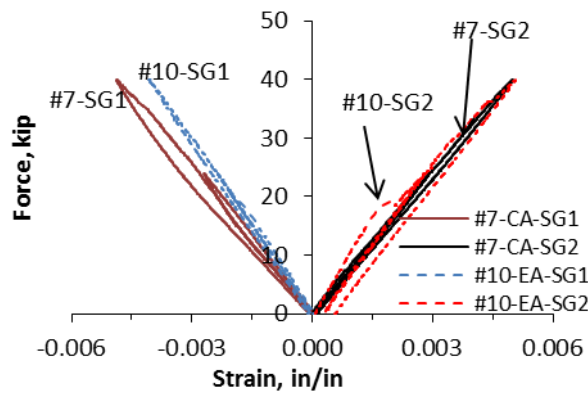


Figure 43. Graph. Load-strain (top & bottom) FRP panels.

CONCLUSIONS

Based on the experimental program developed, the following conclusions can be drawn:

- Load-deflection test of four FRP panels without grout shows that they have similar flexural stiffness ($k=14.32\text{kip/inch}$, with a 2.9 percent variation).
- The flexural stiffness of the epoxy grouted panels (filled in alternate cells) is 45 percent larger, on average, than that of the non-grouted panels, whereas the epoxy grouted panels with cells filled on the narrow side only have a 26 percent increase.
- The cementitious grouted FRP panels only showed an increase of 6.4 percent of flexural stiffness when compared to the empty panels. Very little effect was observed from changes in the location of the filled cells and/or tested position.
- The higher flexural stiffness of the epoxy grouted panels significantly decreases when the grout (or bond between grout and FRP tube) cracks, around 20 kips. Post-cracking stiffness value approaches that of the cementitious panels.
- Even though the position of the cementitious grout does not affect the flexural stiffness of the FRP panels on the elastic range (before first cracking), it does affect the load-deformation behavior in the cracked region.
- Strain data show that the epoxy grouted FRP panel with alternate cells filled has grout cracking (or bond failure) in the tension region at a 20-kip load level.

- Although both grouts achieved fairly highly strength within a short time, the epoxy grout is preferred because of the apparent better bond between it and the FRP surface. Further information about the grouts can be found in Appendix D.

APPENDIX G: PANEL SHEAR TEST

XC Associates fabricated small panels (42 inches long by 17 inches wide) by joining three FRP pultruded tubes and wrapping them with glass fiber wrap (three layers). These specimens were initially designed to evaluate the bond between two adjacent pultruded tubes; however, the wrap was too stiff to be deformed with the test setup available at Penn State to the load level needed to break the bond between the tubes.

The researchers requested a different type of test to evaluate the deformation of one panel between two steel sections with the same top flange width (8 inches) and spacing (24 inches) as the steel girders in the demonstration bridge. The test setup will evaluate the effect of two different load footprints: 20 inches by 10 inches (AASHTO tire contact area) and 6 inches by 6 inches (simulating the effect of a smaller footprint due to debris on the road). In both tests, the panel was loaded up to 25 kips. Deformation was measured from the actuator, as well as a string pot (midspan under panel) and LVDT (top surface of the panel). The sketches in figure 44 and figure 45 show details of the test setup and transducer location for both tests.

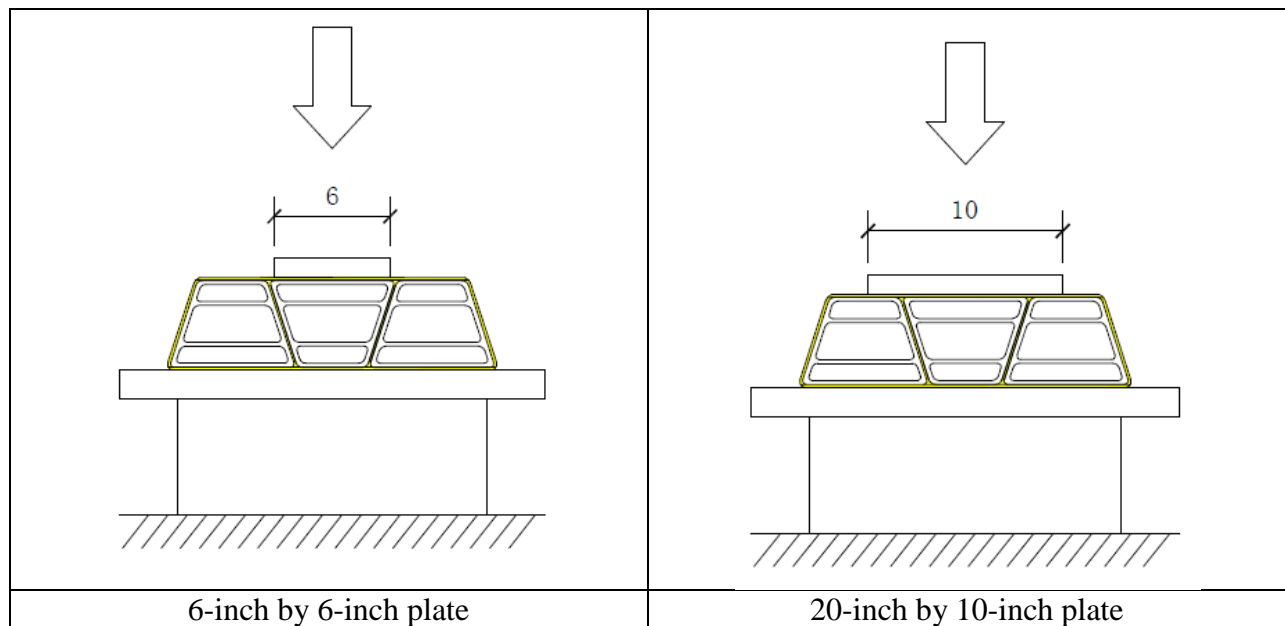


Figure 44. Diagrams. Tested load footprints.

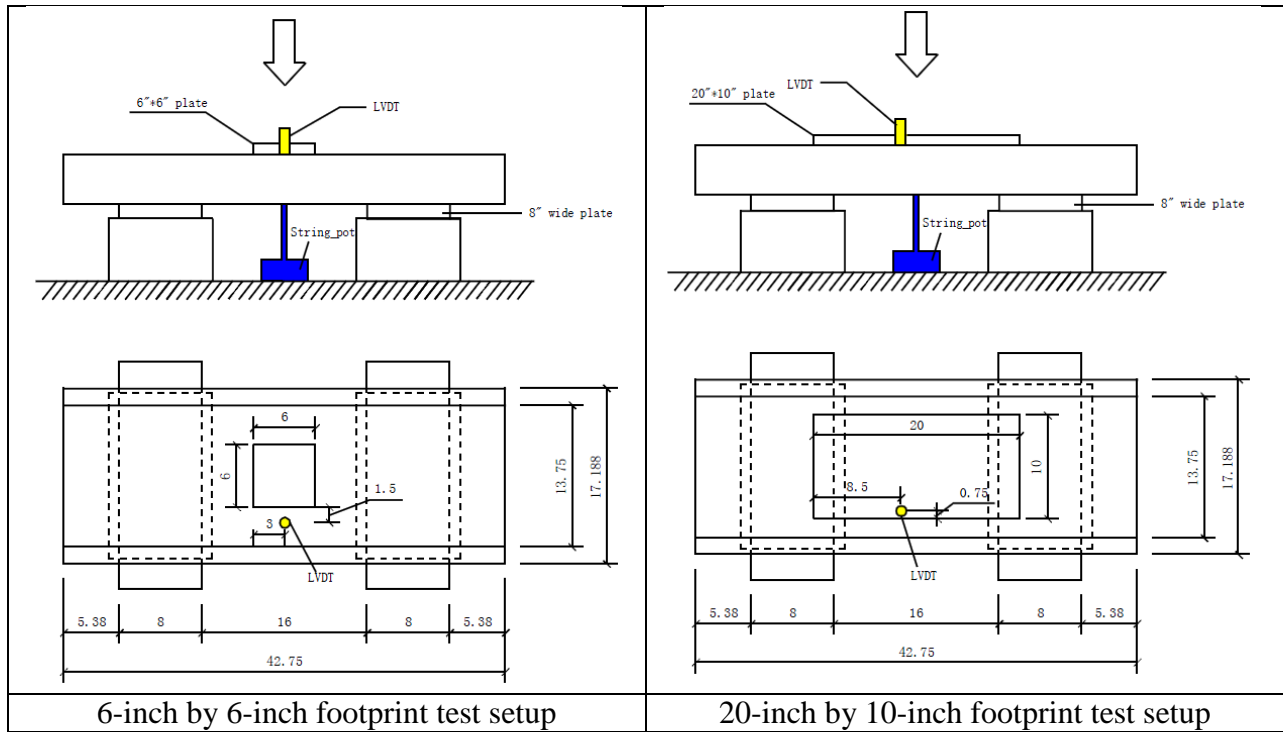
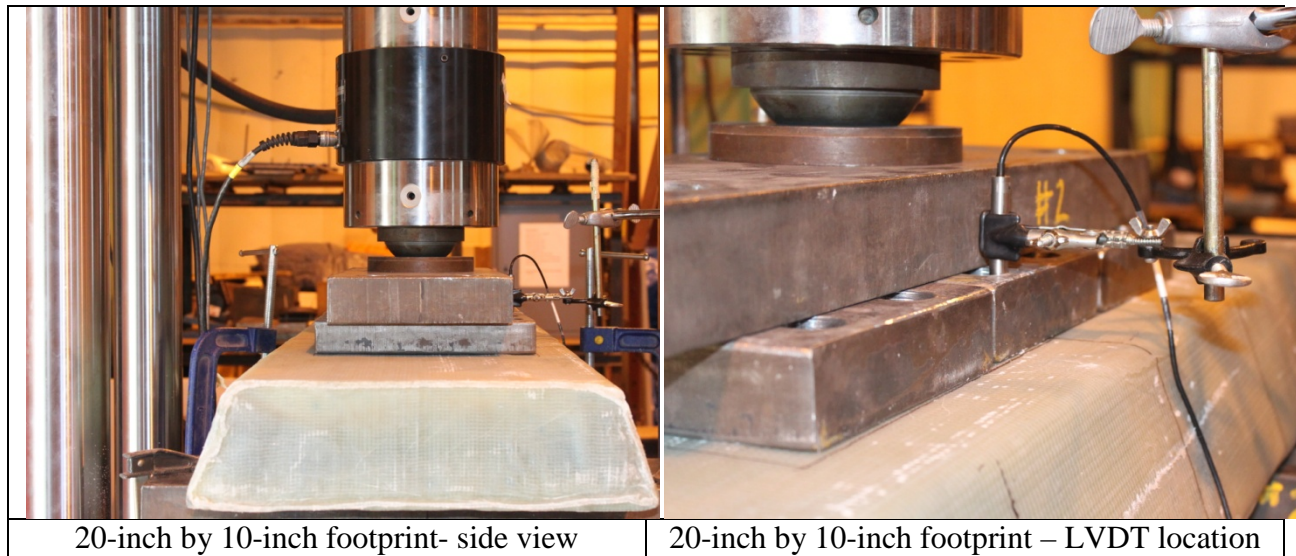


Figure 45. Diagrams. Test setup used to evaluate footprint effect.

Steel plates were used to create the two different footprints. The photographs of different details of the test setup are shown in figure 46.



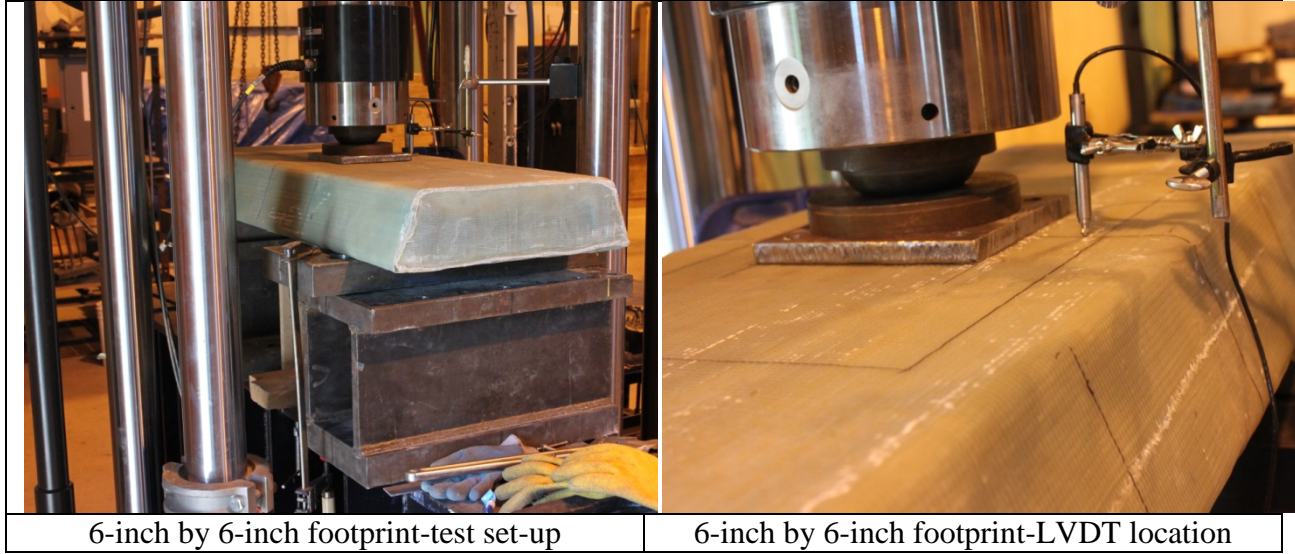


Figure 46. Photos. Test setup details.

During both tests (the same panel was used, first loaded with larger footprint, unloaded, then smaller footprint and unloaded), cracking sounds were heard during the loading phase, but no visible damage or cracks were observed after unloading and removal of the steel plates. The plots in figure 47 show the load-deflection response as captured by the actuator, spring pot (bottom of the panel), and LVDT (top of panel). Results are summarized as follows:

- 6-inch by 6-inch footprint test: Max load is 25.1 kips. Max displacement: 0.146 inch registered by actuator; 0.080 inch by LVDT; 0.092 inch by the string pot.
- 20-inch by 10-inch footprint test: Max load is 25.12 kips. Max displacement: 0.109 inch registered by actuator; 0.074 inch by the LVDT; 0.068 inch by the string pot.

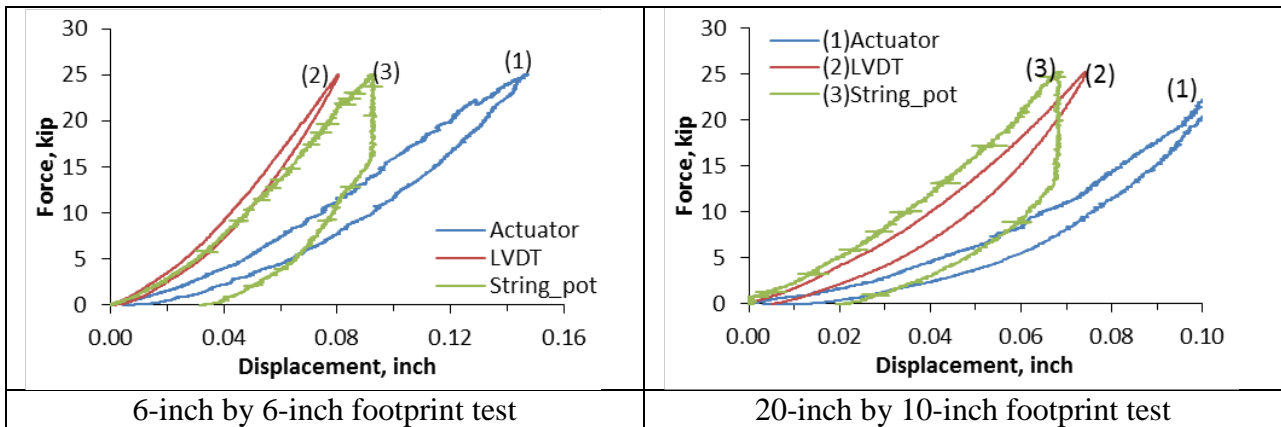


Figure 47. Graphs. Load-deflection responses of the two footprint tests.

APPENDIX H: PANEL FATIGUE TEST REPORT

DESCRIPTION OF THE TESTED SPECIMEN

This appendix reports the details of testing a panel composed of seven FRP tubes with no grout. Manufacturing details are listed in figure 48. The panel was positioned WSD, as shown in figure 49. The length of panel is 11 feet; the cross section dimensions are shown in figure 50.

Test Panel	2	Date:
Panel Size	3'-2" Wide x 11'-0" Long x 4 1/2" High (7 Tubes)	
Tube #'s	3, 4, 12, 14, 19, 23, 26	
Bond	Two layers chop mat and resin	
Weight		
Panel Costs		
Labor Costs		Material Costs
(2hr assem, 1.5 thix, 6 hr. sand)???		(Infill mat, resin, thixo, sanding disk costs)
Photo		Notes
		

Figure 48. Specifications with photo. Manufacturing details of tested panel.



Figure 49. Photo. FRP panel (WSD).

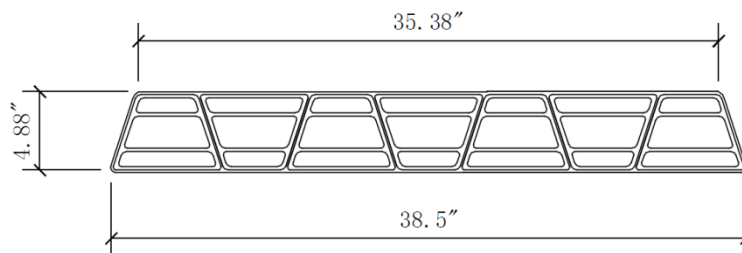


Figure 50. Diagram. Cross section dimensions of the FRP panel tested in fatigue.

DESCRIPTION OF TEST SETUP

Figure 51 shows the fatigue test setup. The FRP panel was tested under three-point loading (hydraulic actuator at midspan). Half-round steel sections were used as support between a 5.5-foot span. A 110-kip load cell was used to collect the load data. To prevent possible “pounding” effects between the FRP deck panel and the supports during testing, two clamps were used at each side. Two steel plates (12 inches by 12 inches by 1.25 inches) were used under the hydraulic actuator to create a 144 in² distributed load over the FRP specimen. One LVDT was placed at the midpoint of bottom face of the panel to measure the deflection during the static load tests; it was used to measure flexure stiffness.

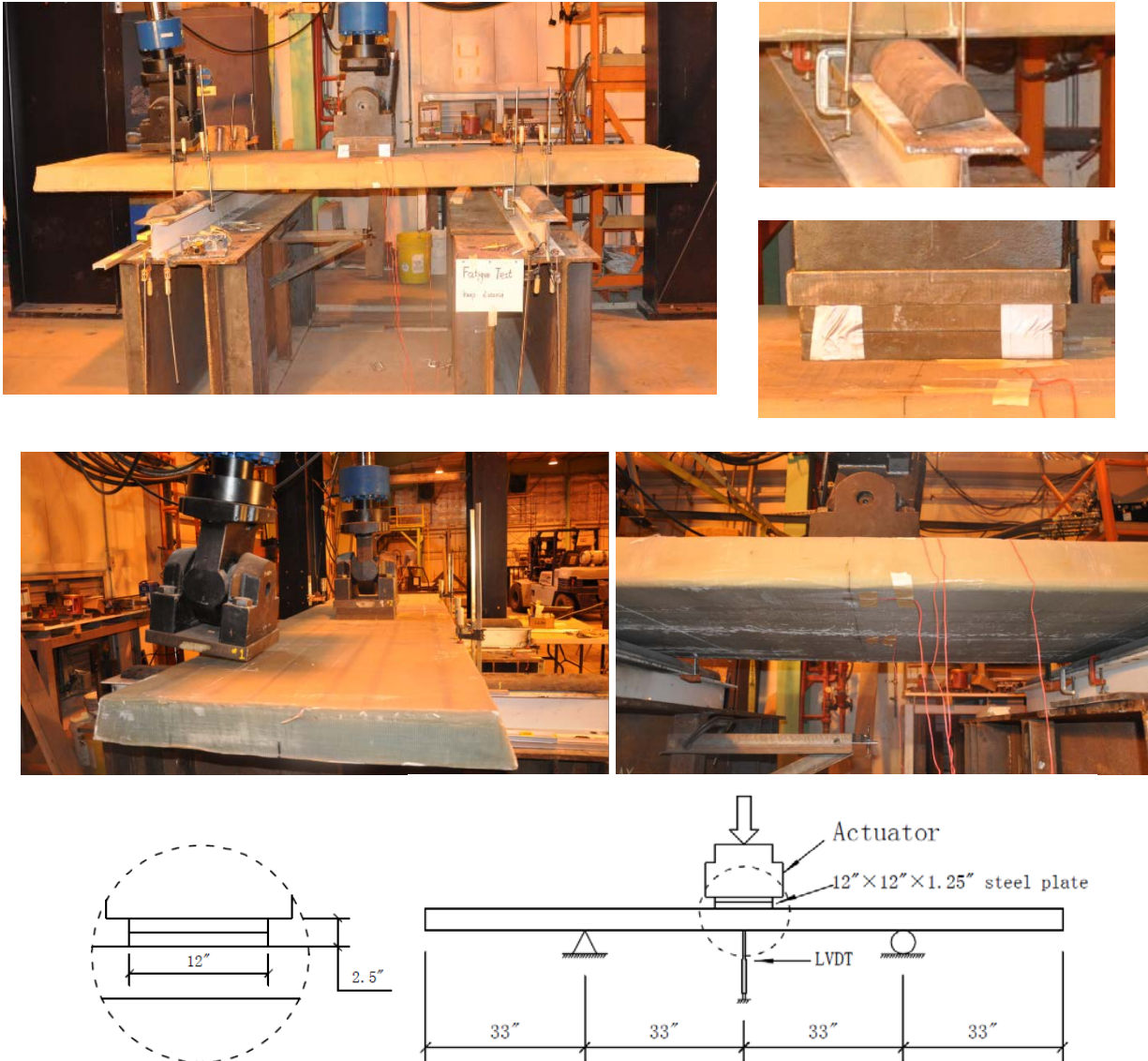


Figure 51. Photos and diagram. Fatigue test setup.

TEST PROGRAM

Load was applied on a range of 1 to 14 kips in flexure (compression on top face of panel) using a hydraulic actuator. A command sinusoidal wave with a 1.5 Hz frequency was used. Testing started at 7:00 am every day and ended at 10:00 pm. This cyclic testing was interrupted one time during the day (at 1:00 pm) to conduct a monotonic test (under displacement control). The specimen was loaded up to 14 kips and unloaded; 14 kips is considered equivalent to the effect of the design truck (16 kips) times the dynamic allowance (1.15) times the load factor assuming a finite life check (0.75). Load, displacement (from LVDT and actuator), and strains at various locations were recorded. Cyclic testing resumed after that. From each monotonic test, flexure stiffness as a function of the number of cycles was calculated (load range of 2 to 12 kips). Table 28 provides this information, as well as the ratio of each stiffness value with respect to that at zero cycles. Figure 52 shows the stiffness ratios as a function of the fatigue load cycles.

Table 28. Flexure stiffness as function of increasing number of fatigue cycles.

Date	Time	Cycle done	LVDT		Actuator	
			Stiffness, kip/in (from 2 kip to 12 kip)	Stiffness/initial stiffness	Stiffness, kip/in (from 2 kip to 12 kip)	Stiffness/initial stiffness
06/18/2012	10:00am.	0	69.11	1.000	51.16	1.000
06/18/2012	3:30pm.	14722	70.44	1.019	53.19	1.040
06/20/2012	1:00pm.	149542	70.49	1.020	53.84	1.052
06/22/2012	1:00pm.	290100	69.59	1.007	53.78	1.051
06/24/2012	1:00pm.	436342	70.02	1.013	53.73	1.050
06/25/2012	1:00pm.	507044	68.84	0.996	53.30	1.042
07/03/2012	1:30pm.	655021	68.36	0.989	53.44	1.045
07/05/2012	1:00pm.	793782	69.01	0.999	55.13	1.078
07/08/2012	1:00pm.	980990	69.07	0.999	55.80	1.091
07/08/2012	9:50pm.	1025326	69.78	1.010	55.46	1.084

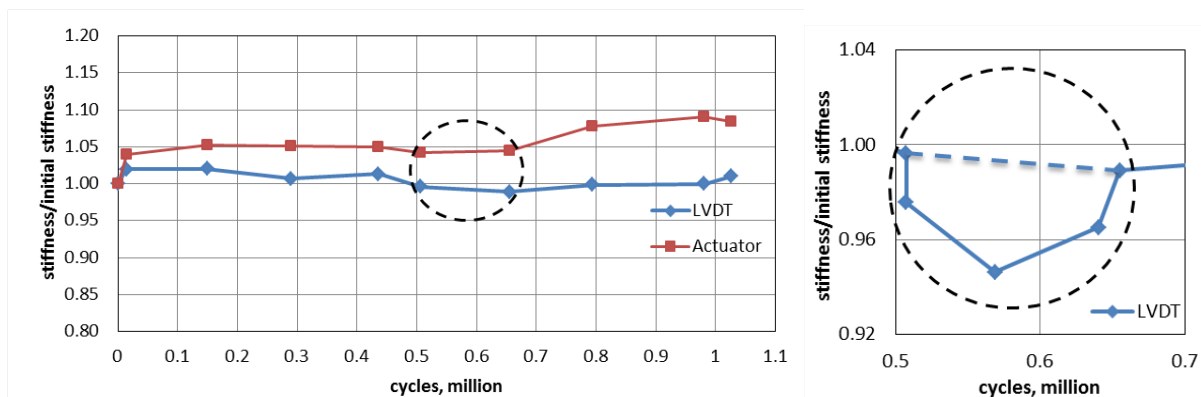
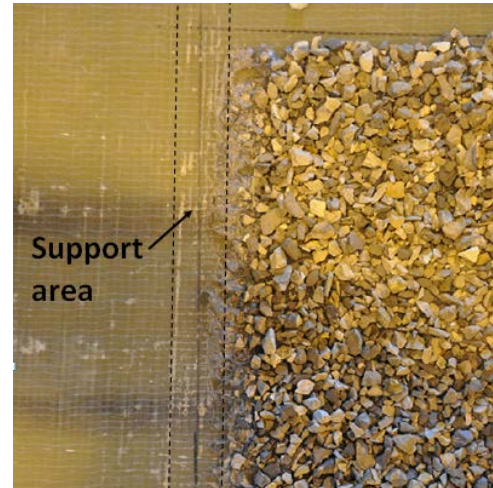
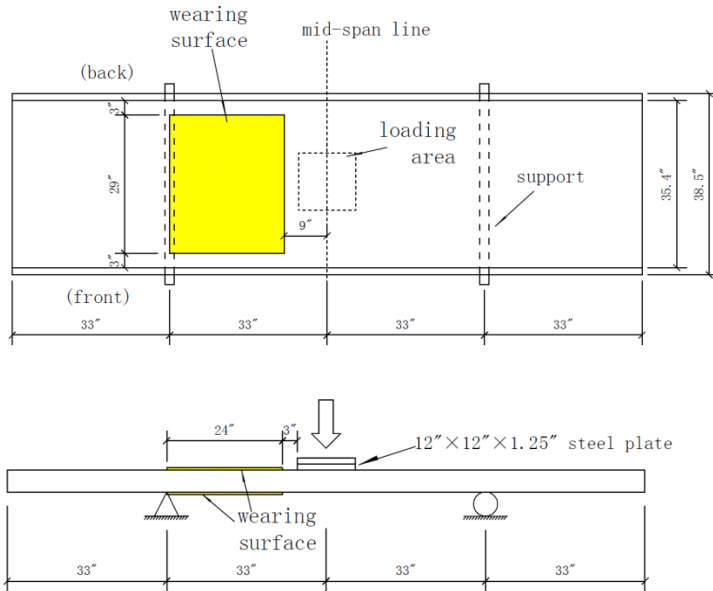


Figure 52. Graphs. Stiffness ratios as function of the number of fatigue load cycles (left); temporary change in stiffness between 500,000 and 650,000 cycles (right).

The graph at the left of figure 52 shows that the stiffness ratios measured at different cycles did not vary more than 3 percent from the original stiffness. It can be concluded that after 1 million

cycles there is no evidence of stiffness degradation. At 500,000 cycles, the test was temporarily stopped so a wearing surface could be applied to the bottom face of the FRP panel deck; see figure 53. After the cyclic testing resumed, a drop on the stiffness ratio was experienced for about 130,000 cycles, as shown in the graph at the right of figure 52. The maximum value corresponded to a 6 percent drop at 570,000 cycles; however, it vanished after that (650,000 cycles). It is hypothesized that because the wearing surface was applied quite close to the support area (see the photograph in figure 53), it might have produced a gap between the support and the panel, which caused the stiffness to temporarily drop.



Wearing surface on bottom side (which is subjected to tension) after 1 million cycles fatigue load

Figure 53. Diagrams and photo. Location of wearing surfaces: applied to top and bottom of deck panel to assess performance in compression and tension.

Figure 54 shows the load-deflection behavior at different fatigue cycles. The load-deflection curve is not quite linear; see for comparison the tangential line drawn in figure 54. The panel becomes “stiffer” after the load reaches 6 kips. The initial load-deflection curve matches well with the curve after 1 million cycles of fatigue loading. The slope of the load-deflection curve at 570,000 fatigue cycles is slightly smaller than the slope of the initial curve, which is indicated as a stiffness drop in figure 52.

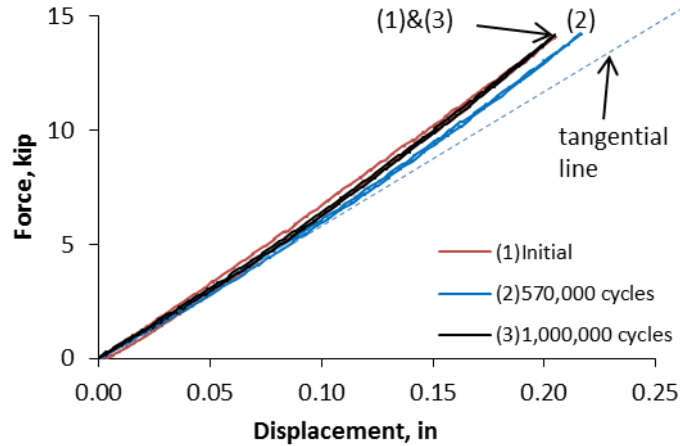


Figure 54. Graph. Load-deflection behavior at different fatigue cycles.

To evaluate the sensitivity of the stiffness measurements to the time of the day when they are taken, the flexure stiffness was measured three times a day from June 22 to June 24, 2012 (at 7:00 am, 1:00 pm, and 10:00 pm.) Results are shown in figure 55. Although these results show that the stiffness measurements change within the day (changes in the order of 2 percent were found), no clear pattern was determined, although it appears that there is a drop of stiffness overnight.

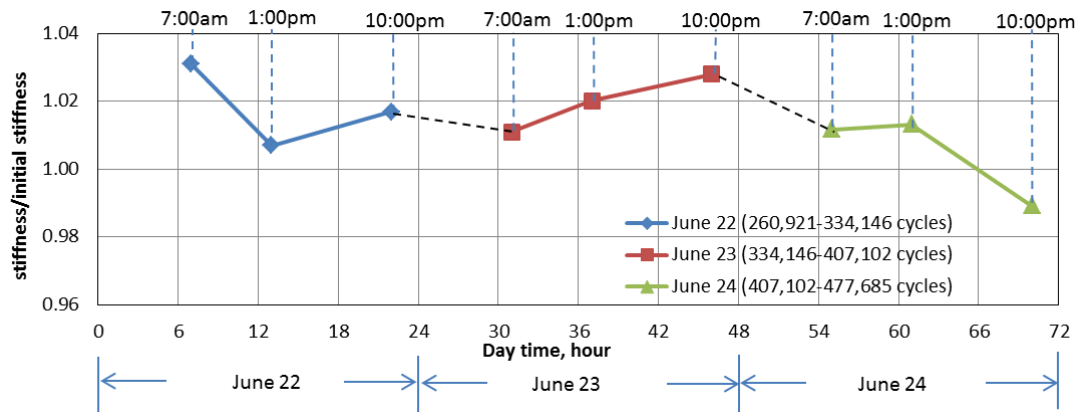


Figure 55. Graph. Stiffness change during daytime.

As indicated before, a wearing surface composed of epoxy compound and exposed aggregate was applied at the bottom of the FRP panel (subjected to tension) at 500,000 fatigue cycles. In addition, the same type of wearing surface was installed at the top of the panel (subjected to compression) at 650,000 fatigue cycles. Both were applied over an area of 29 inches by 24 inches. After 1 million cycles fatigue load, neither the top nor the bottom wearing surfaces showed any visible damage or cracks. Figures 56 and 57 show photographs of the wearing surfaces before and after their respective exposure to cyclic loading.

Figure 58 shows the position of five strain gages (SG1-SG5) installed on the FRP panel surface. SG1 and SG2 were placed on the top face beside the loading steel plate. SG3 (top) and SG4

(bottom) were placed at midspan toward the edge of the panel. SG5 was installed at the midpoint of the bottom face of the panel.



Figure 56. Photos. Bottom wearing surface before and after 500,000 cycles fatigue load.



Figure 57. Photos. Top wearing surface before and after 350,000 cycles fatigue load

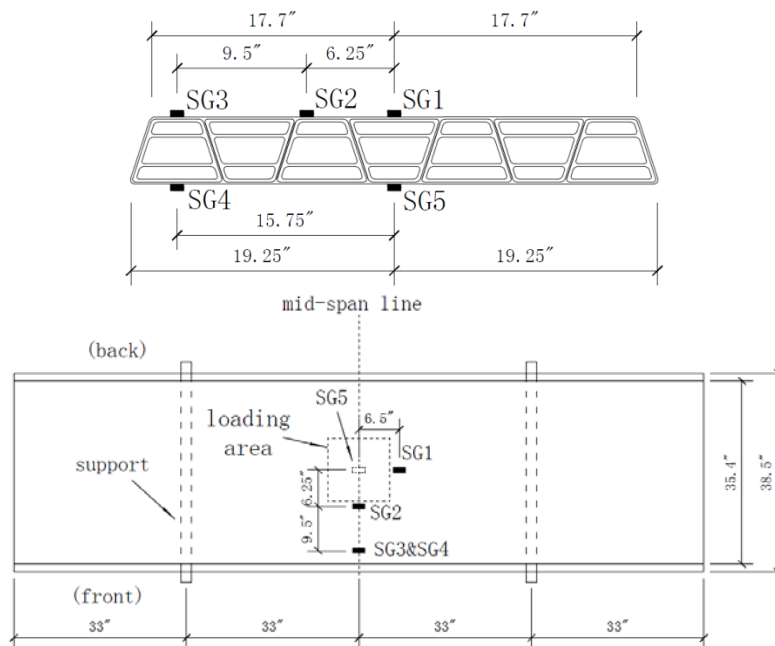


Figure 58. Diagrams. Strain gage position.

Figures 59 through 62 show load-strain behavior for the five strain gages at different fatigue cycles. Despite the presence of small residual strains, load-strain curves for SG1 and SG4 showed little change during the fatigue test (see figures 59 and 60). In figure 61, the slope of the curve for SG3 at 1,000,000 fatigue cycles is almost the same as the initial one. However, the slope at 500,000 fatigue cycles is 21 percent smaller. Figure 62 shows that the slope of the curve for SG5 at 500,000 fatigue cycles is smaller (15 percent) than the initial slope and remains similar at 1,000,000 fatigue cycles. Load-strain behavior of SG2 in figure 63 shows a large residual strain at this location. At 500,000 fatigue cycles, there is a sudden change of slope at 6.5 kips; this may due to the local damage of the FRP deck (or strain gage) at this location. Unfortunately, SG2 was broken due to the slight movement of the loading steel plate at around 600,000 fatigue cycles, so no more data were collected beyond that point.

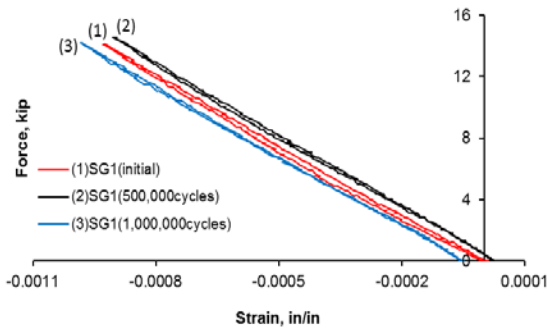


Figure 59. Graph. Load-strain behavior (SG1).

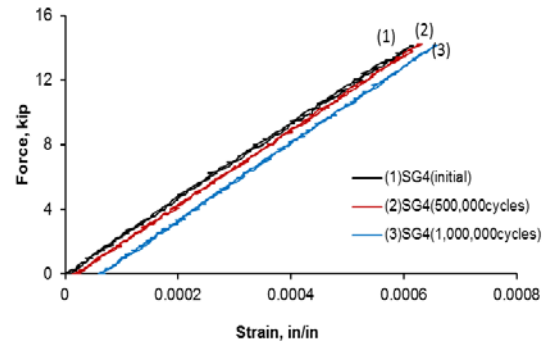


Figure 60. Graph. Load-strain behavior (SG4).

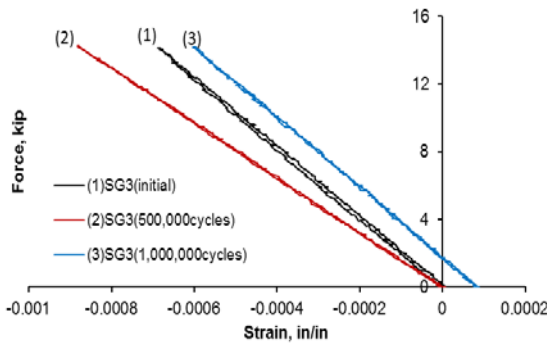


Figure 61. Graph. Load-strain behavior (SG3).

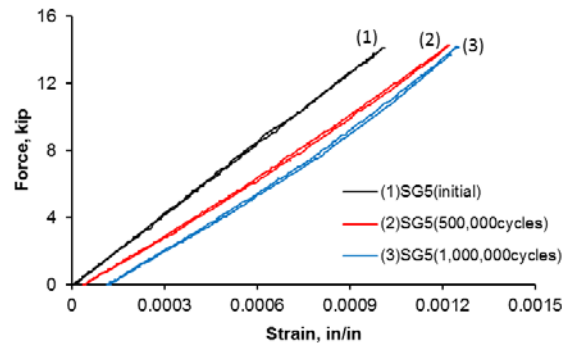


Figure 62. Graph. Load-strain behavior (SG5).

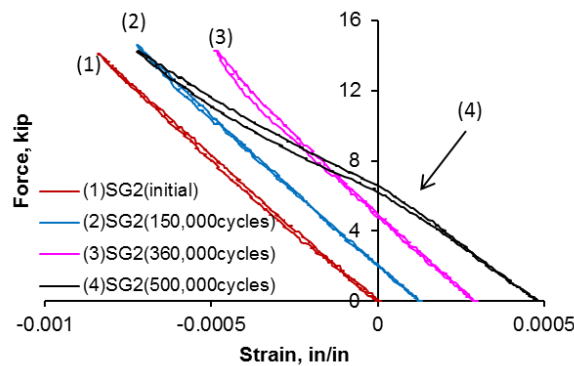


Figure 63. Graph. Load-strain behavior (SG2).

CONCLUSIONS

Based on the experimental program developed, the following conclusions can be drawn:

- The fatigue test shows that there is no stiffness degradation of the FRP panel after 1 million cycles fatigue load (1 to 14 kips of midspan loading).
- Load-deflection plots show a slightly nonlinear behavior of the FRP panel. The panel becomes “stiffer” after the load reaches 6 kips.
- The wearing surface subjected to tension stresses shows no visible damage or cracking after 500,000 cycles fatigue load; the wearing surface subjected to compression shows no visible damage or cracks after 350,000 cycles fatigue load.
- Load-strain behavior of SG2, located on the top surface near the applied loading plate, indicates the possibility of localized damage of the FRP deck (or strain gage) area at that location at 360,000 fatigue cycles.

APPENDIX I: PANEL-TO-PANEL FIELD JOINT REPORT

DESCRIPTION OF TESTED SPECIMEN

The test specimen for a panel-to-panel field connection was made by joining the edges of two small panels together (FRP tubes and outer wrap) and filling the gap between them with an epoxy grout compound and aggregate, as shown in figure 64. The width of the specimen is 18 inches. The cross section dimensions are shown in figure 65.



Figure 64. Photo. Panel-to-panel field joint.

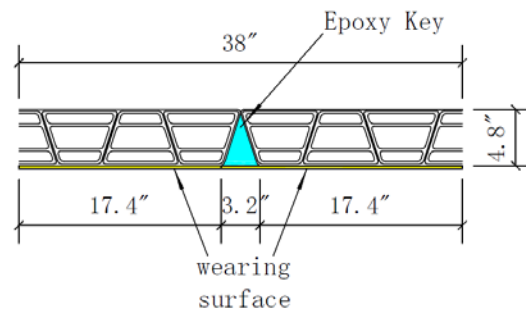


Figure 65. Diagram. Cross section dimensions.

DESCRIPTION OF TEST SETUP

Figure 66 shows the test setup. The FRP panels were loaded using an 18-inch-long steel roller (2 inches in diameter). Two steel I beams (4 inches by 6 inches by 0.2 inches) were used for support between an 8-inch span length (centerline to centerline). Due to the gap created by the wearing surface between the FRP panel and supports, neoprene pads were used on top of the steel supports to more evenly distribute the loading. A 220-kip load cell was used to collect load data. One string pot was placed at the midpoint of bottom face of the specimen (grout key) to measure the vertical displacement. Two LVDTs were placed on the top face of the panel at the centerline of each steel support and 3 inches away from the panel side to measure the deformation of the FRP specimen at the supports; it will be assumed that any deformation at this location will come primarily from the neoprene pads deformation underneath. One strain gage (SG) was installed at the side of the epoxy “key” near the bottom face to measure possible tension strains generated at

this location. The specific locations of the string pot, LVDTs, and strain gage are shown in figure 66.

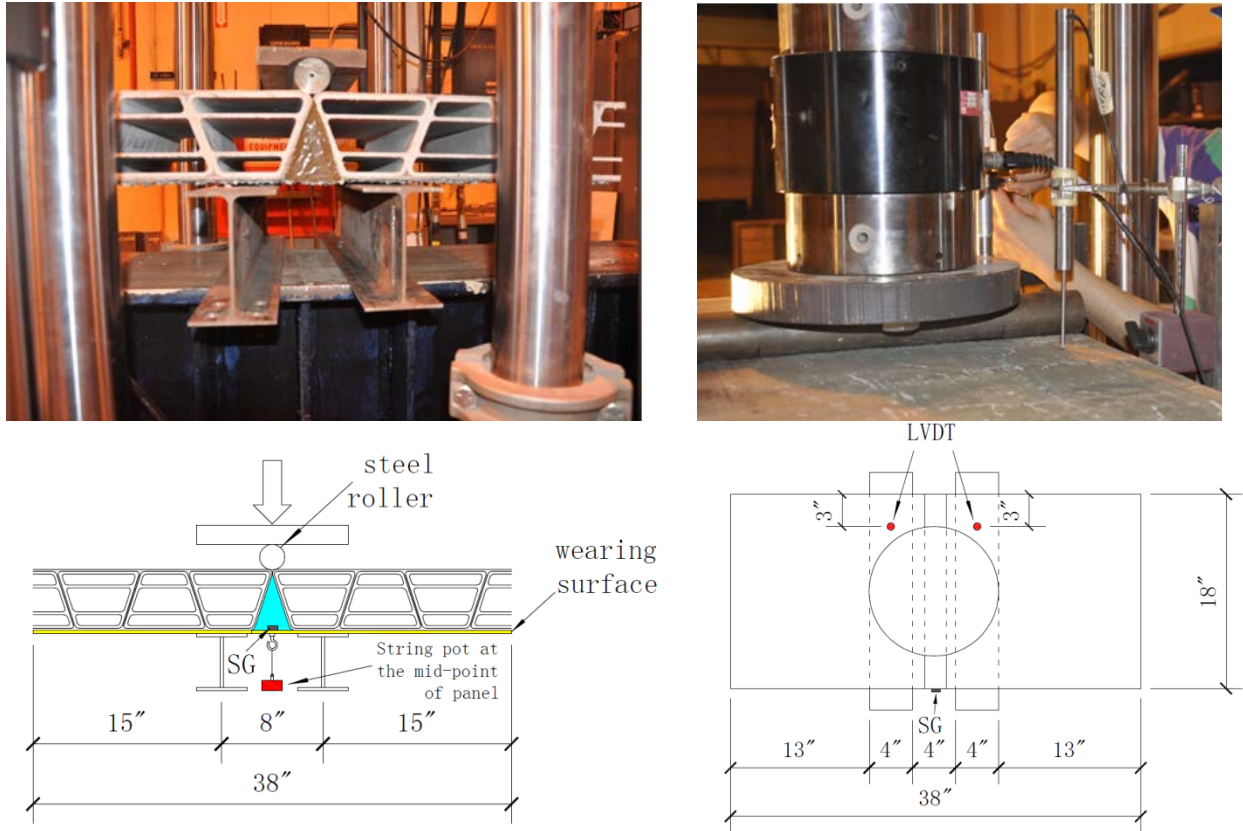


Figure 66. Photos and diagrams. End panel connection test setup.

TEST PROGRAM

The panel was loaded under displacement control. A small cracking sound was heard at 5 kips. A visible crack at the interface between the epoxy key and one of the end panels was observed at a load of 7 kips, as shown in figure 64. A sudden drop of load occurred at 14.7 kips, and the load dropped to 10.7 kips. A large opening of the interfacial crack was observed at this point. The test continued under increasing displacement, and a very small load increase was registered. The crack opening became wider. At a string pot deflection of 0.275 inches and a corresponding load of 11.8 kips, the bond between the epoxy key and the end panel failed, and the specimen separated into two parts, as shown in figure 69.

Figure 70 shows the load-deflection data from the string pot and two LVDTs. The net specimen displacement was taken as the net value between the displacement measured by the string pot and the mean value measured by the two LVDTs. The resulting plot is shown in figure 71. At the maximum load of 14.7 kips, the net displacement of the specimen is 0.06 inches. The net displacement is 0.11 inches at the failure load of 11.8 kips. The negative displacement values in figure 71 may be due to the uneven distribution of reaction forces on the neoprene pads at very small applied loads. It is possible that this caused one of the LVDTs to deform more than the

other one and the string pot at the same load level (up to 5 kips of applied load), as shown in figure 70.

Figure 72 shows the load-strain behavior of the epoxy key. It shows an overall linear behavior. The maximum tensile strain at failure load is $534 \mu\epsilon$.



Figure 67. Photo. Crack at load of 7 kips.



Figure 68. Photo. Crack at maximum load of 14.7 kips.

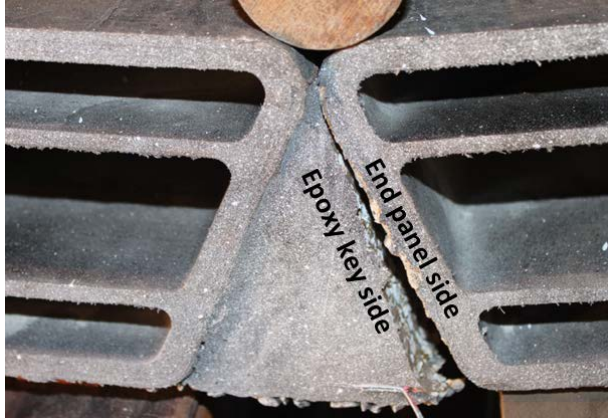


Figure 69. Photo. Failure of the specimen (11.8 kips).

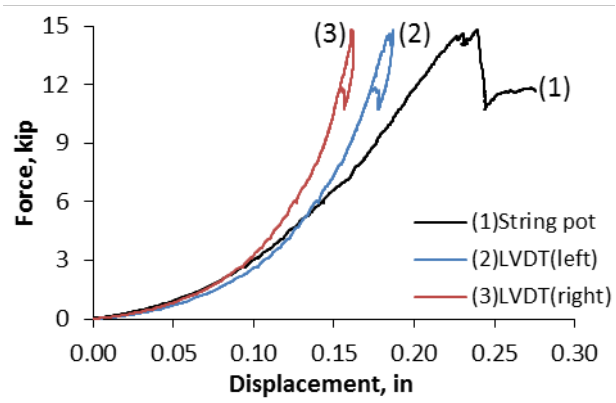


Figure 70. Graph. Load-deflection behavior.

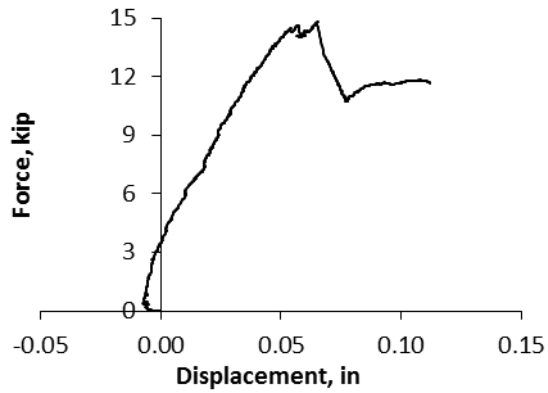


Figure 71. Graph. Net specimen displacement.

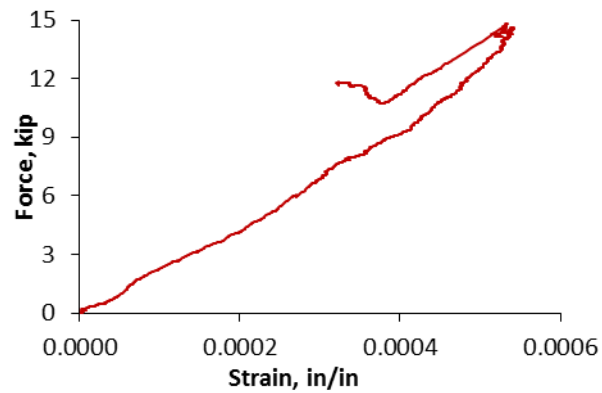


Figure 72. Graph. Load-strain behavior of the epoxy key.

Figure 73 shows the two surfaces of the failed specimen. It should be pointed out that a layer of wearing surface was applied on the surface of the end panel prior to filling out the gap with epoxy compound to form the epoxy key. After failure, it was observed that the aggregates of the wearing surface were almost totally detached from the end panel surface and were primarily attached to the epoxy key side. The end panel failed surface shows a layer of the epoxy from the wearing surface and a small remaining portion of the aggregates. The crack line is shown as a dotted line in Figure 11.

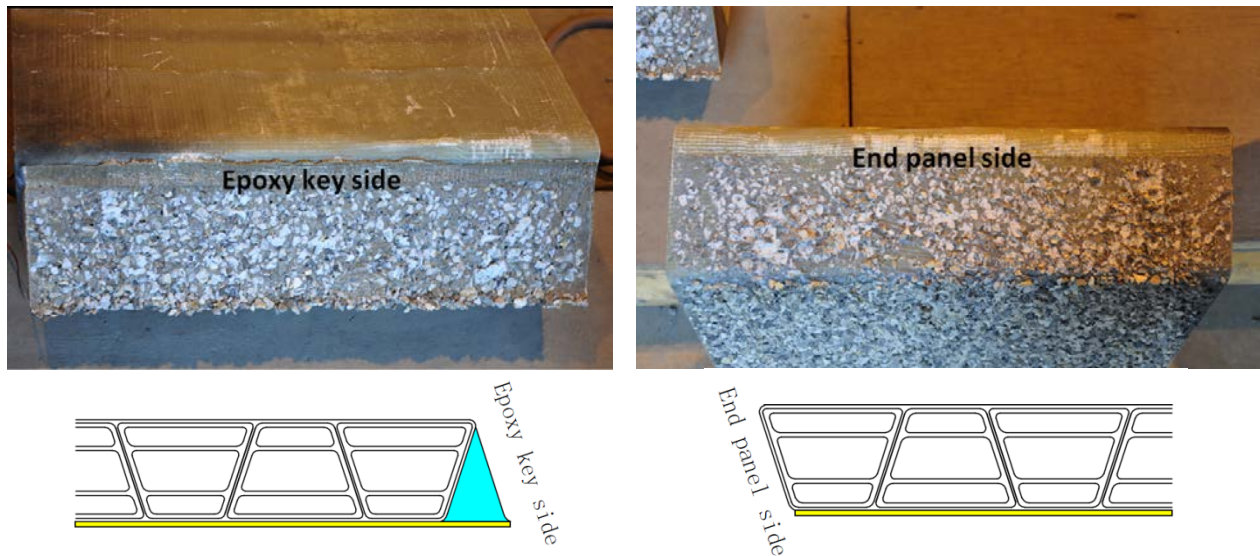


Figure 73.. Photos The two failed surfaces.

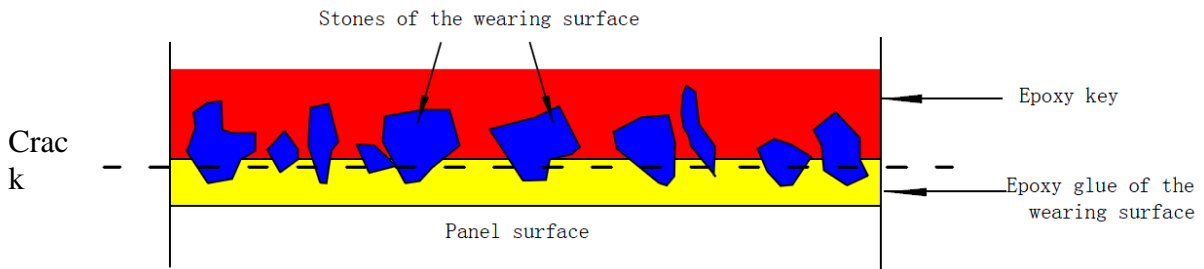


Figure 74. Diagram. Sketch of the crack line.

CONCLUSION

The FRP end panel connection specimen was built joining two smaller end panels (FRP tubes and outer wrap) and filling their gap with an epoxy compound and aggregate. The specimen failed by a crack propagating at the interface between the epoxy key and one of the end panel surfaces. It can be characterized as a bond failure between the wearing surface and the end panel. The maximum obtained load was 14.7 kips; the maximum tensile strain registered on the epoxy key was 534 $\mu\epsilon$. The failed surfaces showed that the aggregates of the wearing surface were almost totally detached from the end panel surface and were primarily attached to the epoxy key side.

APPENDIX J: BRIDGE RAILING POST ANCHORAGE PROOF TEST

DESCRIPTION OF THE TEST SPECIMEN

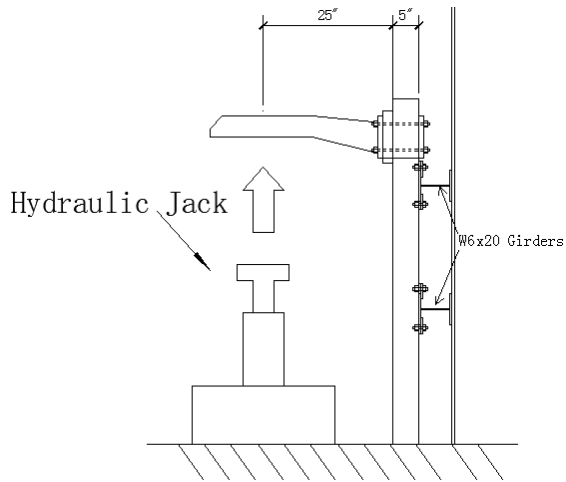
An empty FRP panel, used previously to determine flexure stiffness (panel #3), was selected to fabricate the railing post-FRP deck connection. The FRP panel consisted of seven FRP tubes with the narrow side of the panel facing the rail. A steel railing post was mounted over a high-density polyethylene (HDPE) pad and attached to the FRP deck using four 1-inch threaded anchors, connecting the railing post to a steel base plate on the bottom face of the FRP deck. Figure 75 shows details of the different components of the railing post specimen. The steel base plate had four bolts welded onto the plate; the anchor rods were bolted to the rail base until they felt “snug-tight.”



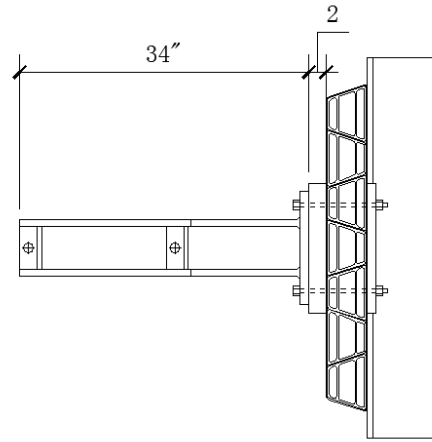
Figure 75. Photos and sketch. Railing post specimen.

DESCRIPTION OF TEST SETUP

Figure 76 shows details of the specimen test setup. Two steel beams (W6x20) were used to attach the FRP panel to a structural frame; their distance to the railing post base as well as to each other was based on the full-scale prototype. A hydraulic ram (22-ton capacity and 6-inch stroke) was used to apply force on the railing post at 25 inches from the base of the deck panel. The FRP deck was connected to the steel beams using hollo-bolts, flat-clips, and washers (see figure 77) similar to those that will be used in the full-scale prototype. The hollo-bolts were tight using the “turn-of-the-nut” procedure: the nuts were turned 1/3 after snug-tight conditions. After the bolts were tensioned, the torque in each bolt torque was verified using a calibrated torque wrench, and it was found to be in the order of 65 to 75 lb-ft.



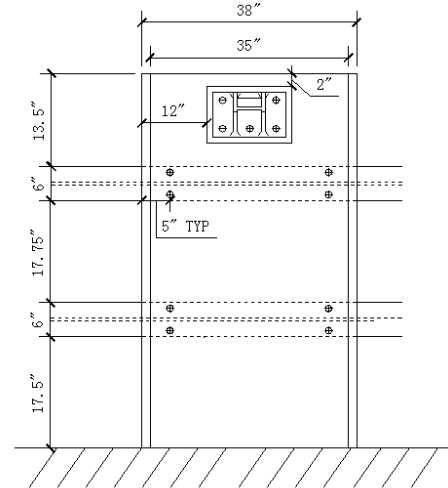
(a) Side View



(b) Top View



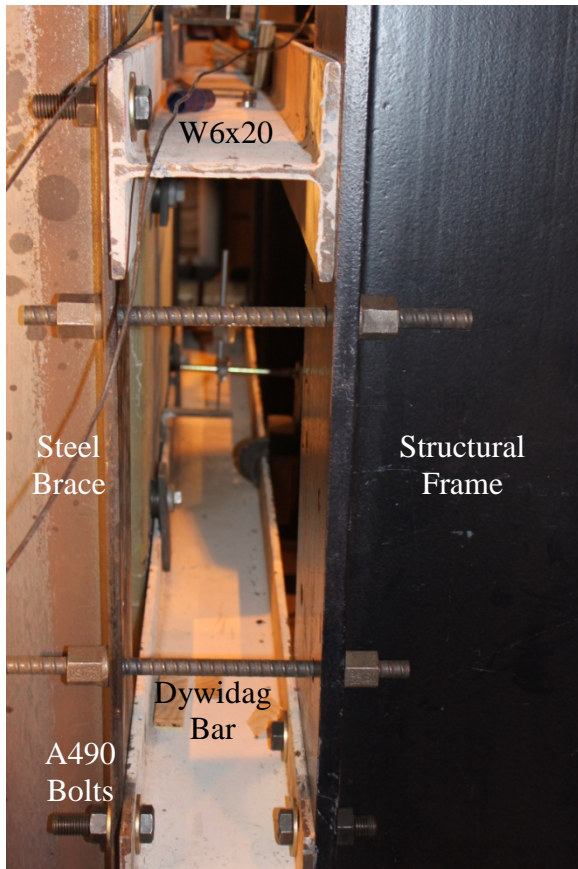
(c) Photograph of Test Set-up



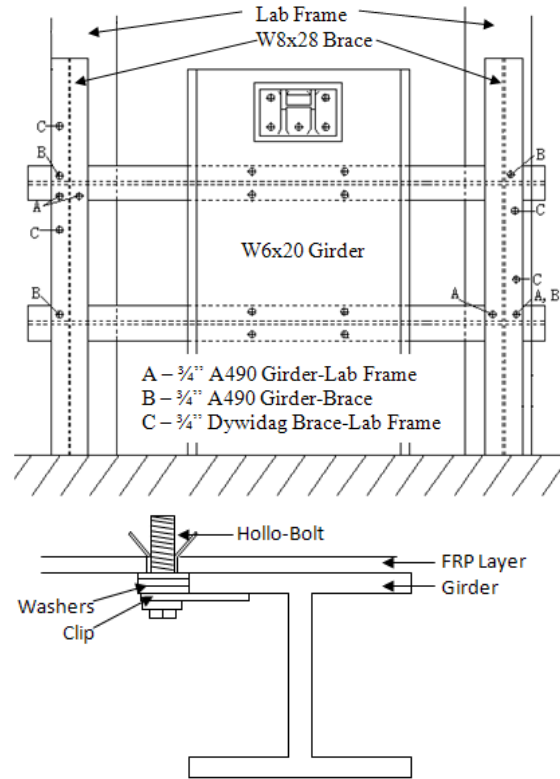
(d) Front View

Figure 76. Photo and diagrams. Railing post test setup.

To secure the W6x20 girders to the structural frame, steel braces, A490 bolts, and dywidag bars were used. Neither the FRP panel nor the braces were directly attached to the floor.



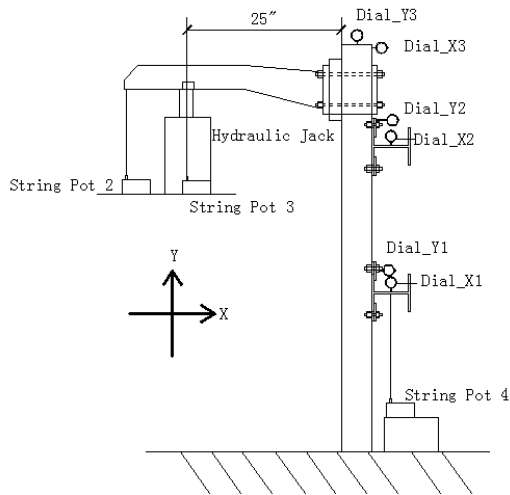
(a) Photograph showing bracing system



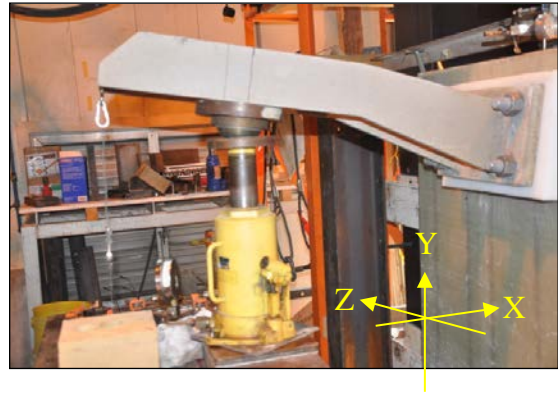
(b) Bracing system & hollo bolt details

Figure 77. Photo and diagram. Detailing of steel beam-structural frame connection.

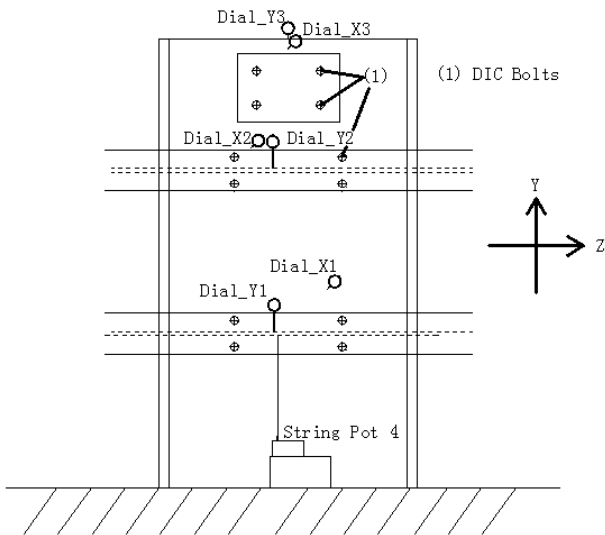
To measure deflections, six dial gages and four string pots were attached to the FRP deck, railing post and W6x20 girders. In addition, digital image correlation was used to monitor the movements of few of the bolts on the back side of the panel. Figure 78 shows photographs and location of all these transducers; their orientation with respect to a Cartesian axis of reference is also indicated in these images.



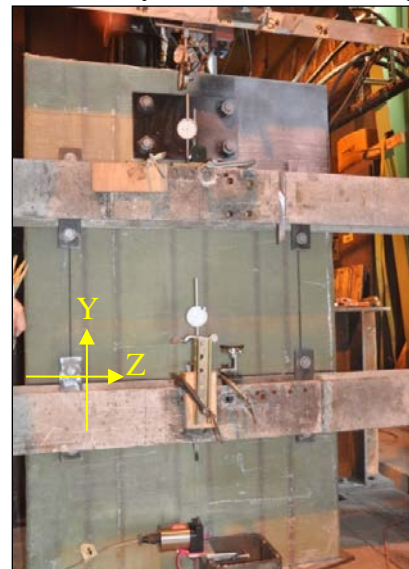
(a) Profile view of gage locations



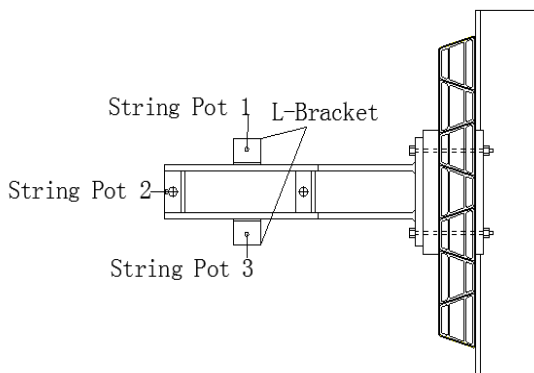
(b) View of hydraulic ram at 32 kip-failure



(c) Back view of gage locations



(d) Photograph of panel back view



(e) Top View of railing post gages



(f) Top view of post & L-brackets - Test 1

Figure 78. Photos and diagrams. Location of transducers used during the test.

TEST PROGRAM

Test Procedure

The first test (Test 1) was completed on July 16, 2012. A 7-inch-diameter steel plate was placed on top of the hydraulic jack to distribute the load; see figure 78f. The specimen was incrementally loaded, and measurements were taken at 0, 3, 6, 9, 12, 13.5, and 15 tons. At 15-ton (30-kip) load, the steel plate sat at a very pronounced angle, so the test was stopped to prevent instability in case of failure. Measurements were not taken during the unloading part.

With a roller support on the ram to increase stability (figure 78b), Test 2 was completed on July 17, 2012. For this test, it was decided to load the specimen to AASHTO TL-2 load level (27 kips), unload incrementally to obtain more complete data, then load the specimen again up to failure (Test 2-Failure) and back down. Table 29 shows the data points recorded for the end rail displacement measured by string pot 2 (see figure 78a) for all tests; figure 79 shows a plot of these data. For Test 2, due to the possibility of large deformations and brittle failures, some transducers were removed (string pots 1 and 3 and the digital image correlation camera); in addition, Dial_X3 and Dial_Y3 replaced two LVDTs to record the data at the same locations.

Table 29. Load-displacement data for string pot 2.

Load (kip)	Deflection (in.)		
	Test 1, Max 30 kip	Test 2, Max 27 kip	Test 2-Failure, Max 32 kip
0	0.000	0.000	0.214
6	0.904	1.171	1.323
12	1.406	1.739	1.916
18	1.941	2.356	2.457
24	2.447	-	2.980
27	2.758	3.114	3.219
30	3.336	-	3.611
32	-	-	4.383
32	-	-	5.208
20	-	2.960	4.850
12	-	-	4.220
10	-	2.205	-
6.4	-	1.815	-
6	-	-	3.520
0	0.419	0.214	1.048

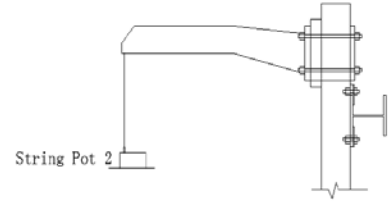
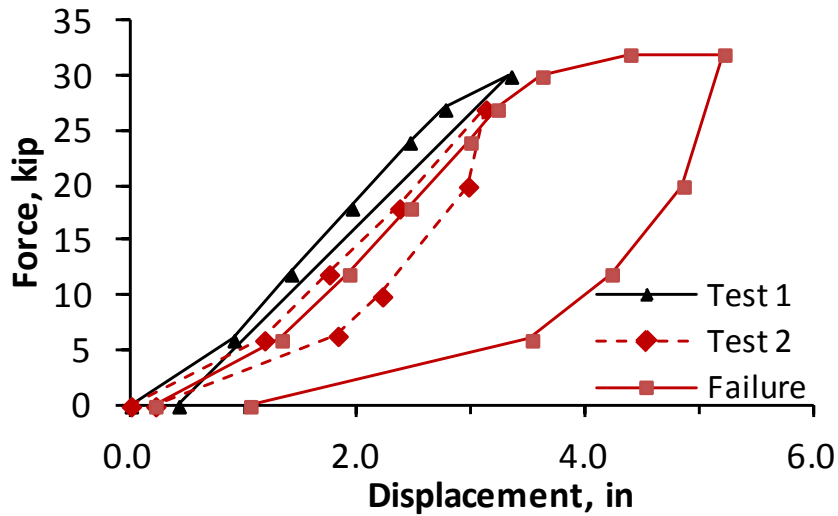
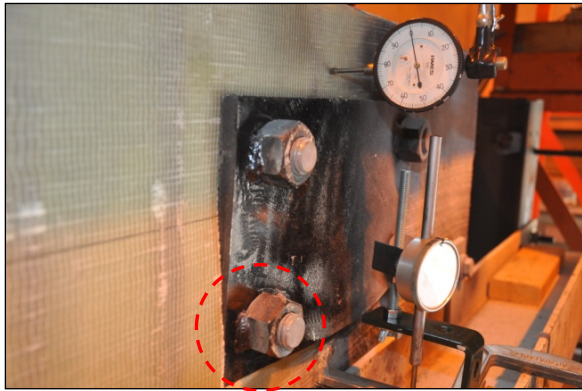


Figure 79. Graph. Load-displacement behavior of railing post end (string pot 2).

Failure Modes

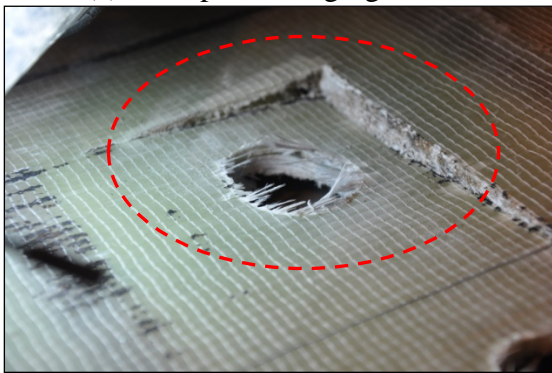
No cracking sound was heard during Test 1 or Test 2 up to 27 kips. When the specimen was reloaded again (Test 2-Failure), cracking sounds were heard around 32 kips. It was also observed that, under increasing displacement, no further load increase was obtained. At a displacement of 5.2 inches, registered by string pot 2 (see figure 78b), the railing post-FRP deck connection failed when a corner of the back steel plate was pulled (wedged) into the FRP deck, as shown in figure 80a. As noted, the significant deformation of the rail base and HDPE pad is believed to be the reason for the increasing pulling forces on the bolts at the bottom of the steel base plate. The steel plate was bent as a result of this pulling effect; figure 80b shows the extent of the deformation. The wedging effect caused a local shear failure of the deck through the first layer of the tubes (aka punching shear), shown in detail in figures 80c and 80d. Post-test visual observations of all bolt holes in the FRP panel both at the railing post and hollo-bolt connections revealed no signs of bearing failure. Figure 79 shows that non-linear deformation (most likely coming from the failure of the connection) started between 30 and 32 kips. Permanent deformation registered by string pot 2 was in the order of 1 inch.



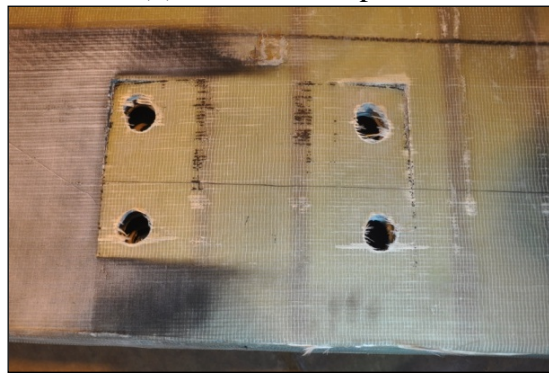
(a) Steel plate wedging failure



(b) Bent on steel plate



(c) FRP deck panel failure-close-up

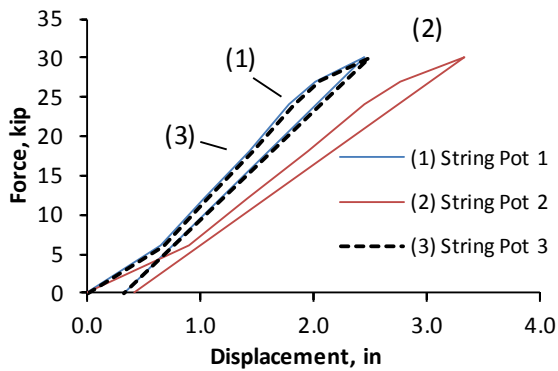


(d) FRP deck failure-photograph post-test

Figure 80. Photos. Failure mode of the railing post-FRP deck panel connection.

Vertical Displacement of the Railing Post

In Test 1, three string pots were attached to the railing post to measure its total vertical displacement relative to the ground. String pots 1 and 3 were used to monitor any possible rotation of the railing post during loading, whereas string pot 2 was placed at the railing post end; see figure 81. Results indicate that the railing post was loaded symmetrically across its width.



(a) Railing post load-displacement behavior



(b) Photograph of 3 string pots used

Figure 81. Graph and photo. Vertical displacement of the railing post, Test 1.

The large amount of vertical displacement registered by the string pots indicates that, in addition to the railing post deformation, other sources of deformation also contributed to this displacement: 1) the rotation and movement of the anchor bolts connecting the post to the FRP deck panel, which in turn allowed for railing post base and HDPE rotation, 2) the HDPE pad deformation, 3) the FRP deck panel deformation, 4) the possible movement of the hollow bolt connections, and 5) movement of the bracing system used to secure the steel beams to the structural frame. Figure 82 shows a sketch illustrating these possible sources of deformation. In the next sections, they will be described in more detail.

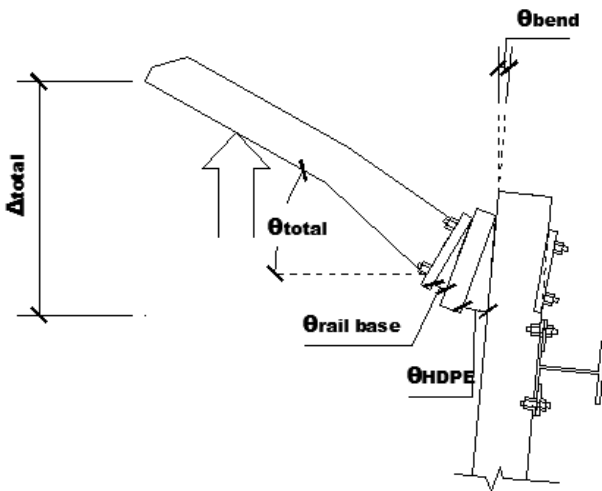


Figure 82. Diagram. Railing post connection (deformed shape, not to scale).

Contributors to the Railing Post Vertical Displacement

The total vertical displacement at the end of the railing post at 27 kips (AASHTO TL-2), and failure (32 kips) was 3.11 inches and 5.21 inches, respectively. The deformation of the HDPE pad was found to be a significant contributor of this vertical displacement. (For reference, the AASHTO Load and Resistance Factor Design Bridge Design Specification for TL-3 and TL-4 uses 54 kips; rail heights are also higher.)

HDPE Deformation

The four corners of the HDPE pad closest to the railing post base were measured against the FRP deck face using calipers. Table 30 shows values of the change in distance from the original position at zero-load for Test 2. Corners A and B are located toward the edge of the FRP deck panel, whereas corners C and D are on the opposite side, see figure 83.

The measurements show that the HDPE pad at corners A and B was compressed under increasing load, whereas corners C and D were stretched. A straight bar was used during testing to confirm that the HDPE pad was bending under increasing load; therefore, it cannot be assumed that it deforms as a rigid plate. After failure of the steel plate and unloading of the specimen, permanent deformation of the HDPE was also measured at the corners.

To estimate the contribution of the HDPE deformation to the vertical railing post displacement, its rotation was calculated based on the deformations recorded in table 30. At 27 kips of applied load, it was estimated that the vertical deflection at the end of the railing post corresponding to the HDPE rotation was in the order of 40 percent of the total value measured by string pot 2. It is also expected that the HDPE deformation would have greatly increased the tension forces in the bottom two bolts of the railing post connection. The gap between the railing post base and the HDPE pad was measured in the vicinity of the maximum load of 32 kips and found to be in the order of 0.125 inches.

Table 30. Test 2 HDPE pad deformation.

Load (kip)	Horizontal Displacement from FRP deck surface (in.)			
	Corner A	Corner B	Corner C	Corner D
0	0.000	0.000	0.000	0.000
12	0.039	0.038	-0.221	-0.171
18	0.047	0.033	-0.269	-0.211
27	0.055	0.055	-0.352	-0.313
30	0.063	0.056	-0.425	-0.386
0	-0.020	0.004	-0.146	-0.094

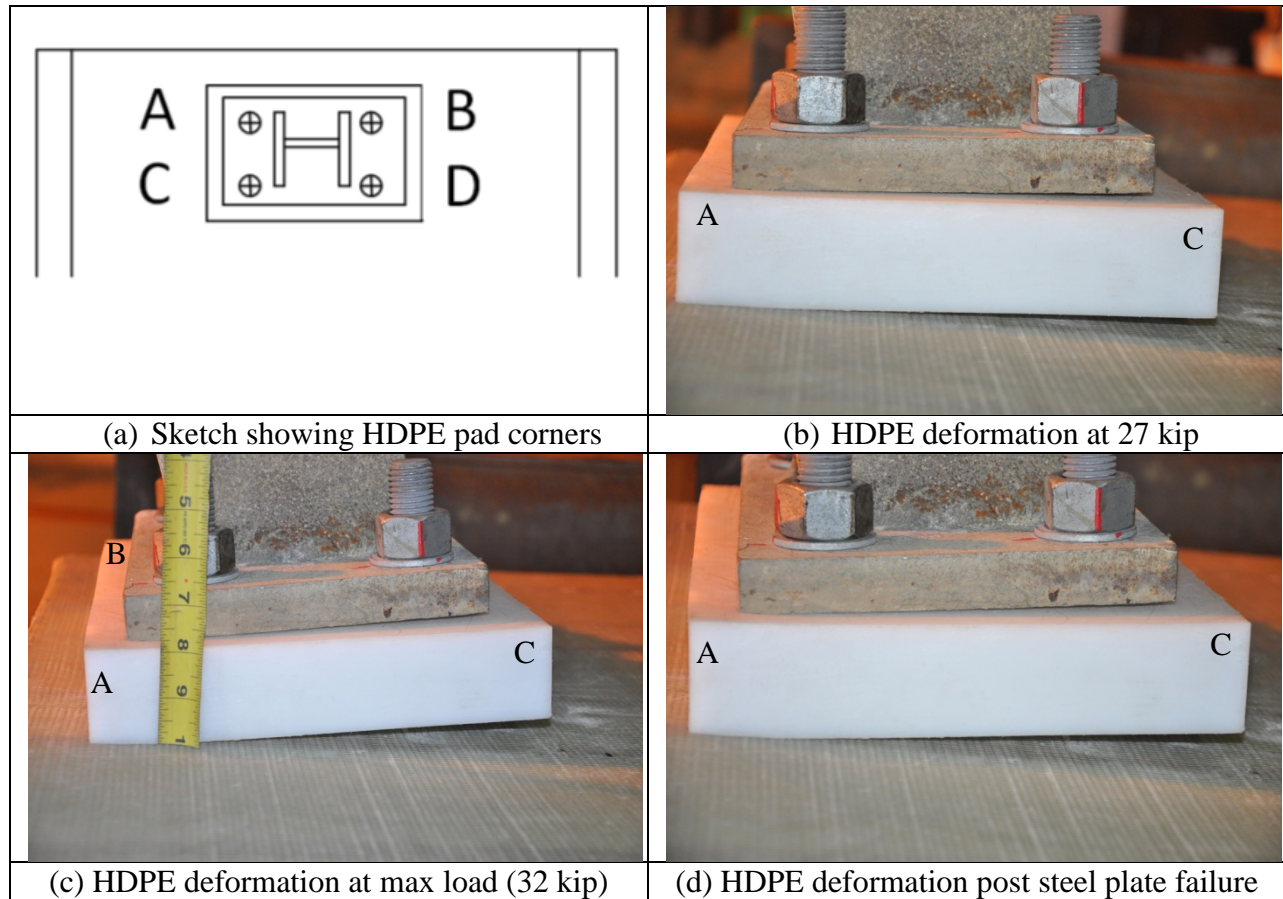


Figure 83. Photos. HDPE deformation at different loading levels, Test 2.

FRP Deck Deformation

Movement of the FRP deck panel in two directions was recorded using LVDTs and dial gages. Displacement in the direction perpendicular to the applied load (x-direction) was estimated from dial gages Dial_X1, Dial_X2, and Dial_X3. Dial_X2 and Dial_X1 measure the FRP deck movement with respect to the top and bottom steel girder, whereas Dial_X3 measures the total movement of the top of the panel relative to the structural frame (attached to the floor). Figure 84 shows these deformations for Test 2. As expected, the deformation of the FRP deck panel is larger toward the cantilever edge and smaller near the steel girder support. At the location near the second (bottom) steel girder, the FRP panel experiences a reversed curvature, thus deforms in the opposite direction than the cantilever edge. The curves on figure 84 show that the FRP deforms linearly up to 30 kips; beyond that load level, non-linear deformations appear, possibly associated with the damage of the railing post connection. At 27 kips, the displacements registered by Dial_X3, Dial_X2 and Dial_X1 are 0.195, 0.188, and -0.233 inches, respectively.

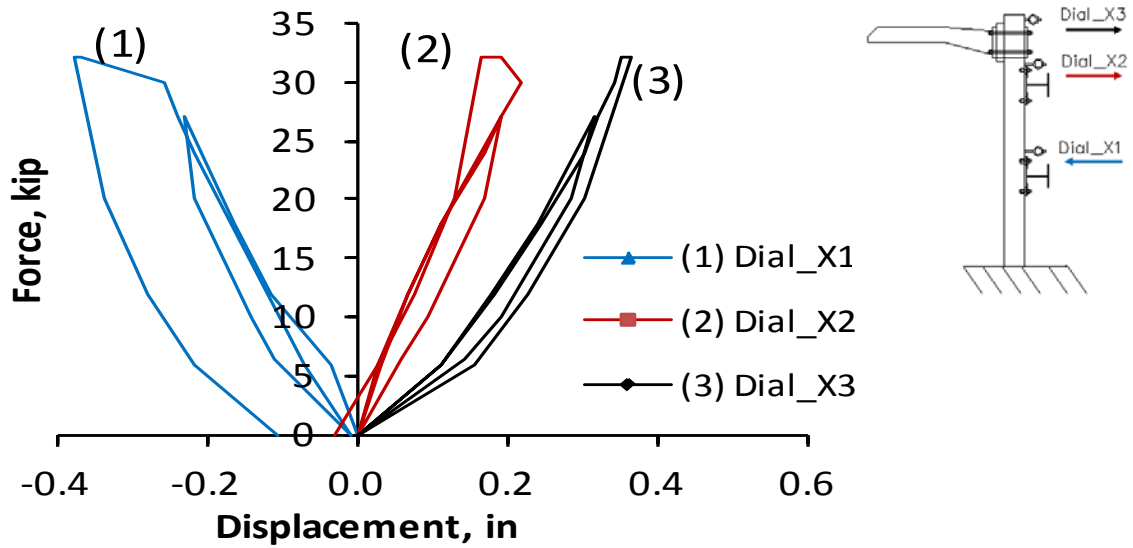


Figure 84. Graph. Horizontal deflection (x-direction), Test 2.

Figure 85 shows the vertical displacements (in the y-direction) recorded by the three dial gages during Test 2. Dial_Y1 and Dial_Y2 measure the vertical movement of the FRP panel relative to the adjacent steel girders while Dial_Y3 measures the overall movement of the top of the FRP panel (with respect to the structural frame, attached to the floor). As expected, the displacement of the top of the FRP panel is larger than those near the steel girders. The behavior of Dial_Y3 shows that the panel does not return to its initial position after the first unloading. After failure of the railing post connection, the specimen was unloaded; the permanent displacement of the FRP deck at the top was found to be 0.058 inches.

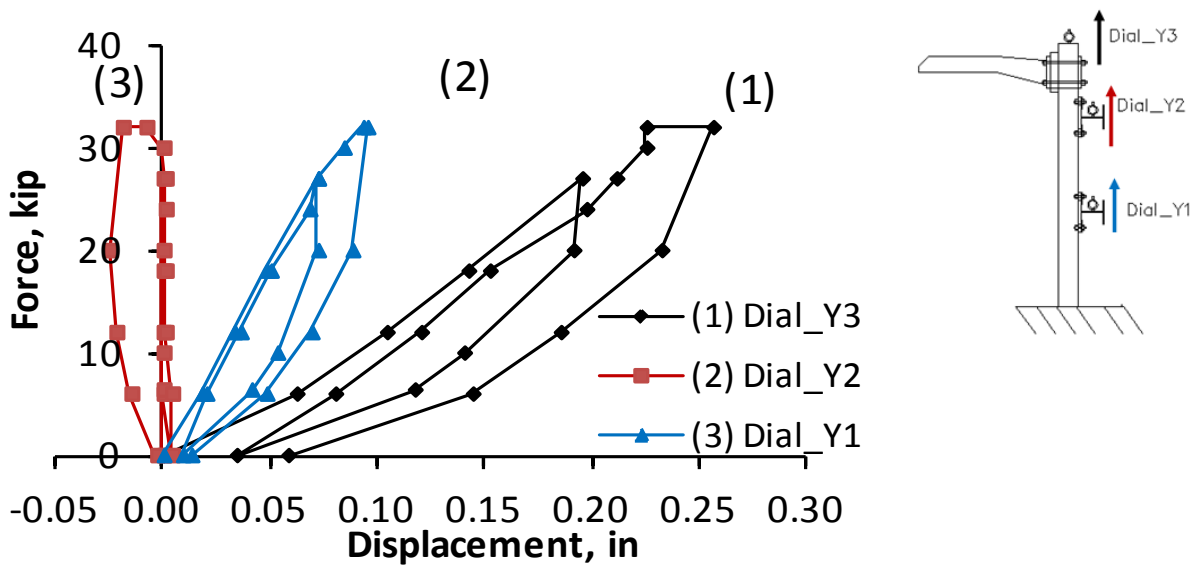


Figure 85. Graph. Vertical displacement (y-direction), Test 2.

The vertical displacement at the top of the FRP panel (Dial_Y3) is a combination of the relative movement of the steel girders with respect to the structural frame, as well as the true “elongation” of the panel under loading. To evaluate the magnitude of the FRP elongation, the deflection of the bottom girder relative to the floor was measured by string pot 4 (see figure 86). At 27 kip of loading, string pot 4 registered 0.082 inches. This small deflection suggests that the brace and bolt system used to hold the steel girders and FRP deck panel system in place, performed well. Overall, this global movement was limited to about 3 percent of the total movement railing post end displacement.

At 27 kip of loading, the top of the FRP deck panel displaced 0.195 inches (captured by Dial_Y3). Assuming that the first steel girder deformed in similar magnitude as the second girder (measured by string pot 4), it can be assumed that the FRP elongated 0.113 inches at this loading (4 percent of the vertical deflection measured by string pot 2, discussed previously).

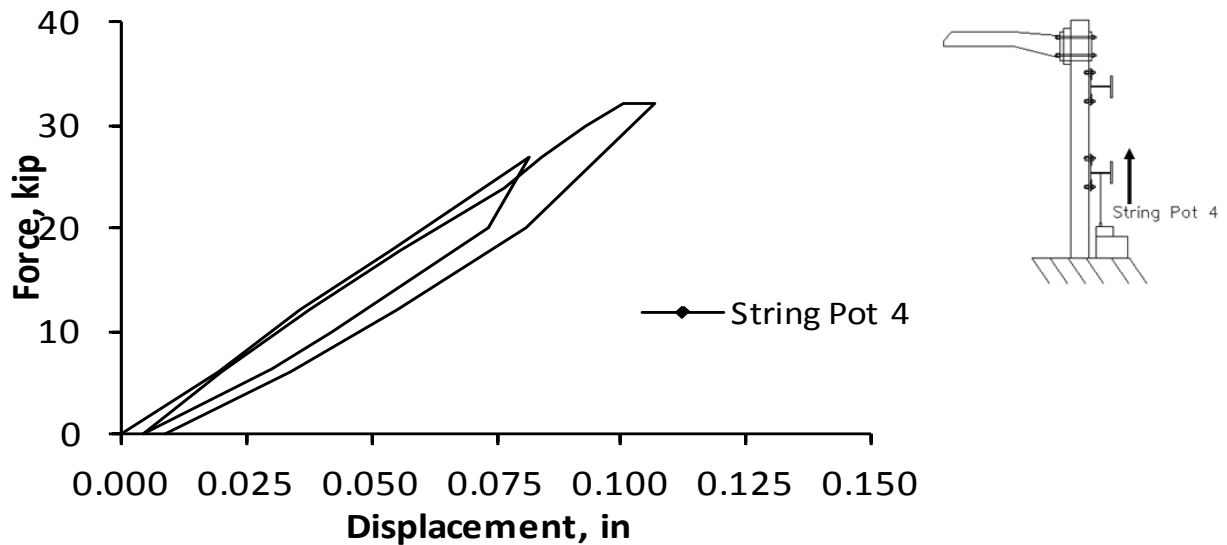
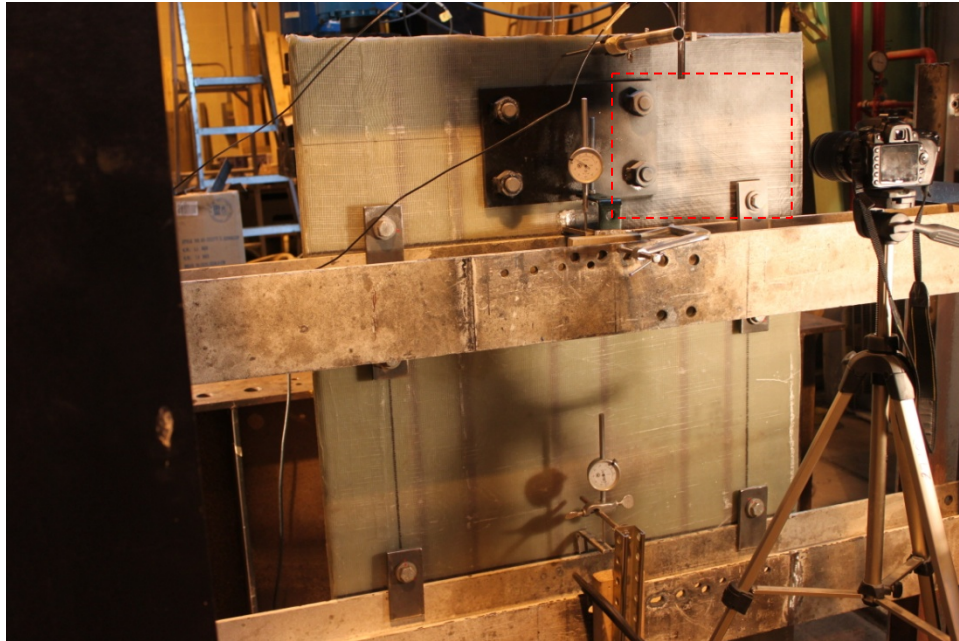


Figure 86. Graph. String pot 4 movement, Test 2.

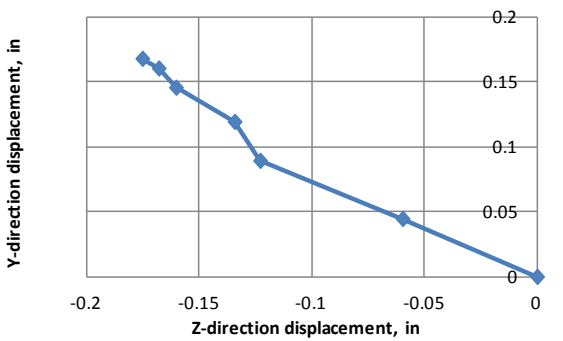
Bolt Movement

The digital image correlation technique was used to monitor the movement of three bolts in the back of the FRP deck panel during Test 1 (loading up to 30 kips and unloading): two bolts on the steel base plate and one on the steel fastening clip. To protect the digital equipment, digital image correlation was not used during Test 2 to failure. Figure 87 shows the location of the monitored bolts as well as their movements, with increasing loading with respect to the Cartesian coordinate system used in this report (y, z axis).

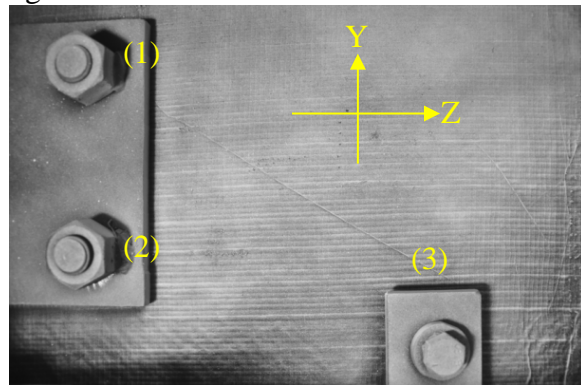
Bolts 1 and 2 were expected to have similar movements with respect to each other since they were both attached to the steel base plate. They both show similar displacements (0.17 inches upward) in the y axis, but their displacements in the z axis are in the opposite directions. Bolt 3 (expansion bolt connecting the FRP panel to the first steel girder) showed smaller displacement values in the y direction (0.10 inch), but similar in magnitude to the global displacement measured by string pot 4.



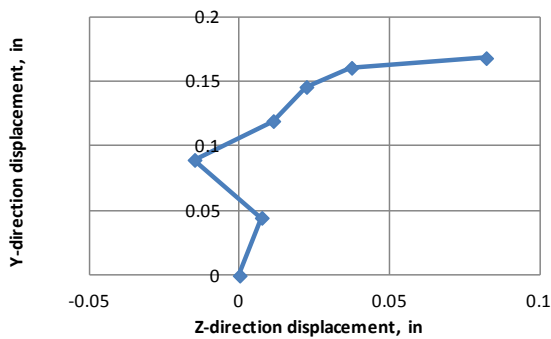
(a) Photograph of the back of the FRP deck; area used for digital image correlation is highlighted



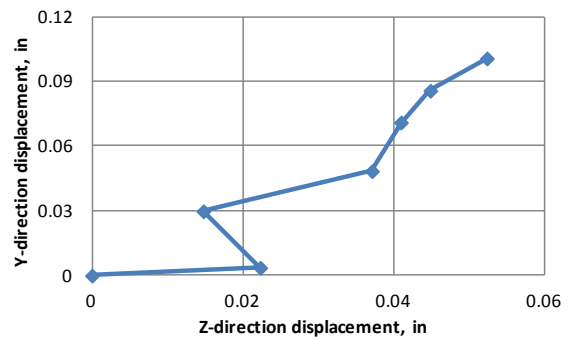
(b) Bolt 1 displacement



(c) Bolt locations



(d) Bolt 2 displacement

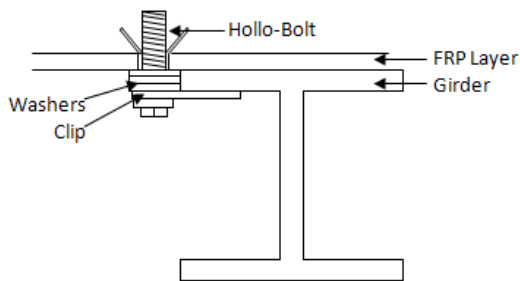


(e) Bolt 3 displacement

Figure 87. Photos and graphs. Movement of three bolts on FRP back panel using digital image correlation, Test 1.

Expansion Bolt Connection

As indicated before, the FRP deck was connected to the steel beams using 5/8-inch-diameter expansion (hollo) bolts, flat-clips, and 3/8-inch-diameter washers (see figure 88a). The expansion bolts were tightened using the “turn-of-the-nut” procedure. The bolt length (3 inches) allowed them to pass through two walls of the FRP tubes, as shown in figure 88b. During the testing of the railing post, the movement of one of the bolts was monitored using digital image correlation, showing very small displacement values that can be related to the movement of the steel girders. After the test was concluded, visual inspection of all the bolt holes in the FRP panel revealed no signs of bearing failure. It can be inferred that the bolted connection was able to effectively hold the FRP panel in place, up to the load and displacement levels when the railing post connection failed.



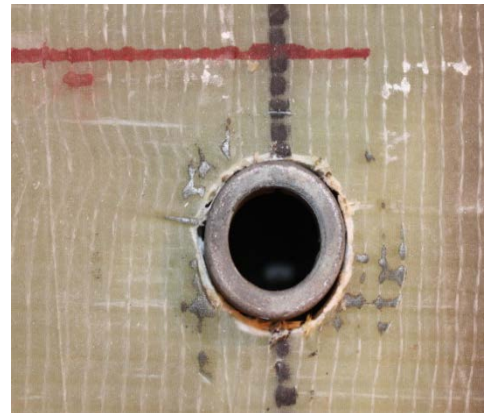
(a) Sketch of bolt connection



(b) Cross section of FRP tube & connection



(c) Profile view of bolted connection



(d) Typical FRP deck hole (post test)

Figure 88. Diagram and photos. Expansion bolt connection.

CONCLUSIONS

- The railing post connection, as tested, meets the AASHTO TL-2 required capacity of 27 kips.
- Under the applied loads, the vertical railing post end displacement was in the range of 3 inches at 27 kips and over 5 inches once loaded to a failure load of 32 kips. This displacement is attributable to many contributing factors.
- Deformations of the HDPE pad were found to significantly contribute to the displacement of the railing post during test.
- At loads between 30 and 32 kips, the corners of the steel base plate were wedged through the first layer of the FRP tube; this was defined as the “failure” stage of the test.
- Based on post-testing observations, none of the bolt holes in the FRP deck panel exhibited bearing failures.
- The bracing system used was effective in limiting the FRP panel/steel girder movement to about 0.1 inches upward.

APPENDIX K: WEARING SURFACE TEST

DESCRIPTION OF THE TEST SPECIMEN

A section of an FRP panel, similar to the specimen used for the end panel connection test (see Appendix I), and with a wearing surface composed of adhesively bonded flint aggregate, was tested following ASTM D 7522 guidelines. The stone was identified as R65-8. The gradation was such that 65 percent is retained on a #8 sieve and 20 to 30 percent is retained on a #6 sieve. Test results provide the pull-off strength of the adhesive bonded to the FRP surface, as well as the pull-off strength of the aggregate embedded into the adhesive. Figure 89 shows photographs of the specimen and the wearing surface.



Figure 89. Photos. FRP specimen used for pull-off tests.

DESCRIPTION OF TEST SETUP

Two test areas were prepared for the two different interfaces (see figure 90). To test the adhesive-FRP pull-off strength, the layer of aggregate was removed with a hand grinder. Special attention was given not to remove the adhesive layer. The area was cleaned, and dollies 1, 2, 3, 7, 8, and 9 were bonded with a two-part epoxy. After 24 hours of curing, the areas around the dollies were scored through the layer of adhesive and into the FRP. To test the pull-off strength of the aggregate to the adhesive, the second test area was cleaned and loose aggregate removed. Zones with an even amount of aggregate were chosen (to minimize bonding of the epoxy and the adhesive). Dollies 4, 5, and 6 were not scored because it was feared the drill would rip the aggregate out as opposed to grinding it.

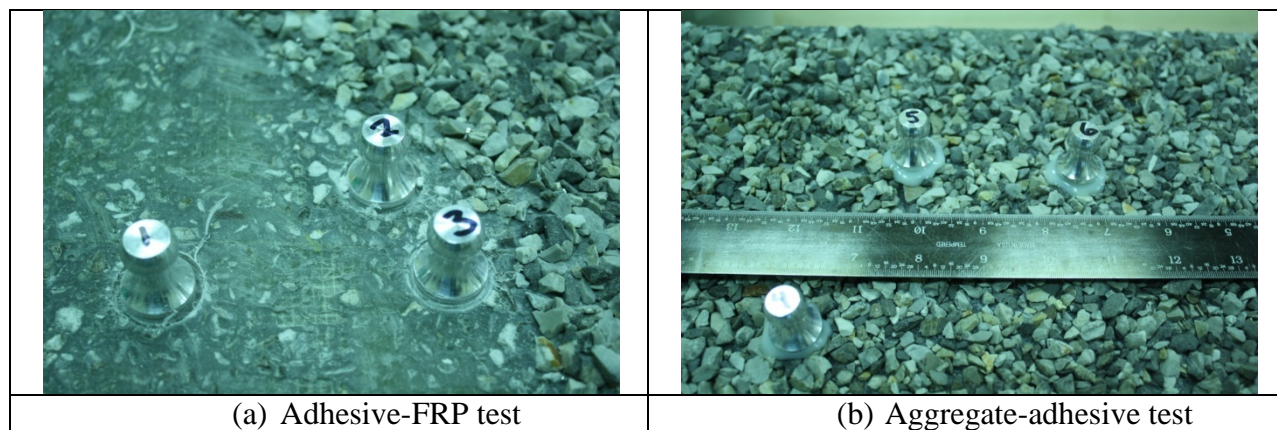


Figure 90. Photos. Dollies mounted to two test areas.

TEST PROGRAM

Using a pull-off adhesion tester, all the dollies were removed. Due to incorrect calibration, data from dollies 1, 2, and 3 were rendered invalid. Results from testing the remaining dollies are presented in table 31.

Table 31. Pull-off test results.

	Specimen	Recorded Stress (psi)	Area Corrected Stress (psi)
Adhesive to Aggregate	4	621	292
	5	886	380
	6	767	372
Adhesive to FRP	7	850	850
	8	900	900
	9	726	726

Figure 91 shows the failure surface for dollies 4, 5, and 6. Since failure did not occur along the dolly perimeter, as the apparatus assumed, the stress was calculated over the area within the aggregate perimeter. The average “area corrected” stress, reported in table 31, was only 348 psi, which reflects how easily individual pieces could be removed by hand on the original specimen prior to testing.



Figure 91. Photos. Failure surfaces of aggregate to adhesive pull-off tests (dollies 4, 5, and 6).

Dollies 7, 8, and 9, shown in figure 92, had higher pull-off strength, with an average of 825 psi. The failure occurred along the adhesive-epoxy interface, so no area correction was required. Some small pieces of aggregate that were too close to the FRP layer to be removed when grinding was done, appeared in the failure surface, thus indicating that the bond strength between the aggregate and the adhesive will always be the weakest layer and that the bond strength between the adhesive and the FRP surface is stronger than 825 psi.

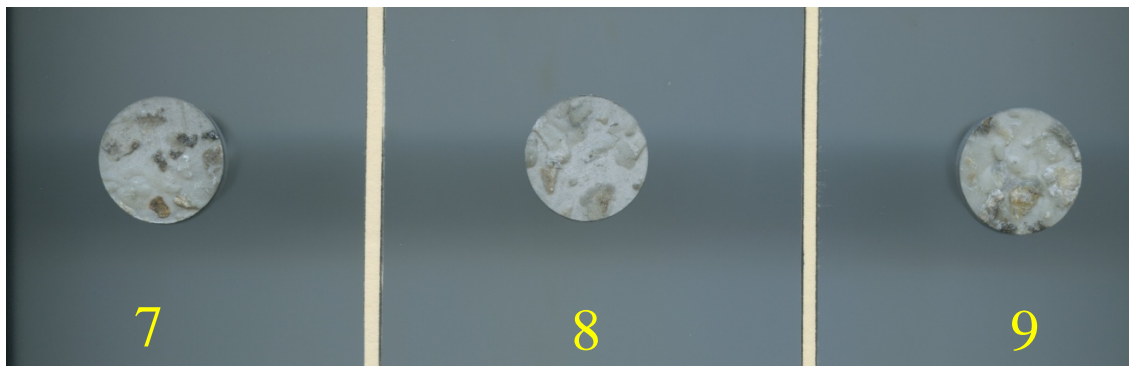


Figure 92. Photos. Failure surfaces of adhesive to FRP pull-off tests (dollies 7, 8, and 9).

APPENDIX L: FIRE TEST REPORT

DESCRIPTION OF TESTED SPECIMEN

A full-depth panel measuring 3 feet by 7 feet was tested to evaluate its fire resistance properties. The standard design of the panel uses fire-resistant resin, but no further protection was provided. It was tested without a wearing surface. See figure 93.



Figure 93. Photo. Test panel mounted on top of fire chamber.

DESCRIPTION OF TEST SETUP

The test specimen was placed over the pilot scale combustion chamber, resting atop and perpendicular to two structural steel support beams (I-beams) spaced 24 inches on center (to be consistent with the proof-of-concept bridge in Allegany County). The support beams each measured 10.5 inches high with 4-inch-wide flanges and 0.25-inch web thickness. The surrounding exposed areas were enclosed with 1-inch-thick non-combustible gypsum shaft liner panels. Only a portion of the length was exposed to the fire over the combustion chamber.

Figure 94 shows the fire test chamber and the steel beams used to support the deck. This picture was taken after the test; note the peeled paint above the fire chamber.



Figure 94. Photo. Support beams spaced at 2 feet.

The panel was loaded to a total superimposed load of 1,600 lb, nominally, using a water-filled steel tank, shown in figure 95, and instrumented with numerous thermocouples. Figure 96 and table 32 detail the placement of the thermocouples. The tank rested on the wood shown at the center of figure 93. This wood was dimensioned to reflect the standard AASHTO 10-inch by 20-inch footprint of a design vehicle.



Figure 95. Photo. 1,600-lb water tank used as concentrated load.

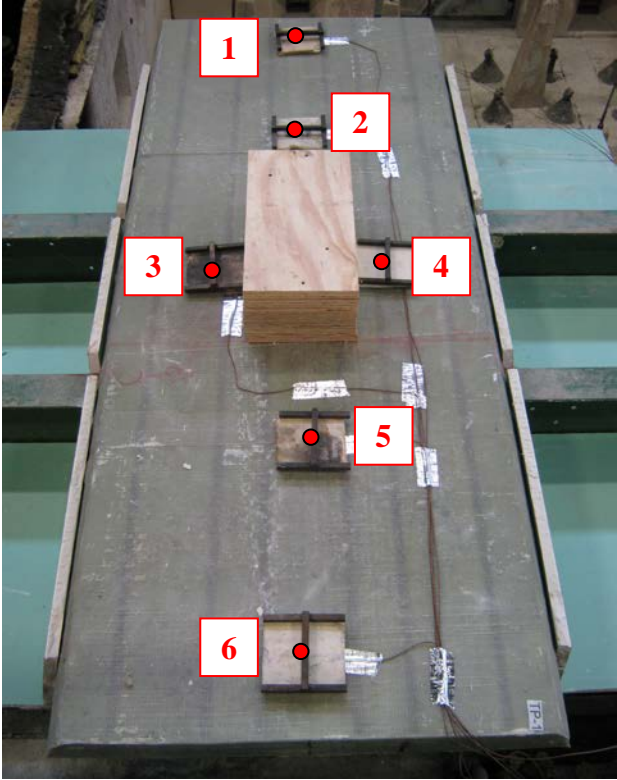


Figure 96. Photos. Placement of thermocouples on the test panel.

Table 32. Details of thermocouple placement.

Thermocouple	X, Y Location	Z Location
TC01	on longitudinal axis, 42" from transverse axis	top surface of deck panel
TC02	on longitudinal axis, 24" from transverse axis	top surface of deck panel
TC03	10" from longitudinal axis, on transverse axis	top surface of deck panel
TC04	10" from longitudinal axis, on transverse axis	top surface of deck panel
TC05	on longitudinal axis, 24" from transverse axis	top surface of deck panel
TC06	on longitudinal axis, 42" from transverse axis	top surface of deck panel
TC07	on longitudinal axis, on transverse axis	1-3/8" from top surface of deck panel
TC08	on longitudinal axis, on transverse axis	3-1/2" from top surface of deck panel
TC09	on longitudinal axis, on transverse axis	4-5/8" from top surface of deck panel

TEST PROGRAM

The panel was loaded with the water tank before igniting the chamber and bringing the temperature to approximately 1,600 degrees Fahrenheit. The heat was applied for 20 minutes, at which time the test was stopped due to excessive smoke. Deflection measurements of the bridge deck panel, provided in table 33, were recorded at 1-minute intervals for the entire test duration. A technician sighted in on a leveling rod to measure the amount of deflection under load.

Table 33. Deflection measurements.

	FC-797	BRIDGE COMPOSITES LLC					K-1084	9/7/2012		
Time (min)	TC01	TC02	TC03	TC04	TC05	TC06	Grp Avg	TC07	TC08	TC09
0.00	76	76	76	76	76	77	76	77	76	78
0.25	77	76	76	76	76	77	76	77	76	78
0.50	76	75	76	76	76	77	76	77	76	78
0.75	76	76	76	76	76	77	76	79	76	77
1.00	76	76	76	76	76	77	76	82	76	78
1.25	76	76	76	75	76	77	76	87	76	78
1.50	76	76	76	76	75	77	76	95	76	77
1.75	76	76	76	76	76	76	76	104	76	78
2.00	76	76	76	76	76	77	76	114	77	78
2.25	76	76	76	76	76	77	76	125	77	78
2.50	76	76	76	76	76	77	76	137	77	78
2.75	76	76	77	76	76	77	76	147	78	77
3.00	76	76	76	76	76	77	76	157	79	78
3.25	76	76	76	76	76	77	76	165	80	78
3.50	76	76	76	76	76	77	76	174	81	78
3.75	76	76	76	76	76	77	76	182	82	78
4.00	76	76	76	76	76	77	76	189	83	78
4.25	76	76	76	76	76	77	76	197	85	78
4.50	76	76	76	76	76	77	76	204	86	78
4.75	76	76	77	76	76	77	76	211	87	78
5.00	76	76	76	76	76	77	76	218	89	78
5.25	76	76	77	76	76	77	76	225	91	78
5.50	76	75	76	76	76	77	76	233	93	78
5.75	76	76	77	76	76	77	76	239	94	78
6.00	76	76	76	76	76	77	76	240	96	78
6.25	76	76	77	75	76	77	76	239	98	78
6.50	76	76	77	77	76	77	76	240	100	78
6.75	76	76	77	77	76	77	76	242	102	78
7.00	76	76	77	77	76	76	76	245	103	78
7.25	76	76	77	77	76	77	77	248	105	78
7.50	77	76	77	77	76	77	77	251	106	78
7.75	77	76	77	77	76	77	77	254	108	77
8.00	77	76	77	77	76	77	77	258	110	78
8.25	77	76	77	77	76	77	77	261	112	79
8.50	77	76	77	77	76	77	77	266	114	79
8.75	77	77	78	77	76	77	77	270	115	79
9.00	77	77	78	77	76	77	77	274	117	79
9.25	77	77	78	77	77	77	77	278	118	79
9.50	77	77	78	77	77	77	77	282	120	79
9.75	77	77	79	77	77	77	77	286	121	79
10.00	78	77	79	78	77	77	77	291	123	79

Table 33. Deflection measurements, continued.

	FC-797	BRIDGE COMPOSITES LLC					K-1084	9/7/2012		
Time (min)	TC01	TC02	TC03	TC04	TC05	TC06	Grp Avg	TC07	TC08	TC09
10.25	78	77	79	78	77	77	78	295	125	79
10.50	77	77	79	78	77	77	77	299	126	79
10.75	78	77	79	78	77	77	78	303	128	79
11.00	78	77	79	78	77	77	78	307	131	79
11.25	78	77	80	76	77	77	78	311	132	80
11.50	78	78	80	77	77	77	78	316	133	80
11.75	78	78	80	79	76	77	78	320	136	80
12.00	79	78	80	79	77	77	78	325	138	80
12.25	79	77	80	79	77	77	78	331	139	80
12.50	79	78	81	80	78	77	79	337	140	80
12.75	79	78	81	80	78	77	79	342	140	80
13.00	80	78	81	80	78	77	79	348	144	80
13.25	80	78	81	80	78	77	79	354	146	81
13.50	80	78	81	80	78	77	79	360	148	81
13.75	80	78	81	80	78	77	79	365	150	81
14.00	80	79	82	81	78	77	79	369	152	81
14.25	81	79	82	81	78	77	80	374	154	81
14.50	81	79	82	81	78	77	80	379	156	82
14.75	81	79	82	81	78	77	80	384	158	82
15.00	81	79	82	81	79	77	80	389	159	82
15.25	81	79	83	81	79	77	80	395	161	82
15.50	81	79	83	82	79	77	80	401	164	83
15.75	82	79	83	82	79	77	80	407	167	83
16.00	82	79	83	82	79	77	80	413	168	83
16.25	82	80	83	82	79	77	81	420	171	83
16.50	82	80	84	81	80	77	81	427	172	84
16.75	83	80	84	83	79	77	81	432	174	84
17.00	83	80	84	83	80	77	81	438	177	84
17.25	83	81	84	83	80	77	81	443	179	84
17.50	83	81	85	84	80	77	82	448	180	85
17.75	84	81	85	84	80	77	82	453	181	85
18.00	84	81	85	84	80	77	82	458	185	85
18.25	84	82	85	85	81	77	82	463	187	85
18.50	84	82	85	85	81	77	82	467	189	86
18.75	85	82	86	85	81	77	83	473	191	86
19.00	85	82	86	85	81	77	83	477	194	87
19.25	85	83	86	86	81	77	83	481	196	87
19.50	85	83	86	86	81	77	83	484	197	88
19.75	86	83	86	86	81	78	83	488	200	88
20.00	86	83	87	87	82	78	84	493	203	89

At the end of the test, the panel was still carrying load and generally structurally sound, although the resin on the bottom had burned off, exposing glass fiber. The following photos illustrate the condition of the specimen afterwards.



Figure 97. Photo. The test panel just after the test stopped. Note that the top surface kept cooler and ended up with little deterioration.



Figure 98. Photo. Specimen immediately after the test. Note the extent of damage on the bottom.



Figure 99. Photo. Close-up of the open end of the panel after the test.



Figure 100. Photo. The glass fiber on the bottom has frayed due to burn-off of the resin matrix.

RESULTS

The deck panel survived 1,600-degree Fahrenheit temperatures relatively well. The top surface did not rise much higher than room temperature (~80 degrees Fahrenheit). Although the bottom surface suffered extensive damage, the multi-celled structure protected the upper part and reduced the spread of flame and high temperatures. The panel carried the full 1,600 lb. superimposed load with a maximum deflection of 5/16 inches. There was no crushing of the tubes observed, no excessive bending, and the panel was still functional at the end of the test.

APPENDIX M: AFTER-TEST REVIEW PRESENTATION

 **BridgeComposites**
Delivering Innovative Technology

Composite Bridge Decking

Report on Testing

A Highways for Life Project
Jerome S. O'Connor, PE

 **BridgeComposites**
Delivering Innovative Technology

Report on Testing

Delivered to the Project Technical Advisory Panel (TAP) via GoToMeeting on 8/14/12 as part of

Task 13

Design Review II (After-Test Review)

A Highways for Life Project
Jerome S. O'Connor, PE, Project Director

 **BridgeComposites**
Delivering Innovative Technology

Composite Bridge Decking for Moveable Bridges

Report on Testing

- Description w/ Details
- Analysis & Testing
- Performance
- Summary

 **BridgeComposites**
Delivering Innovative Technology

Composite Bridge Decking for Moveable Bridges

Technical Advisory Panel

1. Ray Bottenberg, OR DOT
2. Duane Daniels, Larson Design Group
3. Jeremy Ferris, Allegany County
4. Paul Fossier, LA DOTD
5. Paul Liles, GA DOT
6. George Patton, E.C. Driver & Associates
7. William Potter, FL DOT
8. Herbert Protin, HDR
9. Tom Sheehan, NYSTA Canals Division
10. Kevin Thompson, Caltrans (retired)
11. Art Yannotti, NY DOT (retired)

Design Approach -

Priority of Design Parameters

1. Performance
 - Strength - given
 - Stiffness – very important because it affects serviceability issues and long term durability (cracking/spalling of wearing surface, deterioration of attachment detailing and panel-panel joints)
2. Constructability
3. Weight
4. Cost
5. Speed of installation

 **BridgeComposites**
Delivering Innovative Technology

Composite Bridge Decking for Moveable Bridges

Description



Panel type	Weight	Weight w/ thin wearing surface
Empty	16 psf	20 psf
Alternating E-grout	27 psf	31 psf
E-grout in top cells	24 psf	28 psf

Depth:
5 3/8"





 Composite Bridge Decking for Moveable Bridges

Details



 Composite Bridge Decking for Moveable Bridges

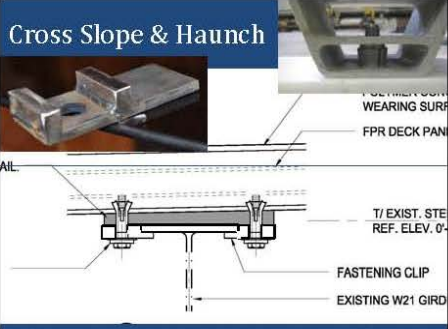
“Details”

- o Connection to supporting steel
- o Cross slope and haunch provisions
- o Field Joint between panels
- o Wearing surface
- o Bridge railing



 Composite Bridge Decking for Moveable Bridges

Cross Slope & Haunch



WEARING SURF
 FPR DECK PANEL
 T/ EXIST. STE
 REF. ELEV. 0'-
 FASTENING CLIP
 EXISTING W21 GIRD



 Composite Bridge Decking for Moveable Bridges

Wearing Surface

- o 1st course: 3/8" stone shop applied w/ adhesive

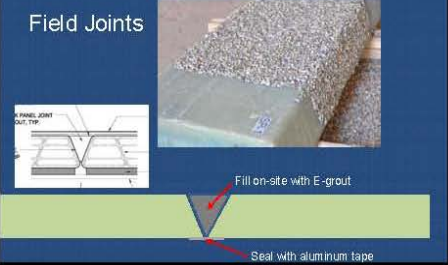



- o 2nd course: field applied



 Composite Bridge Decking for Moveable Bridges

Field Joints



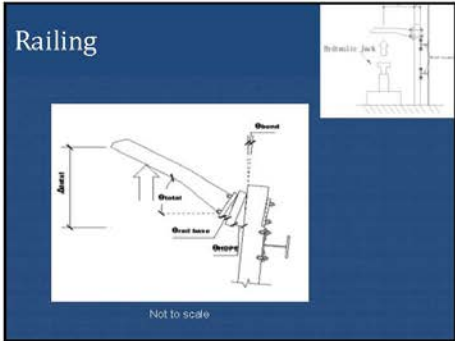
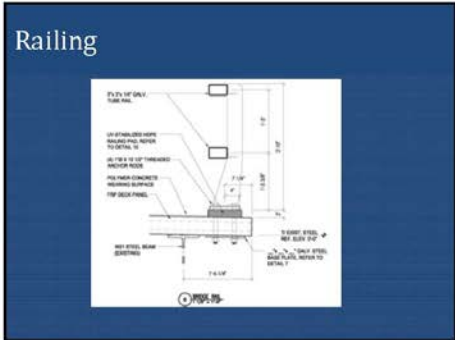
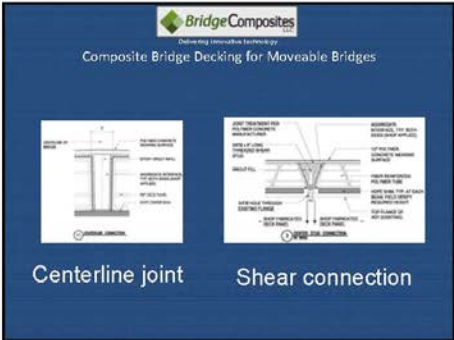
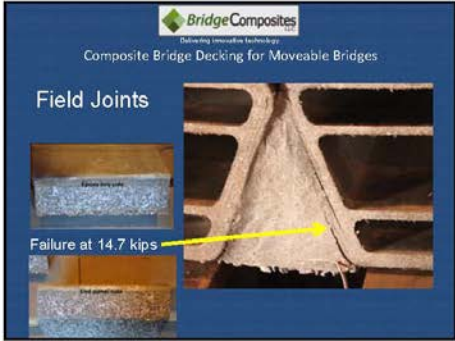
PANEL JOINT
 CUT TOP
 Fill on-site with E-grout
 Seal with aluminum tape

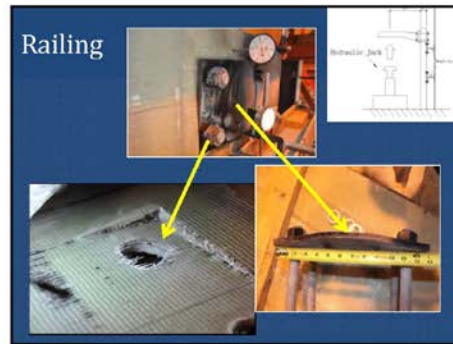
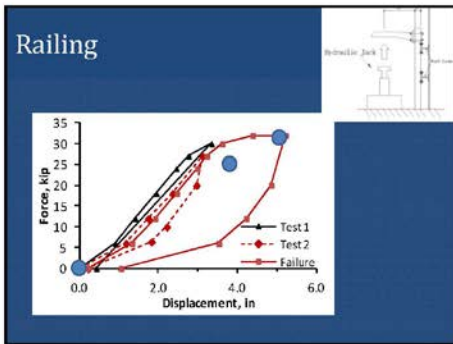


 Composite Bridge Decking for Moveable Bridges

Field Joints



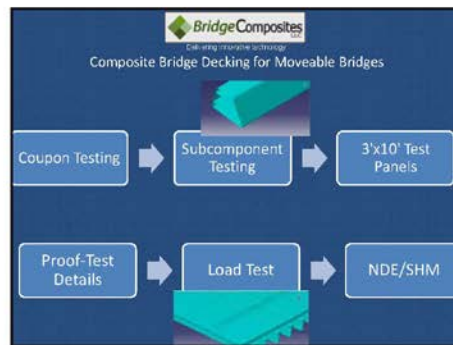




BridgeComposites
Delivering innovative solutions

Composite Bridge Decking for Moveable Bridges

Analysis / Testing



- BridgeComposites
Delivering innovative solutions
- Composite Bridge Decking for Moveable Bridges
- Material Testing
 - Tube Testing
 - Panel Testing
 - Flexure
 - Fatigue
 - Ultimate
 - Shear
 - Fire resistance

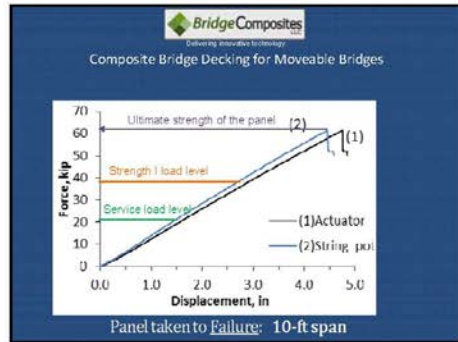
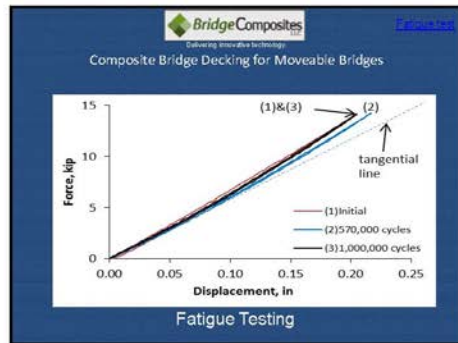
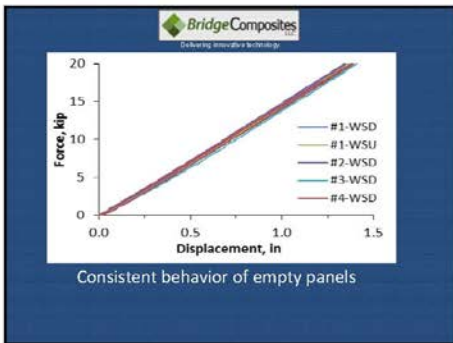
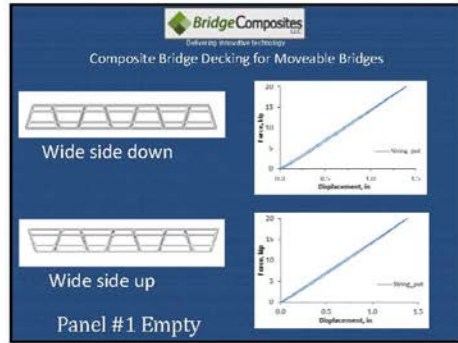
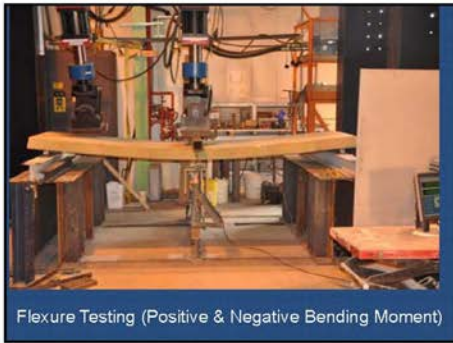
BridgeComposites
Delivering innovative solutions

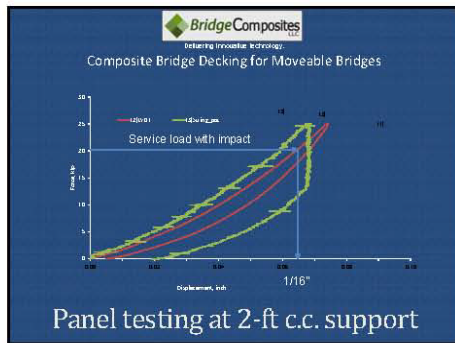
Composite Bridge Decking for Moveable Bridges

Testing Nomenclature

WSU=wide side up (testing position)
 WSD=wide side down
 SG1=strain gage 1
 for tubes:
 EW=epoxy grout & filled with wide cell (grout type and grouted cell)
 EN=epoxy grout & filled with narrow cell
 CW=cementitious grout & filled with wide cell
 CN=cementitious grout & filled with narrow cell

for panels: (the figure 2 in panel testing report may help better understand these nomenclatures)
 EN=epoxy grout & filled with narrow side cells
 EA=epoxy grout & filled with alternate cells
 CN=cementitious grout & filled with narrow side cells
 CA=cementitious grout & filled with alternate cells



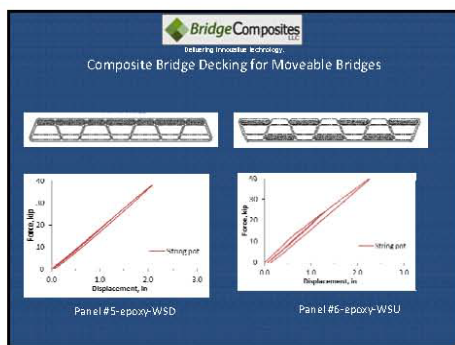


BridgeComposites LLC
Delivering Innovative Technology

Composite Bridge Decking for Moveable Bridges

Summary of Empty Panel Tests
10' span

Panel ID No.	Instrument used	Cross-section position	Max deflection (in)	Displacement at max deflection (in)	Average deflection (in)	Test date
A1	Stringer & VWF & 10' tie back out	WSU	28	1.28	1.48	05/22/2012
A2	Stringer & VWF & 10' tie back out	WSU	28	1.28	1.4	05/22/2012
A3	Stringer & VWF & 10' tie back out	WSU	28	1.27	1.42	05/22/2012
A4	Stringer & VWF & 10' tie back out	WSU	28	1.24	1.42	05/22/2012
A5	Stringer & VWF & 10' tie back out	WSU	28	1.23	1.38	05/24/2012
A6	Stringer & VWF & 10' tie back out	WSU	28	1.4	1.48	05/24/2012



BridgeComposites LLC
Delivering Innovative Technology

Summary of panel tests 10' span

Panel ID No.	Instrument used	Cross-section position	Max deflection (in)	Displacement at max deflection (in)	Average deflection (in)	Test date
W5-FU	Stringer & VWF & 10' tie back out	WSD	208.38	1.2182.09	17.24 (5.20)	05/23/2012
W6-FU	Stringer & VWF & 10' tie back out	WSU	248.40	1.2582.25	20.38 (5.30)	06/02/2012
W7-CA	Stringer & VWF & 10' tie back out	WSD	248.40	1.5382.63	15.88 (4.51)	06/04/2012
W8-FU	Stringer & VWF & 10' tie back out	WSU	208.38	1.4282.71	15.07 (5.21)	05/30/2012
W9-FU	Stringer & VWF & 10' tie back out	WSU	228.38	1.3482.60	18.09 (5.30)	05/31/2012
W10-CA	Stringer & VWF & 10' tie back out	WSD	248.40	1.2782.23	20.72 (5.30)	06/04/2012
W11-CA	Stringer & VWF & 10' tie back out	WSU	248.40	1.5082.57	15.02 (4.51)	06/04/2012
W12-CA	Stringer & VWF & 10' tie back out	WSD	228.38	1.2682.25	15.23 (4.41)	05/30/2012

BridgeComposites LLC
Delivering Innovative Technology

Composite Bridge Decking for Moveable Bridges

Summary

-
- BridgeComposites LLC
Delivering Innovative Technology
- Composite Bridge Decking for Moveable Bridges
- ## Penn State Conclusions
1. Tubes are very elastic.
 2. Epoxy grout can increase panel stiffness by 45%.
 3. Symmetrical section is good for + & - bending.
 4. Failure mode of unfilled section is compressive failure of tubes.
 5. Fatigue results in very small loss of stiffness.



Composite Bridge Decking for Moveable Bridges

Summary

1. Strength demands are easily met.
2. Very stiff section, especially at spacing < 5.5'.
3. Alternating epoxy grout fill enhances stiffness by 45%; other means available to provide stiffness.
4. Pseudo-ductile failure; some capacity remains after failure.
5. Empty section: weighs 16 psf w/o wearing surface.
6. Pliable adhesive ensures bond of wearing surface.
7. Options exist for attaching and providing cross slope.
8. Low modulus epoxy grout is used to prevent cracking at field joints.



Composite Bridge Decking for Moveable Bridges

Next Steps

1. Proof of Concept Deck Installation
2. Compare field data to FEA



Future Demonstration Project



Composite Bridge Decking for Moveable Bridges



jerome.oconnor@bridgecomposites.com
 (607) 725-0442
 50 Seneca Street, Hornell, NY

COMMENTS APPRECIATED !



Composite Bridge Decking for Moveable Bridges

1. Question (Herb): How is the wearing surface repaired / refreshed?

Response: Since the second course of the wearing surface is only 1/4" thick, a new 1/4" surface can be applied if the additional 3 psf weight is not critical. Otherwise, the polymer concrete wearing surface can be milled off and resurfaced with a fresh course of the same material.



Composite Bridge Decking for Moveable Bridges

2. Question (Herb): Will this be available in various panel sections/sizes? Will there be a table for design engineers to use as a design guide.

Response: The deck design is valid for a range of spans and this can be tabulated to give designers the ability to pick the suitable deck type for their stringer spacing. Spans between 2' and 10' were tested. Sections were tested with various stiffening materials: empty, epoxy grout in the top only, epoxy grout alternating between top and bottom.



Composite Bridge Decking for Moveable Bridges

3. Question (Herb): What about dynamic loading?

Response: An impact factor was applied to the AASHTO design load. The field testing that is planned may provide additional information about the actual dynamic loading induced by truck loads.



Composite Bridge Decking for Moveable Bridges

4. Question (Paul): Previous FRP decks have had trouble with the deck-deck joints, deck-steel connections, and the wearing surface. What has been done to prevent those problems?

Response: "Details" have been given a lot of attention in the design/analysis, material testing, and proof testing stages of the project. The modeling and subsequent testing assures us that the proposed details will function well in service.



Composite Bridge Decking for Moveable Bridges

5. Comment (Ray): In the preliminary design stage, his only concern had been about the type of grout used. He was pleased to see that we addressed that issue by selecting a low-modulus grout (called E-Flex) that will be compatible with the fairly flexible deck panels.